BIOCHEMICAL INVESTIGATIONS OF *Artocarpus* spp. FOR COSMECEUTICAL APPLICATIONS

HAZWANI MAT SAAD

FACULTY OF SCIENCE
UNIVERSITI MALAYA
KUALA LUMPUR

2022

BIOCHEMICAL INVESTIGATIONS OF *Artocarpus* spp. FOR COSMECEUTICAL APPLICATIONS

HAZWANI MAT SAAD

THESIS SUBMITTED IN FULFILMENT OF THE REQUIREMENTS FOR THE DEGREE OF DOCTOR OF PHILOSOPHY

INSTITUTE OF BIOLOGICAL SCIENCES
FACULTY OF SCIENCE
UNIVERSITI MALAYA
KUALA LUMPUR

2022

UNIVERSITI MALAYA

ORIGINAL LITERARY WORK DECLARATION

Name of Candidate: **HAZWANI MAT SAAD**

Matric No: **17058009/4**

Name of Degree: **DOCTOR OF PHILOSOPHY**

Title of Project Paper/Research Report/Dissertation/Thesis ("this Work"):

BIOCHEMICAL INVESTIGATIONS OF *Artocarpus* spp. FOR COSMECEUTICAL APPLICATIONS

Field of Study: **BIOCHEMISTRY (BIOLOGY AND BIOCHEMISTRY)**

I do solemnly and sincerely declare that:

(1)   I am the sole author/writer of this Work;
(2)   This Work is original;
(3)   Any use of any work in which copyright exists was done by way of fair dealing and for permitted purposes and any excerpt or extract from, or reference to or reproduction of any copyright work has been disclosed expressly and sufficiently and the title of the Work and its authorship have been acknowledged in this Work;
(4)   I do not have any actual knowledge nor do I ought reasonably to know that the making of this work constitutes an infringement of any copyright work;
(5)   I hereby assign all and every rights in the copyright to this Work to the University of Malaya ("UM"), who henceforth shall be owner of the copyright in this Work and that any reproduction or use in any form or by any means whatsoever is prohibited without the written consent of UM having been first had and obtained;
(6)   I am fully aware that if in the course of making this Work I have infringed any copyright whether intentionally or otherwise, I may be subject to legal action or any other action as may be determined by UM.

Candidate's Signature   Date: 26.10.2022

Subscribed and solemnly declared before,

Witness's Signature   Date: 26.10.2022

Name:

Designation:

BIOCHEMICAL INVESTIGATIONS OF *Artocarpus* spp. FOR COSMECEUTICAL APPLICATIONS

ABSTRACT

Cosmeceutical agents from natural origins which are presumably non-invasive, highly efficacious, and cost effective are exceptionally in demand by consumers nowadays. This study aimed to explore the potential of fifteen ethanolic extracts from the leaf, peel, and stem bark of five Malayan *Artocarpus* species, namely *Artocarpus altilis* (Parkinson) Fosberg, *Artocarpus heterophyllus* Lam., *Artocarpus integer* (Thunb.) Merr., *Artocarpus elasticus* Reinw. ex Blume, and *Artocarpus rigidus* Blume for their application in skin-lightening cosmeceutical by performing *in vitro* evaluations including anti-melanogenesis, radical scavenging, and ultraviolet (UV) protective activities. The study was then narrowed down to the bioassay-guided fractionation of the bioactive extract, followed by mechanistic analysis and encapsulation of the bioactive fraction. The *A. heterophyllus* stem bark and peel extracts showed potent anti-melanogenesis activity in reducing melanin content to 23–24% and inhibited the cellular tyrosinase activity with 1.85 and 1.42 folds stronger than kojic acid (positive control) at the concentration of 50 µg/mL. Whilst, the *A. elasticus* peel extract exhibited a remarkable radical scavenging activity on 2,2-diphenyl-1-picrylhydrazyl (DPPH•), 2,2'-azino-bis(3-ethylbenzothiazoline-6-sulphonic acid) (ABTS$^{+•}$), and superoxide anion (O$_2^{-•}$). The *A. heterophyllus* stem bark extract which was identified as the bioactive extract in exerting anti-melanogenesis effect in B16F10 melanoma cells was selected for further analysis. A semi-purified fraction (H-3) from *A. heterophyllus* stem bark extract demonstrated the most pronounced anti-melanogenesis effect at 12.00 µg/mL by reducing melanin content to 22.86 ± 2.90% and inhibiting cellular tyrosinase activity at treatment concentration 33-folds lower than kojic acid, without being cytotoxic against B16F10 melanoma cells. Six chemical constituents in H-3 including two fatty acids and four

flavonoids were identified *via* liquid chromatography-mass spectrometry (LCMS) analysis. Moreover, treatment with H-3 for 24 and 48 hours substantially scavenged intracellular reactive oxygen species (ROS) of hydrogen peroxide(H_2O_2)-challenged B16F10 melanoma cells by 1.8 and 4.4%, respectively. Based on the microarray profiling and real-time polymerase chain reaction (qPCR) analysis, H-3 downregulated *Creb3l1, Creb3l2*, *Creb3l3*, *Mitf, Tyr*, *Tyrp1*, and *Dct* genes in B16F10 melanoma cells, whereas the expression of *Map3k20*, *Mapk14* (p38), and *Foxo3* genes were markedly increased. Generally, these results demonstrated that H-3 exhibited its anti-melanogenesis activity in B16F10 melanoma cells through scavenging ROS and concurrent inhibition of the cyclic adenosine monophosphate (cAMP) and activation of the p38/mitogen-activated protein kinase (MAPK) signaling pathways. Due to the outstanding anti-melanogenesis effect of H-3, this bioactive fraction was encapsulated into the liposomes in order to enhance its cosmeceutical value. The incorporation of H-3 in liposomes yields vesicles with a particle size of 185 nm, a zeta potential of −38 mV, and encapsulation efficiency of 79%. The obtained results suggest that the encapsulation of H-3 in liposomes retained the anti-melanogenesis activity in B16F10 melanoma cells. Altogether, these findings indicate that H-3 from *A. heterophyllus* stem bark extract has the potential to be used as skin-lightening cosmeceutical agent in the treatment of skin hyperpigmentation.

Keywords: *Artocarpus*, melanin, tyrosinase, radical scavenging, microarray profiling, liposomes.

PENYIASATAN BIOKIMIA TERHADAP spp. *Artocarpus* UNTUK APLIKASI KOSMESIUTIKAL

ABSTRAK

Ejen kosmesiutikal daripada sumber semula jadi yang dianggap tidak invasif, sangat berkesan, dan menjimatkan kos mempunyai permintaan yang luar biasa pada masa kini. Kajian ini bertujuan untuk menerokai potensi lima belas ekstrak etanol daripada daun, kulit buah, dan kulit batang lima spesies *Artocarpus* Malayan, iaitu *Artocarpus altilis* (Parkinson) Fosberg, *Artocarpus heterophyllus* Lam., *Artocarpus integer* (Thunb.) Merr., *Artocarpus elasticus* Reinw. ex Blume, dan *Artocarpus rigidus* Blume untuk aplikasi kosmesiutikal mereka dalam pencerahan kulit dengan melakukan penilaian *in vitro* termasuk aktiviti anti-melanogenesis, penghapusan radikal, dan perlindungan ultraungu (UV). Seterusnya, kajian ini diperincikan lagi dengan menjalani pemecahan berpandukan bioesei bagi ekstrak bioaktif, dan disusuli dengan analisis mekanistik serta enkapsulasi bagi pecahan bioaktif. Ekstrak kulit batang dan kulit buah *A. heterophyllus* menunjukkan aktiviti anti-melanogenesis yang kuat dalam pengurangan kandungan melanin kepada 23–24% dan menghalang aktiviti tirosinasa selular dengan 1.85 dan 1.42 kali ganda lebih kuat berbanding asid kojik (kawalan positif) pada kepekatan 50 µg/mL. Manakala, ekstrak kulit buah *A. elasticus* mempamerkan aktiviti penghapusan radical yang luar biasa ke atas 2,2-difenil-1-pikrilhidrazil (DPPH•), 2,2'-azino-bis(3-etilbenzotiazolin-6-asid sulfonik) ($ABTS^{+•}$), dan anion superoksida ($O_2^{-•}$). Ekstrak kulit batang *A. heterophyllus* yang dikenal pasti sebagai ekstrak bioaktif dalam mempamerkan kesan anti-melanogenesis terhadap sel melanoma B16F10 telah dipilih untuk analisis selanjutnya. Pecahan separa tulen (H-3) daripada ekstrak kulit batang *A. heterophyllus* menunjukkan kesan anti-melanogenesis yang ketara pada 12.00 µg/mL dengan menurunkan kandungan melanin kepada 22.86 ± 2.90% serta menghalang aktiviti tirosinasa selular pada kepekatan 33 kali ganda lebih rendah berbanding asid kojik tanpa kesan toksiksiti pada

sel melanoma B16F10. Enam konstituen kimia dalam H-3 yang merangkumi dua asid lemak dan empat flavonoid telah dikenal pasti melalui analisa kromatografi cecair-spectrometri jisim (LCMS). Tambahan pula, rawatan dengan H-3 selama 24 dan 48 jam dapat menghapuskan spesis oksigen reaktif (ROS) intrasel daripada sel melanoma B16F10 yang dicabar dengan hydrogen peroksida (H_2O_2) dengan ketara masing-masing sebanyak 1.8 dan 4.4%. Berdasarkan profil jujukan mikro dan analisis reaksi berantai polymerase masa nyata (qPCR), H-3 menurunkan gen *Creb3l1*, *Creb3l2*, *Creb3l3*, *Mitf*, *Tyr*, *Tyrp1*, dan *Dct* dalam sel B16F10, manakala ekspresi bagi gen *Map3k20*, *Mapk14* (p38), dan *Foxo3* telah meningkat dengan ketara. Secara amnya, keputusan ini menunjukkan bahawa H-3 mempamerkan aktiviti anti-melanogenesis dalam sel melanoma B16F10 dengan mengikis ROS intrasel dan pada masa yang sama menghalang laluan isyarat kitaran edenosin monofosfat (cAMP) serta mengaktifkan isyarat lalauan p38/protein kinasa diaktifkan mitogen (MAPK). Disebabkan oleh kesan anti-melanogenesis H-3 yang luar biasa, pecahan bioaktif ini telah dikapsulkan ke dalam liposom untuk meningkatkan nilai kosmesiutikalnya. Penggabungan H-3 dalam liposom menghasilkan vesikel yang bersaiz 185 nm, potensi zeta −38 mV, dan kecekapan enkapsulasi sebanyak 79%. Hasil dapatan ini mencadangkan enkapsulasi H-3 dalam liposom mengekalkan aktiviti anti-melanogenesisnya dalam sel melanoma B16F10. Secara keseluruhannya, penemuan ini menunjukkan bahawa H-3 daripada ekstrak kulit batang *A. heterophyllus* berpotensi untuk digunakan sebagai agen kosmeseutikal pencerah kulit dalam rawatan hiperpigmentasi kulit.

Kata kunci: *Artocarpus*, melanin, tirosinasa, pengikis radikal, profil jujukan mikro, liposom.

ACKNOWLEDGEMENTS

First and foremost, I would like to express my deepest gratitude to my supervisors Assoc. Prof. Dr. Sim Kae Shin, Dr. Sugumaran Manickam from the Institute of Biological Sciences, Faculty of Science, and Dr. Lim Siew Huah from the Department of Chemistry, Faculty of Science for their unwavering guidance, advice, support, and encouragement throughout the whole project.

I would like to extend my gratitude to Assoc. Prof. Dr. Teo Yin Yin from Department of Chemistry, Faculty of Science for her guidance and for allowing me to utilize the equipment and facilities in her laboratory for the encapsulation studies. I also owe my gratitude to Prof. Dr. Misni bin Misran from Department of Chemistry, Faculty of Science, Assoc. Prof. Dr. Bong Chui Wei, and Prof. Dr. Saiful Anuar bin Karsani from Institute of Biological Sciences, Faculty of Science for allowing me to use their equipment and facilities.

A special thanks and gratitude to Dr. Tan Chun Hoe, Ms. Tang Sin Yee, Mr. Wong Soon Kit, and Mr. Tang Yi Sheng for their help and motivation in carrying out the experiment despite their hectic schedules. Also, a warm thanks to my family for their constant encouragement and fellow friends for all the help and support.

TABLE OF CONTENTS

LIST OF FIGURES

LIST OF TABLES

LIST OF SYMBOLS AND ABBREVIATIONS

A	:	Absorbance
Abs	:	Absorbance
C	:	Absorbance
CF	:	Correction factor
EE	:	Erythemal effect spectrum
$\cdot OH$	:	Hydroxyl radical
λ	:	Lambda
O	:	Molar extinction coefficient of AlamarBlue®
I	:	Solar intensity spectrum
$^1O_2$	:	Singlet oxygen
2SCD	:	2-S-cysteinyldopa
5SCD	:	5-S-cysteinyldopa
α-MSH	:	Alpha melanocyte stimulating hormone
AAI	:	Antioxidant index
ABTS	:	2,2'-Azino-bis(3-ethylbenzothiazoline-6-sulphonic acid)
AEBSF	:	4-(2-Aminoethyl)benzenesulfonyl fluoride hydrochloride
ANOVA	:	Analysis of variance

ATCC®	:	American Type Culture Collection
CA	:	California
cAMP	:	Cyclic adenosine monophosphate
cDNA	:	Complimentary deoxyribonucleic acid
cGMP	:	Cyclic guanosine 3',5'-monophosphate
CREB	:	cAMP-responsive element binding protein
cRNA	:	Complementary ribonucleic acid
Cy3	:	Canine-3
DCT	:	Dopachrome tautomerase
DEG	:	Differentially expressed genes
DHI	:	6-Dihydroxyindole
DHICA	:	5,6-Dihydroxyindole-2-carboxylic acid
DMEM	:	Dulbecco's Modified Eagle's Medium
DMSO	:	Dimethyl sulfoxide
DNA	:	Deoxyribonucleic acid
DPPH	:	2,2-Diphenyl-1-picrylhydrazyl
EE	:	Encapsulation efficiency
ERK	:	Extracellular signal-regulated kinase
ESI	:	Electrospray ionization

FBS	:	Fetal bovine serum
FC	:	Fold change
FDA	:	Food and Drug Administration
FDR	:	False discovery rate
Fe^{2+}	:	Ferrous ion
FOXO3a	:	Forkhead Box O3
FRAP	:	Ferric reducing antioxidant power
GC	:	Gas chromatography
GO	:	Gene ontology
GPCR	:	G-protein-coupled receptor
GSK-3β	:	Glycogen synthase kinase-3β
GTP	:	Guanosine-5'-triphosphate
GUV	:	Giant unilamellar vesicles
H_2DCFDA	:	2',7'-Dichlorodihydrofluorescein diacetate
H_2O_2	:	Hydrogen peroxide
HBTA	:	5-Hydroxy-1,4-benzothiazinylalanine
HCl	:	Hydrochloric acid
HIV	:	Human immunodeficiency virus
HUVEC	:	Human umbilical vein endothelial cell

i.e.	:	That is
IC$_{50}$	:	Half maximal inhibitory concentration
ICAQ	:	Indole-2-carboxylic acid-5,6-quinone
iNOS	:	Inducible nitric oxide
IQ	:	Indole-5,6-quinone
LC	:	Liquid chromatography
L-DOPA	:	L-3,4-Dihydroxyphenilalanine
LEF1	:	Lymphoid enhancer-binding factor 1
LUV	:	Large unilamellar vesicles
MAPK	:	Mitogen-activated protein kinase
MC1R	:	Melanocortin 1 receptor
MED	:	Minimal erythema dose
MIQE	:	Minimum Information for Publication of Quantitative Real-Time PCR Experiments
MITF	:	Microphthalmia-associated transcription factor
MLV	:	Multilamellar vesicles
mRNA	:	Messenger RNA
MS	:	Mass spectrometer
NA	:	Not applicable
NADH	:	Reduced nicotinamide adenine nucleotide

NADPH	:	Reduced nicotinamide adenine nucleotide phosphate
NBT	:	Nitrobluetetrazolium
ND	:	Not detected
NO	:	Nitric oxide
$O_2{}^{-\bullet}$	:	Superoxide anion radical
OK1	:	Human oral keratinocytes 1
OLV	:	Oligolamellar vesicles
ORAC	:	Oxygen radical absorbance capacity
PAX3	:	Paired box gene 3
PBS	:	Phosphate buffered saline
PCR	:	Polymerase chain reaction
PDI	:	Polydispersity index
PI3K	:	Phosphatidylinositol 3-kinase
PKA	:	Protein kinase A
PMS	:	Phenazine methosulfate
qPCR	:	Real-time polymerase chain reaction
Q-TOF	:	Quadrupole Time-of-Flight
RIN	:	RNA integrity number
RNA	:	Ribonucleic acid

ROS	:	Reactive oxygen species
SOX10	:	SRY (sex-determining region Y)-box 10
SOX9	:	SRY (sex-determining region Y)-box 9
SPF	:	Sun protection factor
SUV	:	Small unilamellar vesicles
TCF	:	T-cell factor
TNF-α	:	Tumour necrosis factor alpha
TRP1	:	Tyrosinase related protein-1
TYR	:	Tyrosinase
UK	:	United Kingdom
ULK1	:	Unc-51-like kinase 1
USA	:	United States of America
USD	:	United States Dollar
UV	:	Ultraviolet
viz.	:	Namely
Zp	:	Zeta potential

LIST OF APPENDICES

CHAPTER 1: INTRODUCTION

1.0   Introduction

Huge demand for skin lighteners is driven by a desire to moderate the conditions related to abnormal melanin deposition in the skin, resulting in the formation of freckles, melasma, age spots, and other hyperpigmentation related conditions (Han et al., 2015). The global cosmeceutical market is experiencing a constant increase and expected to reach USD 98.7 billion by 2026 (Sotelo et al., 2021). About 15% of the population in the world has invested heavily in skin-lightening agents, where much of this trade is predominantly from Asia (Pillaiyar et al., 2017b). In this regard, a wide search for effective anti-melanogenesis treatment has been popular among researchers in the field of cosmeceutical products. Compared to instrumental approaches such as laser surgery in the treatment of hyperpigmentation, topical cosmeceutical containing anti-melanogenesis agents is relatively non-invasive, efficacious, and cost-effective alternative treatment.

In the light of the toxicological safety and adverse effects of synthetic chemicals, consumers would prefer to use anti-melanogenesis agents from natural sources (Fowler Jr et al., 2010). The genus *Artocarpus* (Moraceae) consists of approximately 50 different species that are widely distributed throughout the South and South-East Asia, New Guinea, and Southern Pacific, where the plants can be found mostly at the altitude below 1,000 m (Jagtap & Bapat, 2010). Despite the usefulness of various *Artocarpus* species as reported in the literature (Jagtap & Bapat, 2010), little study has been carried out on the cosmeceutical properties of the three well-known *Artocarpus* species in Malaysia such as *Artocarpus altilis* (Parkinson) Fosberg*, Artocarpus heterophyllus* Lam., and *Artocarpus integer* (Thunb.) Merr. The two lesser-known species, i.e., *Artocarpus elasticus* Reinw. ex Blume and *Artocarpus rigidus* Blume have hardly been studied in this aspect especially on the non-edible parts of the plant (leaf, peel, and stem bark).

By aiming to contribute new insights in developing cosmeceutical from various parts of *Artocarpus* species, 15 extracts from the leaf, peel, and stem bark of the selected *Artocarpus* species were evaluated through several parameters. The anti-melanogenesis potential of the *Artocarpus* species was first assessed using mushroom tyrosinase assay (non-cellular), followed by cellular assays using B16F10 melanoma cells, including cell viability assay, measurement of intracellular melanin content, and cellular tyrosinase assay. Since ROS plays a significant role in melanogenesis regulation (Huang et al., 2012), the radical scavenging potential of *Artocarpus* species was determined using DPPH•, ABTS$^{+•}$, and O$_2^{-•}$ radical scavenging assays. The UV protective (sun screening) potential of the extracts was also assessed by spectrophotometry in this study. The bioactive extract with a pronounced anti-melanogenesis effect was then identified and subjected to pesticide residue testing, proximate composition, along with bioassay-guided fractionation. Cell viability and melanin content assays were performed to identify the bioactive fraction. Following that, the bioactive fraction was chosen for further analysis, including identification of chemical constituents through LCMS analysis, measurement of intracellular ROS by using a flow cytometer, as well as determination of anti-melanogenesis mechanisms through microarray profiling and qPCR analysis. Nowadays, the process of encapsulation of the active ingredients is more focused on the delivery of the substance itself and also to protect its contents from breaking down (Casanova & Santos, 2016). In order to enhance the cosmeceutical properties, the bioactive fraction in this study was encapsulated into liposomes, followed by cosmeceutical evaluations. The outline of the experimental design is depicted in Figure 1.1.

1.1   Objectives of study

The current study aims to explore the potential of *Artocarpus* species in skin-lightening cosmeceutical applications. This may be achieved through the following objectives:

i.   To determine the anti-melanogenesis effect of selected *Artocarpus* species;

ii.   To analyse the UV light absorption pattern of selected *Artocarpus* species;

iii. To evaluate the radical scavenging activity of selected *Artocarpus* species;

iv.   To identify the chemical constituents in the bioactive fraction obtained through bioassay-guided fractionation using modern spectroscopic method;

v.   To investigate the cosmeceutical properties of the bioactive fraction and determine the molecular mechanisms involve in its anti-melanogenesis activity;

vi.   To encapsulate the bioactive fraction and examine the effect of encapsulation on the anti-melanogenesis activity.

Collection of fresh *Artocarpus* samples

↓

Species identification and herbarium sample preparation

↓ Cleaned, dried, and ground

Dried and ground plant materials

↓ Extraction with ethanol and concentrated under reduced pressure

Ethanol extracts

Anti-melanogenesis activity
- Mushroom tyrosinase assay
- Cell viability assay
- Intracellular melanin content assay
- Cellular tyrosinase assay

Radical scavenging activity
- DPPH scavenging activity
- ABTS cation scavenging activity
- Superoxide anion scavenging activity

UV absorption analysis

↓

Identification of bioactive extract → Pesticide residue testing

→ Proximate composition

↓ Bioassay-guided fractionation

Identification of bioactive fraction

↓

Measurement of intracellular ROS

Identification of chemical constituents

Determination of anti-melanogenesis molecular mechanisms

↓ Encapsulation

Physicochemical evaluation

↓

Cosmeceutical evaluation

Figure 1.1: Outline of the experimental design of the study.

CHAPTER 2: LITERATURE REVIEW

2.1 The skin

2.1.1 Structure and function of facial skin

Skin is the largest organ covering the whole surface of the body where it contributes about 15% of the total body weight (Kanitakis, 2002). The skin has three main layers; epidermis (the outermost layer), dermis (the second layer below the epidermis), and subcutaneous layer (the deepest layer of the skin) (Figure 2.1). The epidermis is a stratified squamous keratinized epithelium that renews by itself continuously. Keratinocytes are the majority of cells in the epidermis with a percentage of the population around 90–95% (Brody, 1960; Kanitakis, 2002). Epidermal keratinocytes are produced from the stem cells of the basal layer. The newly produced keratinocytes will migrate towards the skin surface while undergoing morphological and biochemical differentiation. After 30 days, dead keratinocytes will shed from the skin surface and will be replaced with new cells (Kanitakis, 2002). The other cells that reside in the epidermis are melanin-producing tactile antigen-presenting Langerhans cells, Merkel cells, and melanocytes. These cells make up around five to ten percent of the total population in the epidermis (Arda et al., 2014).
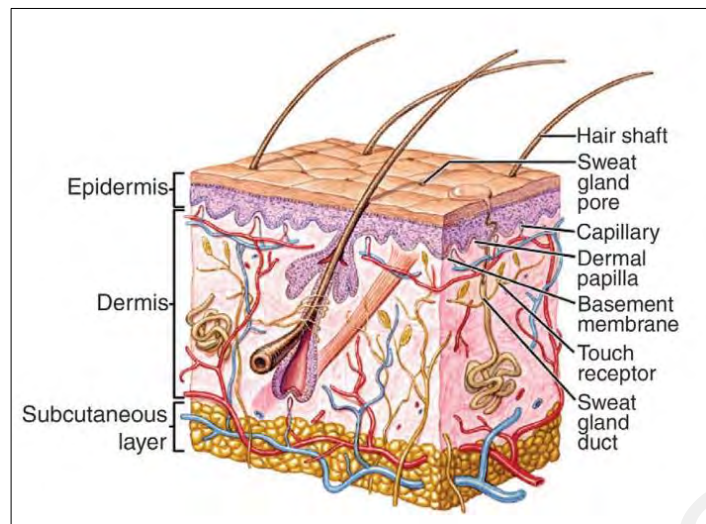
Figure 2.1: Structure of human skin. Photo sourced from MacNeil (2008).

The epidermis of facial skin is composed of four layers. The descending order of the epidermis layers is stratum corneum, stratum granulosum, stratum spinosum, and stratum basale (Figure 2.2) (Yousef et al., 2020). The outermost layer of the epidermis is the most lipophilic which contains only 13% water whereas the deeper layer of the epidermis becomes significantly hydrophilic which containing about 50% water (Matthias et al., 2009). The stratum corneum is the outermost layer of the epidermis is made up of a heterogeneous layer (15–20 layers) of lipid-depleted corneocytes embedded in a lipid-enriched extracellular matrix (Elias, 2005).
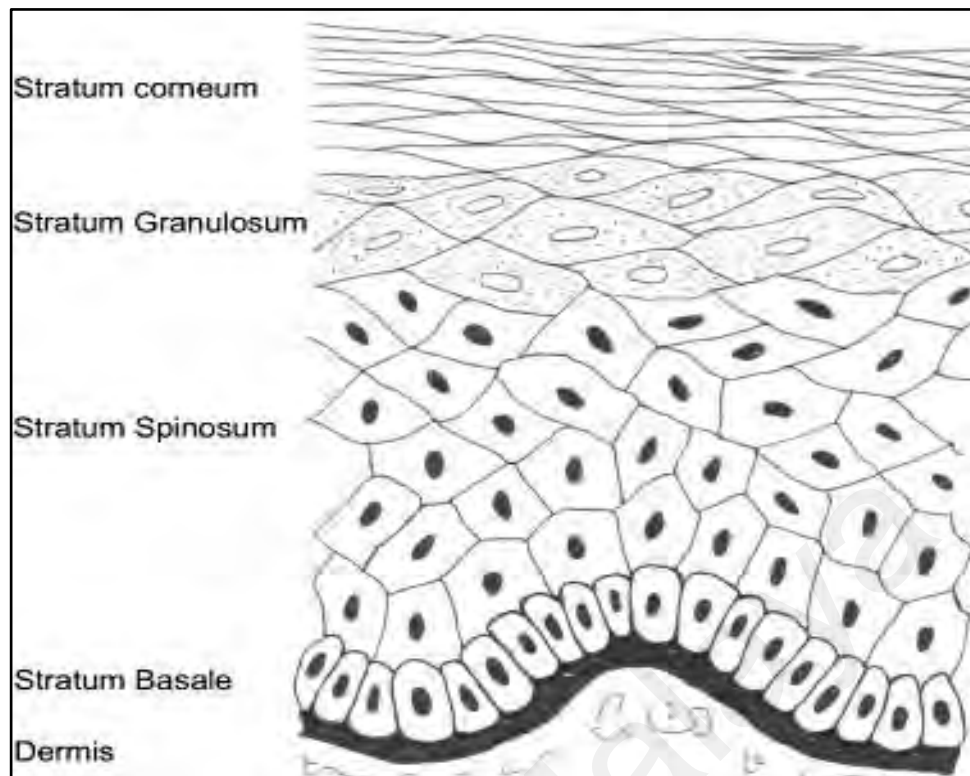
Figure 2.2: Layers of the epidermis. Photo sourced from Wickett and Visscher (2006).

According to Elias (2005), the structure of the stratum corneum has been proposed as a 'brick and mortar model' (Figure 2.3). The anucleated corneocyte which is 'welded' together by corneodesmosomes being the brick and the continuous matrix of specialized lipid matrix is the mortar (Harding, 2004; Lane, 2013). The corneocytes protect the stratum corneum from abrasion by chemical and physical injury while the lipid function as the water barrier (Harding, 2004). The characteristics of the specialized cells in the stratum corneum contribute to the resilient framework (Madison, 2003) which act as the first line barrier against the penetration of toxic chemicals, bacteria, and UV radiation into the skin at the same time maintaining the skin integrity by preventing the loss of fluids and electrolytes (Baroni et al., 2012; Elias, 2005).
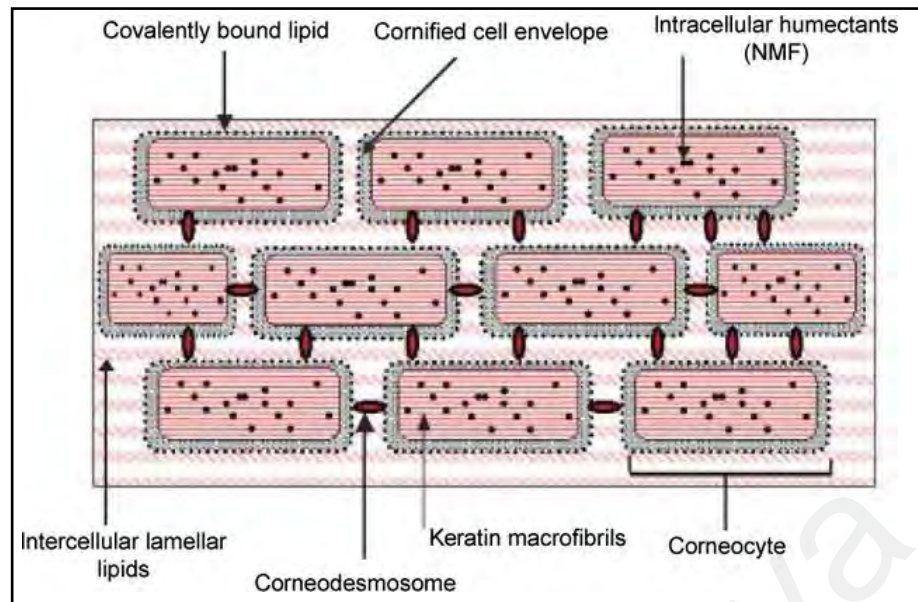
Figure 2.3: Schematic 'brick and mortar' model of the stratum corneum. Photo sourced from Harding (2004).

The dermis tissue is elastic and compressible which is important in supporting and protecting the epidermis as well as vascular and nervous plexuses running through it (Kanitakis, 2002). The dermis is made of 90% fibers (mainly collagen type I and III) and the ground substance filling the space between fibers (Arda et al., 2014; Kanitakis, 2002). The cells that reside in the dermis are fibroblasts, dermal dendrocytes, and mast cells. Fibroblasts are the most important cells in the dermis and all connective tissues; appear as spindle-shaped or stellate cells and contain a well-developed rough endoplasmic reticulum. All types of fibers and ground substances in the dermis are synthesized in fibroblasts (Kanitakis, 2002). The dermis is more hydrophilic compared to the epidermis where the water content in the dermis is about 70% (Matthias et al., 2009). The subcutaneous layer is located beneath the reticular layer of the dermis and is largely composed of fat cells (Arda et al., 2014; Shimizu, 2016). Subcutaneous tissue stores neutral fats that function as the cushion protecting the skin against physical pressure, retains moisture, and protection from heat and cold (Shimizu, 2016).

The glands on the facial skin include sweat glands (eccrine and apocrine) and sebaceous glands (Figure 2.4) (Baker, 2019; Shi et al., 2015). The eccrine sweat gland is a simple coiled tubular gland that is not associated with hair follicles (Arda et al., 2014). The sweat secreted from the eccrine sweat gland is mostly water and sodium chloride. Sometimes, the sweat from the eccrine gland also contains a mixture of chemicals from interstitial fluids and the eccrine gland itself (Baker, 2019). The main function of the eccrine sweat gland is to regulate the body temperature via evaporative heat loss (Hodge et al., 2018). The apocrine sweat gland is larger compared to the eccrine sweat gland and is associated with hair follicles (Arda et al., 2014; Baker, 2019). The apocrine sweat gland is known as the odiferous sweat gland where the sweat produced from this gland is rich in lipids and other components such as proteins, sugars, and ammonia (Baker, 2019; Hodge et al., 2018).

The sebaceous gland is a holocrine gland made up of sebocytes, located in the dermis (Szöllősi et al., 2017). This gland is associated with hair follicles and is highly distributed at the T-zone of the face area (Shi et al., 2015). The sebaceous gland produces a viscous lipid-rich fluid called sebum which helps to prevent desiccation of the skin by retaining its moisture (Baker, 2019; Hoover et al., 2020). The lipid components in sebum include triglycerides (30–50%), free fatty acids (15–30%), wax esters (26–30%), cholesterol (1.5–2.5%), cholesterol esters (3–6%), and squalene (12–20%) (Picardo et al., 2009; Szöllősi et al., 2017). In addition, sebum also plays other functions in the skin including photoprotection, anti-microbial, anti-fungal, pro-and anti-inflammatory activities, and delivery of fat-soluble antioxidant to the skin surface (Baker, 2019; Picardo et al., 2009).
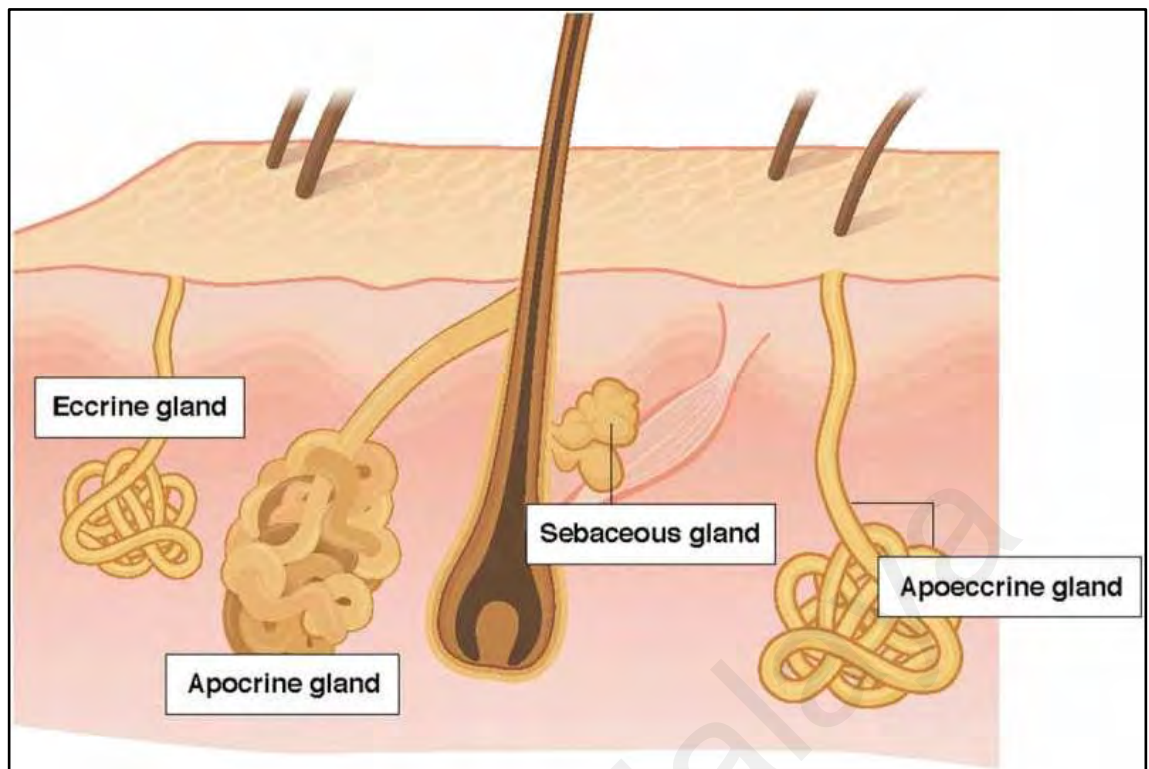
Figure 2.4: The glands on the skin. The apoeccrine gland is absent on the face and only available at the axillary region. Photo sourced from Baker (2019).

In addition to providing a protective barrier against external stimuli, the facial skin is responsible for wound healing and injury repair to restore the normal structure and function of the skin. In other aspects, facial skin is an important part of our appearance in reflecting our identity, personality, and emotions (Figure 2.5) to the people around us (Arda et al., 2014).

Figure 2.5: Faces with different emotions. Photo sourced from Praditsangthong et al. (2021).

2.1.2 Skin penetration pathways

The penetration of molecules through the epidermis is limited to molecules of molecular mass (< 500 Dalton) and moderate lipophilicity (partition coefficients log $K_{octanol/water}$ values between 1 and 3) (Matthias et al., 2009; Prausnitz et al., 2004). There are several possible pathways for the penetration of molecules through the stratum corneum of the epidermis which includes intercellular, transcellular, and transappendageal pathways (Figure 2.6) (Ammala, 2013; Lane, 2013). The intercellular route takes place at the interface between cells through the lipid bilayers while the transcellular pathway takes place directly through the cells (Ammala, 2013). The

transappendageal pathway takes place through eccrine sweat glands or hair follicles. This pathway is not considered to be a crucial pathway since these glands occupy only a small area of the skin, which is about 0.1%. However, this route is still possible and applicable for slowly diffusing compounds and very high molecular weight substances (Lane, 2013).
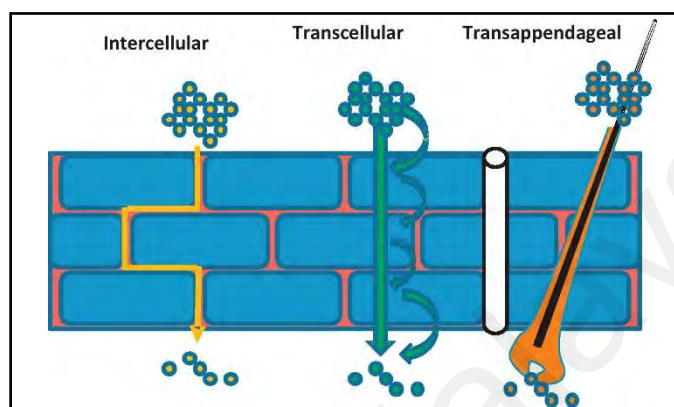
Figure 2.6: Possible transport pathways through the stratum corneum. Photo sourced from Lane (2013).

2.1.3   Skin colour and skin phototyping

Skin colour has three main variations, namely black, brown and white (Figure 2.7), which are determined by several pigments including melanin, haemoglobin, bilirubin, and carotenoids (Gupta & Sharma, 2019). Constitutive skin colour is determined by the genetic information which codes for the levels, types, and distribution of skin pigments (Sturm, 2009). In addition, the regulatory activity by cutaneous and follicular melanocytes also plays a significant role in determining skin colour (Yamaguchi et al., 2007). Whilst, facultative skin colour is an increment of skin pigment resulted from environmental (UV light) or hormonal factors (Gupta & Sharma, 2019).

Figure 2.7: Varieties of the skin colour. Photo sourced from Gupta and Sharma (2019).

Skin phototyping is a skin classification system based on the tendency of skin to experience sunburn and the ability to tan after expose to direct sunlight (Fitzpatrick, 1988). The Fitzpatrick system is commonly used to determine skin phototyping (Gupta & Sharma, 2019). This system was introduced by Thomas B. Fitzpatrick (1919–2004) on his outdoor sunscreen study at Brisbane, Australia in 1972. The skin reactivity post-sun exposure of the Australian citizens initially was classified into three groups (Group I, II, and III). Group I was for those who sunburn at ease without tan at all. Group II was for those who experience sunburn easily and tan with difficulty. Group III was for those who experience sunburn moderately, instant pigment darkening reaction, and tan at average after expose to the sun for 60 minutes at midday (Pathak, 2004). After some time, skin type IV was identified as having white skin that tan more than average, but seldom experienced burn after exposure to sunlight for an hour or less (Fitzpatrick, 1988). The development of the Fitzpatrick system later takes into account several other factors like tanning patterns, the response of skin to sunlight, and genetic predisposition (Gupta & Sharma, 2019). The examples of skin colour according to the Fitzpatrick system is presented in Figure 2.8.
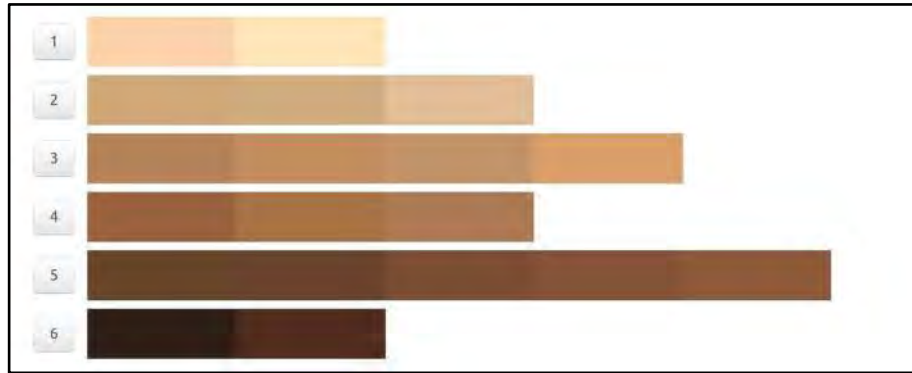
Figure 2.8: Colour of the skin based on colour bar survey item following Fitzpatrick skin classification. The colour bar was compared to the skin tone on the inside part of upper arm. Photo sourced from Ho and Robinson (2015).

Different skin phototypes require different sun protection factors (SPF) to prevent the skin from experiencing tanning and sunburn. SPF is defined as the UV energy required to produce a minimal erythemal dose (MED) in protected skin, divided by the UV energy required to produce a MED in unprotected skin (Kaur & Saraf, 2010). A lighter skin from skin type I, and II need higher SPF values (≥ 20) while darker skin type V and VI require lower SPF values (≤ 10). The updated list of skin phototyping using the Fitzpatrick system together with recommended SPF values is listed in Table 2.1.

Table 2.1: Fitzpatrick classification of skin and recommended SPF. Adapted from Fonseca and Rafaela (2013) and Plensdorf and Martinez (2009).

Skin type	Skin colour	Characteristics	Recommended SPF
I	White; very fair; freckles	Always burns, never tans	> 40
II	White; fair	Usually burns, tans with difficulty	20–40
III	Cream white; fair	Sometimes mild burns, gradually tans	7–20
IV	Brown; typical Mediterranean skin	Rarely burns, tans with ease	6–15
V	Dark brown; Middle Eastern skin types	Very rarely burns, tans very easily	5–10
VI	Black	Never burns, tans very easily	4

2.2 Cosmeceutical

2.2.1 Overview of cosmeceutical

The word cosmetic is defined as a substance of diverse origin, scientifically compounded used to cleanse, alleviate skin troubles, cover up imperfections, and beautify (Patkar, 2008). The ancient science of cosmetology is believed to have originated in Egypt and India (Patkar, 2008). Examples of cosmetic substances used in ancient cultures include castor oil, beeswax, olive oil, and rose water (Charles Dorni et al., 2017). The increasing consumer awareness about healthcare and advanced scientific understanding about skin physiology lead to the innovation of cosmeceutical (Charles Dorni et al., 2017).

Cosmeceutical is an over-the-counter topical skincare product containing biologically active ingredients intended to enhance both the beauty and health of the skin (Tetali et al., 2020). The term "cosmeceutical" was coined in 1961 by Raymond Reed, a founding member of the United States Society of Cosmetic Chemists (Newburger, 2009). He interpreted cosmeceutical word in four complementary points: (1) A cosmeceutical is a scientifically designed product intended for external application to the human body; (2)

A cosmeceutical produces a useful, desired result; (3) A cosmeceutical has desirable aesthetic properties; (4) A cosmeceutical meets the rigid chemical, physical and medical standard (Charles Dorni et al., 2017).

Cosmeceuticals represent the hybrids of both drug and cosmetic products however, it does not include the intensive safety and efficacy regime as drugs (Pieroni et al., 2004; Tetali et al., 2020). The grey line between cosmetic and pharmaceutical products enable cosmeceuticals avoid the strict regulation of the Food and Drug Administration (FDA). The concentration of active ingredients incorporated in the cosmeceutical formulations is lesser than prescriptions therefore it is classified as cosmetics rather than drugs. The efficacy of cosmeceutical formulations is always tested using replicas of skin from silicone, followed by clinical trials that normally uses randomized, placebo-controlled trials or randomized, double-blind trials. Despite a cosmeceutical product undergoing non-intensive testing compared to a drug, patients with skin problems seem to always choose cosmeceuticals as their main option before consulting a dermatologist. As pointed out by Tetali et al. (2020), two of the main reasons for a consumer to opt for cosmeceuticals first before consulting a dermatologist (which will often end up in prescriptions) are, cosmeceuticals are easily accessible and the prices are often more affordable.

The cosmeceutical formulations exist in various types such as cream, lotions, and ointments (Alves et al., 2020). The medicinal properties of cosmeceutical include the treatment of acne, hyperpigmentation, aging, skin inflammation, wrinkle, scarring, and photoprotective activity which take place at the cellular level (Charles Dorni et al., 2017). Botanical extracts are very popular source for cosmeceutical ingredients as plants are rich in phytochemical components including essential oil, vitamin, phenylpropanoids and their derivatives, peptides, alkaloids, and terpenes (Marchev & Georgiev, 2020). The other sources for cosmeceutical ingredients are animal-based, marine-based, endogenous

agents, and inorganic compounds (Nguyen et al., 2020; Tetali et al., 2020). The examples of bioactive ingredients incorporated into cosmeceutical formulation are listed in Table 2.2.

Some of the active ingredients are effective when applied as a single therapy. For instance, Kwon et al. (2018) demonstrated that treatment using a cream containing retinaldehyde at 0.05% and 0.1% was shown to improve skin hydration and texture. However, some of the active ingredients work best when combining with more active ingredients. Moyal et al. (2007) have presented that the combination of vitamin C and E with ferulic acid enhanced the protective effect against UVA-induced erythema compared to the combination of Vitamin E and Vitamin C or Vitamin E and ferulic acid alone. The increasing efficacy for the formulation with more active ingredients is contributed by the additive and synergistic effects of these ingredients (Malakooti et al., 2020).

Table 2.2: Example of bioactive ingredients incorporated into cosmeceutical formulations (years 2009-2020).

Source	Bioactive component	Potential indication(s) on the skin	Reference(s)
Plants	α-tocopherol	Reduce post-surgical scar	Tetali et al. (2020)
	Ascorbic acid	Reduce fine lines, roughness, and pigmentation	Tetali et al. (2020); Sunder (2019)
	Mulberry extract	Reduce pigmentation	Glen Alvin et al. (2011)
	Niacinamide	Reduce wrinkles, roughness, UV-induced erythema, inflammation, and pigmentation	Kawada et al. (2009); Tetali et al. (2020)
	Retinaldehyde	Reduce wrinkles, roughness, and pigmentation. Improve hydration and brightness	Kwon et al. (2018); Tetali et al. (2020)
	Retinyl retinoate	Reduce wrinkles and roughness	Kim et al. (2010)
	Stem cell extracts	Skin rejuvenation	Tetali et al. (2020)
Animals	Bee venom	Treatment of acne, skin rejuvenation, and reduce pigmentation	Nguyen et al. (2020)
	Propolis	Treatment of acne and UV protection	Nguyen et al. (2020)
	Snail mucin	Skin rejuvenation and reduce pigmentation	Nguyen et al. (2020)
Marines	Microalgae	Skin rejuvenation, reduce pigmentation, and UV protection	Nguyen et al. (2020)
	Pearl powder	Skin rejuvenation, reduce pigmentation, and improve hydration	Nguyen et al. (2020)

Table 2.2, continued.

Source	Bioactive component	Potential indication(s) on the skin	Reference(s)
Endogenous agents	Alpha hydroxy acid	Reduce fine lines and wrinkles and improve hydration	Sunder (2019)
	Hyaluronic acid	Reduce wrinkles and improve hydration, firmness, and elasticity	Jegasothy et al. (2014)
	Tranexamic acid	Reduce pigmentation	Atefi et al. (2017); Chung et al. (2016)
Fungi/yeast derivatives	Azelaic acid	Treatment of papulopustular rosacea and acne	Draelos et al. (2015); Searle et al. (2022)
	Kojic acid	Reduce pigmentation	Tetali et al. (2020)
Minerals	Charcoal	Adsorb toxin from skin	Tetali et al. (2020)
	Gold	Skin rejuvenation, reduce pigmentation, and promote collagen and elastin production	Nguyen et al. (2020)

2.2.2 Encapsulation

Encapsulation which yields small particles comprising of active agents surrounded by a natural or synthetic polymeric membrane (Martins et al., 2014) has the potential of delivering active ingredients into the skin in a pain-free, safe, targeted, and effective manner. Encapsulation also protects fragrances or volatile compounds from evaporation, keeps the active ingredients from deterioration caused by moisture, light, and heat, and controls the release rate of active ingredients at the targeted site (Casanova & Santos, 2016). Examples of encapsulation techniques that have been reported in cosmeceutical applications are liposomes, chitosan nanoparticles, cyclodextrins, solid-lipid nanoparticles, vesicles, nanostructured lipid carriers, and emulsions (Ephrem et al., 2017).

In recent decades, the liposomal delivery system consisting of phospholipids bilayer membranes (Figure 2.9) has received considerable attention in cosmeceutical application (Deb et al., 2019; Liu & Park, 2009). The advantages of using liposomes as encapsulation materials are non-reactive, excreted easily from the body through a simple metabolic process, the ability to modify the surface properties and size, and low toxicity (Van Tran et al., 2019). Moreover, liposomes can encapsulate both hydrophilic and hydrophobic molecules due to their bilayer compositions. The hydrophilic molecules will be incorporated at the inner core which is surrounded by the hydrophilic head of the phospholipids whereas the hydrophobic molecules tend to remain around the hydrophobic portion of the phospholipids bilayer (Deb et al., 2019). The natural sources of phospholipid for large scale production are commonly egg yolk and soybean (Li et al., 2015). Liposomes are categorized into five types based on the size and bilayer numbers (Table 2.3 and Figure 2.10) (Van Tran et al., 2019). Conventional liposomes only contain phospholipids with or without cholesterol while the modification of liposomes includes additional skin penetration enhancers such as eucalyptol or oleic acid (Abd et al., 2016;

Maghraby et al., 2006). Further innovation has introduced transferosomes, ethosomes, and niosomes. Transferosomes are ultradeformable liposomes with the addition non-ionic surfactant as edge activator whereas ethosome also phospholipid vesicles which include ethanol to increase the elasticity. Niosomes are mainly comprised of non-ionic surfactants together with cholesterol and a small proportion of phospholipids (Abd et al., 2016; Maghraby et al., 2006).
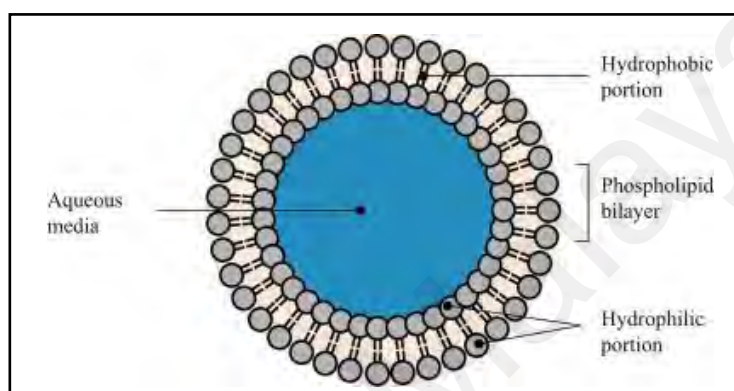
Figure 2.9: Structure of liposome. Photo sourced from Deb et al. (2019).

Table 2.3: Classification of liposomes based on size and lamellarity. Adapted from Van Tran et al. (2019).

Type of liposomes	Size (nm)
Small unilamellar vesicles (SUV) / nanoliposome	20–100
Large unilamellar vesicles (LUV)	> 100
Giant unilamellar vesicles (GUV)	> 1000
Oligolamellar vesicles (OLV)	100–1000
Multilamellar vesicles (MLV)	> 500
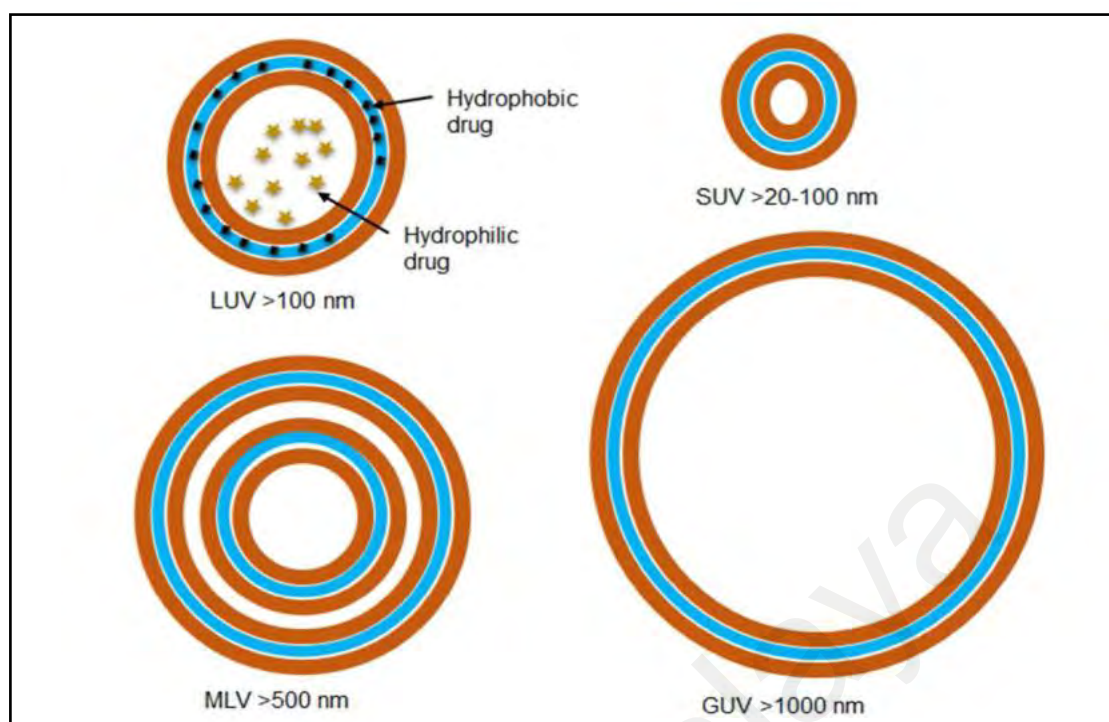
Figure 2.10: Different liposomes types based on size and lamellarity. Photo sourced from Pattni et al. (2015). Copyright 2015, American Chemical Society.

In order to enhance the cosmeceutical value, active ingredients such as arbutin (Wen et al., 2006), azelaic acid (Esposito et al., 2004), resveratrol (Caddeo et al., 2008), tretinoin (Sinico et al., 2005), and linoleic acid (Shigeta et al., 2004) have been reported to be successfully incorporated into the liposomes. Furthermore, some of the cosmeceuticals that are actively incorporated with liposomal delivery systems have been patented such as vitamin A derivatives (Aust et al., 2001), hydroquinone, kojic acid, and mulberry extract (Meybeck & Dumas, 1992), and ascorbic acid (Ephrem et al., 2017).

2.3   Melanogenesis and hyperpigmentation

2.3.1   Overview of melanogenesis

Melanogenesis is a process of synthesizing the skin pigment (melanin) in highly specialized cells called melanocytes. In the skin, melanocytes are located in the stratum basal of the epidermis, connected to keratinocytes through its dendrites. Melanocytes are distributed regularly among basal keratinocytes at the ratio of one melanocyte to 4–10 basal keratinocytes. The connection between melanocytes and keratinocytes enables the melanocytes to transfer the melanin to keratinocytes and this association determines skin colour (Tsatmali et al., 2002). The density of melanocytes reaches 500–2000 cells per mm of the cutaneous surface with regional variation (Kanitakis, 2002). Melanin also functions to protect the skin from the damaging effect of UV light by scavenging the radicals generated in the skin upon exposure to sunlight (Parvez et al., 2006). Melanin synthesized by melanocytes has two variations: brown-black eumelanin and yellow-red pheomelanin. Eumelanin is dominant in dark skin individuals while phaeomelanin is dominant in red hair and fair skin individual with skin types I and II (Fitzpatrick classification of skin, Table 2.1) (Thody et al., 1991).

In melanocytes, melanogenesis takes place in special organelles called melanosomes (Slominski et al., 2004). Melanogenesis involves enzymatic and chemical reactions. The first step is the rate-limiting step which involves the hydroxylation of tyrosine into L-3,4-dihydroxyphenylalanine (L-DOPA), followed by oxidation to dopaquinone by copper-containing enzyme, tyrosinase. Dopaquinone spontaneously cyclizes to form an orange intermediate of dopachrome if intramelanosomal cysteine is depleted (Yamaguchi et al., 2007). The spontaneous removal of the carboxylic acid chain from dopachrome generates 6-dihydroxyindole (DHI) which rapidly oxidize and polymerizes to form eumelanin. In the presence of dopachrome tautomerase (DCT) (also known as tyrosinase related protein-2 (TRP-2)), dopachrome will then be tautomerized without losing its carboxylic

acid group to form DHI-2-carboxylic acid (DHICA). DHICA will be oxidized to form indole-2-carboxylic acid-5,6-quinone (ICAQ) intermediate in the presence of tyrosinase related protein-1 (TRP-1). Subsequently, eumelanin is formed from DHICA or ICAQ intermediates. In the presence of amino acid cysteine or glutathione, dopaquinone will be converted into 5-S-cysteinyldopa (5SCD) and 2-S-cysteinyldopa (2SCD). These intermediates will be converted into 5-hydroxy-1,4-benzothiazinylalanine (HBTA) and finally formed pheomelanin by polymerization process (Figure 2.11) (Bino et al., 2018; Chang, 2009; Halaban et al., 2002).

In the process of transferring melanin to the neighbouring keratinocytes, the melanin granules in melanosomes are departed from the perinuclear zone to the tips of melanocytes dendrites through microtubules (Ali et al., 2015). Kinesin, dynein, GTPase (ras related protein Rab27a) together with its effector protein melanophilin, and myosin-Va are examples of proteins involved in the transport of melanosomes to the keratinocytes by tethering to the peripheral actin network (Hara et al., 2000; Hume et al., 2002).
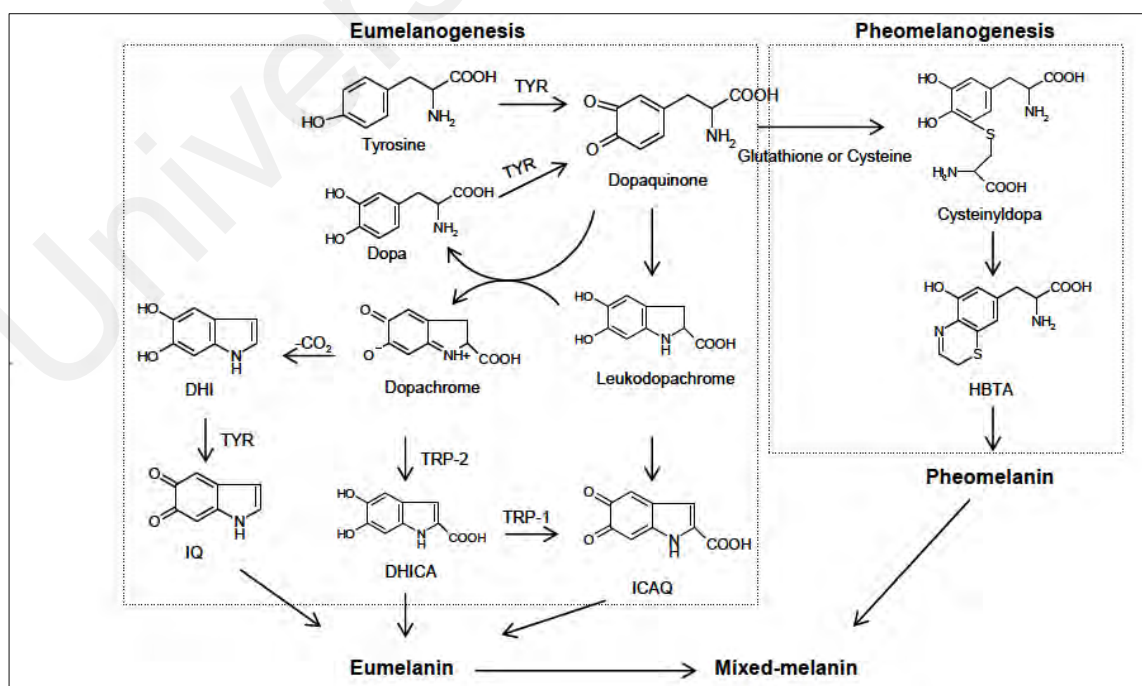
Figure 2.11: Biosynthesis of melanin. TYR: tyrosinase; IQ: indole-5,6-quinone. Photo sourced from Chang (2009).

2.3.2 Regulation of melanogenesis

At the cellular level, melanogenesis is regulated by controlling melanosome production with varying sizes, numbers, and densities while the regulation of melanogenesis at the subcellular level involves the regulation of gene expression of melanogenesis-related proteins and signaling pathways (Chang, 2012). Hormones, growth factors, interferons, interleukins, and prostaglandins play a crucial role to initiate the signaling pathways as well as determining the quality and quantity of synthesized melanin (Chang, 2012). The cAMP-dependent protein kinase A (PKA), Wnt/β-catenin, extracellular signal-regulated kinase (ERK), and nitric oxide (NO) signaling pathways are four common signaling pathways involved in melanogenesis regulation in melanocytes (Figure 2.12) (Pillaiyar et al., 2017a). These signaling pathways involve the regulation of microphthalmia-associated transcription factor (MITF) expression. MITF protein regulates the expression of the melanogenesis-related genes which including *Tyr* (tyrosinase), *Tyrp1* (TYRP1), and *Dct* (DCT) by binding to the M-box (AGTCATGTGCT) or E-box (CATGTG) motifs (Sun et al., 2020). As a master regulator of melanogenesis, the expression of MITF protein is regulated transcriptionally and post-translationally. At transcription level, MITF is regulated by transcription factor MITF itself, one cut domain 2 (ONECUT-2), MAPK pathway (Hsiao & Fisher, 2014), cAMP-responsive element binding protein (CREB) (Price et al., 1998), SRY (sex-determining region Y)-box 9 (SOX9) (Lee et al., 2016), SRY (sex-determining region Y)-box 10 (SOX10), paired box gene 3 (PAX3) (Bondurand et al., 2000), and lymphoid enhancer-binding factor 1/T-cell factor (LEF1/TCF) (Saito et al., 2002). The post-translational modification of MITF includes phosphorylation (Mansky et al., 2002), sumoylation (Murakami & Arnheiter, 2005), and ubiquitination (Wu et al., 2000).

Regulation of melanogenesis by alpha melanocyte stimulating hormone (α-MSH) takes place through the cAMP-dependent pathway. The binding of α-MSH to melanocortin 1 receptor (MC1R) located on the membrane of melanocytes will activate the G-protein-coupled receptor (GPCR). Activated GPCR will activate adenylate cyclase to produce cAMP as intracellular second messenger cAMP which to amplify the signal and activate PKA. PKA will migrate into the nucleus and bind to CREB. The binding of PKA with CREB at a specific CREB-binding element will activate the expression of MITF. The expression of MITF will in turn activate the expression of melanogenesis-related proteins (Busca & Ballotti, 2000).

Activation of the Wnt pathway will deactivate glycogen synthase kinase-3β (GSK-3β). Deactivation of GSK-3β will inhibit the phosphorylation of β-catenin and lead to β-catenin accumulation in the cytoplasm. β-catenin will enter the nucleus, form a complex with both TCF and LEF to up-regulate the expression of the MITF (Bellei et al., 2012).

Upon activation of the ERK pathway, MITF will be phosphorylated at Ser73 which leading to MITF ubiquitination and proteasomal degradation. ERK pathway regulates melanogenesis by degrading MITF, thus inhibit the melanogenesis process (Kim et al., 2003). In contrast, activation of ERK will in turn phosphorylate CREB. Phosphorylated CREB will bind to the MITF promoter region and upregulate MITF expression. The activation of p38 leads to two diverse effects either inducing (Kim et al., 2015) or inhibiting melanin production (Ko et al., 2019; Ko et al., 2014).

In UV-induced melanogenesis, the NO signaling pathway plays a crucial role in regulating melanogenesis. In response to UVA and UVB radiation, keratinocytes which is known as the neighbouring cells of melanocytes will secrete NO (Roméro-Graillet et al., 1997). NO activates guanylyl cyclase, a heme-containing protein that induces the production of cyclic guanosine 3',5'-monophosphate (cGMP). The induction of cGMP

promotes the expression of MITF and the melanogenesis process in melanocytes (Pillaiyar et al., 2017a).

Phosphatidylinositol 3-kinase (PI3K)/Akt signaling pathway regulates melanogenesis without upregulating the MITF expression. This pathway involved the inactivation of PI3K by cAMP. The inactivation of PI3K will inhibit Akt phosphorylation and its activity. The inhibition of Akt decreased the phosphorylation of GSK-3β and stimulated its activity. Activation of GSK-3β by cAMP facilitates the binding of MITF to the tyrosinase promoter, leading to the activation of transcription of tyrosinase-related genes and stimulation of melanogenesis (Khaled et al., 2002).
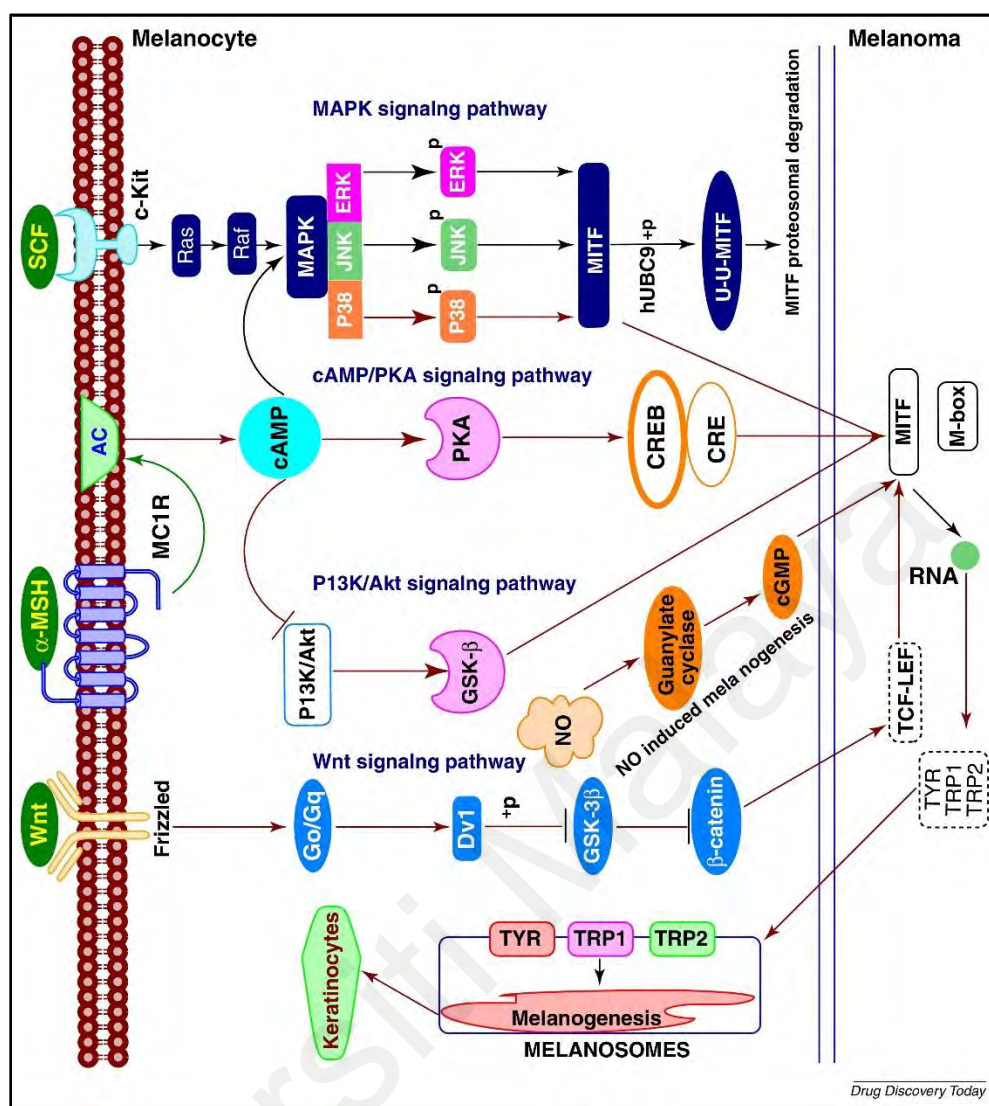
Figure 2.12: Regulation of melanogenesis through main signaling pathways. Photo sourced from Pillaiyar et al. (2017a).

2.3.3 Skin problems related to hyperpigmentation

Hyperpigmentation is a darkening of the skin due to the excessive deposition of melanin pigment at the epidermis or/and dermis layer and such condition negatively affects the aesthetics as well as the quality of life (Ali et al., 2015; Kaufman et al., 2018). Several factors overstimulate melanogenesis in the skin such as autoimmune conditions, overexposure to UV radiations, genetic factors, hormonal changes, hormonal therapy, medications, drug reactions, and frequent rubbing of the skin (Ali et al., 2015). Examples of hyperpigmentation-related disorders are postinflammatory hyperpigmentation,

melasma, solar lentigines, and ephelides (Pandya & Guevara, 2000; Plensdorf & Martinez, 2009).

The pattern of hyperpigmented skin varies for different disorders. Postinflammatory hyperpigmentation (Figure 2.13) is an acquired hypermelanosis characterized by a darkening of the skin in the area of previous injury or inflammation (Davis & Callender, 2010). The melanocytes are believed to respond to cytokines, chemokines, ROS, other inflammatory mediators leading to melanin synthesis and distribution of melanin to neighbouring keratinocytes (Callender et al., 2011). The deposition of melanin at the epidermis (epidermal postinflammatory hyperpigmentation) causes the skin to become tan to dark brown lesions (Kaufman et al., 2018). Dermal postinflammatory hyperpigmentation is characterized by darker brown or blue/gray discoloration of the skin (Kaufman et al., 2018). The accumulation of melanophages at the upper dermis which phagocytized the destructed basal keratinocytes which contain a high concentration of melanin causes such intense pigmentation to appear on the skin (Callender et al., 2011). Postinflammatory hyperpigmentation can occur in any age, skin type, and gender (Callender et al., 2011). However, this disorder is more common in skin type III–VI (Fitzpatrick classification of skin, Table 2.1). In addition, the visibility of hypermelanosis tends to be more clinically apparent and lasts longer in darkly pigmented skin (Taylor et al., 2009). The proposed reason for this condition could be due to the ability of inflammation to elicit intense responses to hyper-reactive melanocytes in this skin type (Callender et al., 2011). The etiologies that lead to postinflammatory hyperpigmentation includes immunologic skin conditions (lupus erythematosus), allergic/hypersensitivity (contact dermatitis and arthropod bite), inflammatory skin conditions (psoriasis, lichen planus, and acne), viral infection (herpes simplex), bacterial or fungal infection (dermatophytosis), physical injury, drug-induced, dermatologic procedures (cryotherapy,

dermabrasion, lasers, chemical peels, and intense pulse light), and neoplastic (Kaufman et al., 2018).

Figure 2.13: Appearance of postinflammatory hyperpigmentation due to acne. Photo sourced from Sharad (2013).

Melasma is an acquired hypermelanosis involving sun-exposed skin, especially on the cheek, nose, forehead, chin, and upper lip where the affected skin appears as irregular non-scaling macules with light to dark brown in colour (Figure 2.14) (Pandya & Guevara, 2000; Rajanala et al., 2019; Victor et al., 2004). In addition to pigmentation, the pathologic findings of melasma include solar elastosis (an accumulation of abnormal elastic tissues in the dermis as a result of prolonged sun exposure), disrupted basement membranes, and an increase of vascularity and mast cells in the dermis (Kwon et al., 2016). The occurrence of melasma is more common in women with 90% of reported cases are this gender (Rendon et al., 2006). However, the occurrence of melasma in men is not uncommon (Sarkar et al., 2018). Early studies classified melasma as either

epidermal, dermal, and mixed type. The classification was made based on the location of melanin accumulated in the skin. In the epidermal type, melanin is deposited in the basal and superbasal of the epidermis whereas, for the dermal type, the melanin-laden macrophages in a perivascular location are resided in the superficial and mid-dermis (Victor et al., 2004). Later, the general pathophysiology of melasma was proposed to be a mixed type only (Passeron & Picardo, 2018). In women, melasma is associated with pregnancy, oral contraceptives, or anticonvulsants. Melasma is more prominent in Asian, Middle Eastern, or South American women with skin type IV–VI (Fitzpatrick classification of skin, Table 2.1) (Pandya & Guevara, 2000; Plensdorf & Martinez, 2009). Recently, melasma has been shown to be a hallmark of a skin photoaging disorder affecting genetically predisposed individuals (Passeron & Picardo, 2018).

Figure 2.14: Appearance of melasma on the forehead. Photo sourced from Pandya and Guevara (2000).

Solar lentigines are acquired pigmented spots on sun-exposed skin such as on the face, forearms, hands, chest, back, and shins (Figure 2.15). They are identified by the appearance of well-circumscribed hyperpigmented lesions (light yellow to dark brown) with size ranges from 1–3 cm (Plensdorf & Martinez, 2009). The other names that commonly refer to solar lentigines are age spots and liver spots. Solar lentigines are prominent with increasing age and these lesions are mainly associated with chronic or

intermittent sun exposure which subsequently increased the proliferation of basal melanocytes (Bastiaens et al., 2004; Plensdorf & Martinez, 2009). Over time, these lesions will increase in size to larger macules or patches (Ortonne et al., 2006). These lesions are also known as the hallmark for photoaged skin (Nakamura et al., 2015). White or Asian persons with skin types I and III (Fitzpatrick classification of skin, Table 2.1) are the most common to develop this disorder (Plensdorf & Martinez, 2009). However, a darker skin type (type IV, Fitzpatrick classification of skin, Table 2.1) is also prone to this sun-induced skin disorder (Praetorius et al., 2014).
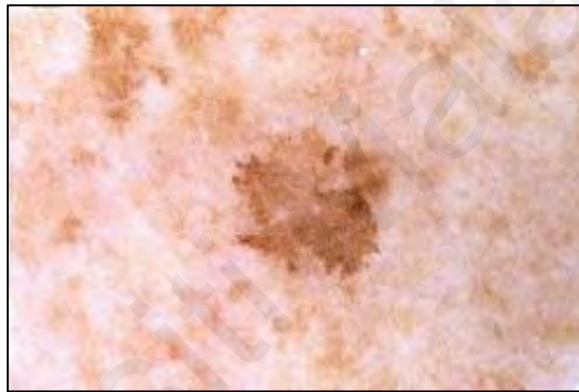
Figure 2.15: Appearance of solar lentigines. Photo sourced from Praetorius et al. (2014).

Ephelides or freckles are small (1–2 mm), sharply define macular lesions of uniform colour (from red to tan to light brown) as a result of increased melanin synthesis (Figure 2.16) (Plensdorf & Martinez, 2009). The features of melanocytes in ephelides are larger in size, a higher number of melanosomes, and numerous dendrites compared to normal melanocytes (Praetorius et al., 2014). Ephelides can be found on the face, neck, chest, and arms with various numbers from a few to hundreds. The disorder emerges post-sun exposure and is largely determined by genetic factors (Plensdorf & Martinez, 2009; Praetorius et al., 2014). The presence of *MC1R* genes variant, *IRF4*, *ASIP*, *TYR*, and *BNC2* are important in the formation of ephelides (Bastiaens et al., 2004; Praetorius et

al., 2014). They are asymptomatic and the onset of disorder commonly happens during childhood. Ephelides are more prominent in an individual with skin types I and II (Fitzpatrick classification of skin, Table 2.1) and tend to fade away during the winter season (Plensdorf & Martinez, 2009). In addition, Asians also have been reported to develop such disorders which partially fade away with age (Jang et al., 2000). Ephelides are considered fashionable in Western culture while Asians consider ephelides as cosmetic disfiguration that need to be eradicated (Jang et al., 2000; Praetorius et al., 2014).

Figure 2.16: Appearance of freckles in a young boy. Photo sourced from Praetorius et al. (2014).

2.4   UV radiation and adverse effect on the skin

UV light has three main regions, UVC (from 100 to 290 nm), UVB (from 290 to 320 nm), and UVA (from 320 to 400 nm) (Walters et al., 1997). The ozone layer absorbs UV radiation up to 310 nm. Hence, UVC which characterize as the most dangerous light with strong mutagenicity is being absorbed by the ozone layer before reaching the earth's surface (Figure 2.17). In addition to UVC, the ozone layer also effectively absorbs UVB radiation up to 95%. However, the deterioration of the ozone layer increases the intensity of UVB that reaches the ground (Svobodova et al., 2006).

UVB will penetrate the epidermis layer of the skin (Figure 2.17) and is mainly responsible for the manifestation of sunburn, photodamage, and photoaging. In addition, UVB induced delayed tanning which involving the synthesis of melanin that develops several days after UVB exposure and persists for weeks (Moan et al., 2012). Once UVB reaches the epidermis layer, it is absorbed by deoxyribonucleic acid (DNA), aromatic amino acids of proteins, reduced nicotinamide adenine dinucleotide (NADH), reduced nicotinamide adenine dinucleotide phosphate (NADPH), flavins, porphyrins, lipids, carotenoids, quinones, eu- or pheomelanin, and urocanic acid (Kammeyer & Luiten, 2015). The absorption of UVB radiation by DNA causing cumulative DNA damage by directly interact with DNA to produce thymine dimer photoproduct (Gu et al., 2020). UVB also being absorbed by ribonucleic acid (RNA), resulting in mutated messenger RNA (mRNA). The accumulation of unrepaired mutation leads to the production of dysfunctional protein and subsequently causes cell arrest and apoptosis. Besides that, the unrepaired mutations can twist apoptotic programs into malignancies on the skin (Kammeyer & Luiten, 2015).

UVA is a weaker mutagen but, has a stronger penetration ability than UVB which can penetrate both epidermis and dermis layers (Figure 2.17). UVA affects the deeper layer of the dermis and even subcutaneous tissue area, whereby UVA causes damage to the extracellular matrix, leading to photoaging. The deteriorative effect of UVA will be visible on the skin after chronic exposure, even at low intensity (Gu et al., 2020; Kammeyer & Luiten, 2015; Latha et al., 2013). In addition, UVA is 1,000 times more effective in oxidizing the melanin in the epidermis, subsequently causing the immediate tanning effect (Svobodova et al., 2006).
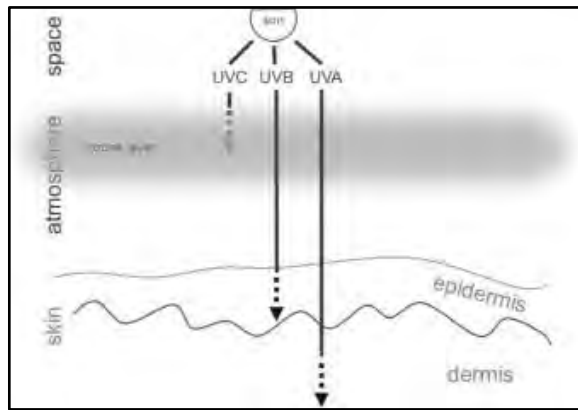
Figure 2.17: Pathway of solar UV radiation through the atmosphere into the skin. Photo sourced from Kammeyer and Luiten (2015).

Exposure to UVB and UVA radiations produces a higher concentration of ROS in the skin through the indirect way. This event occurs when the activated photosensitizer on the skin reacts with oxygen resulting generation of ROS including $O_2^{-\bullet}$ and singlet oxygen ($^1O_2$). Superoxide dismutase will then convert $O_2^{-\bullet}$ into H_2O_2. H_2O_2 can cross cell membrane easily and a chemical reaction with transitional ferrous ion (Fe^{2+}) will produce highly toxic hydroxyl radical ($\bullet OH$). Therefore, both $^1O_2$ and $\bullet OH$ will initiate lipid peroxidation on the cell membrane leading to cellular damage (Wlaschek et al., 2001). In addition to cellular damage, ROS accumulation causes keratinocytes to release several factors that induce massive melanin production in melanocytes which leads to hyperpigmentation (Maddodi et al., 2012).

2.5   The genus *Artocarpus*

Species classified in the genus *Artocarpus* are evergreen or deciduous and monoecious with sizes ranging from small to large trees. The special characteristic of this genus is all parts of the tree contain white latex (Jagtap & Bapat, 2010). Besides having appreciable importance as a source of edible fruits (Li et al., 2010), these species are a good source of wood for constructing buildings and in making furniture (Jagtap & Bapat, 2010).

Based on the literature search (Table 2.4), the secondary metabolites from *Artocarpus* species exhibited various pharmacological and biological properties including anti-cancer, anti-viral, anti-allergic, anti-tyrosinase, anti-inflammatory, and anti-microbial activities. These biological activities of *Artocarpus* species somewhat validate the traditional uses of the genus as a remedy for skin ailments, dermatitis, malarial fever, diarrhea, wound healing, and tuberculosis (Jagtap & Bapat, 2010).

Table 2.4: Reported biological activities of *Artocarpus* species (years 2006-2021).

Species	Local name	Part(s)	Bioactive component(s)	Biological activity	Reference(s)
A. altilis	Sukun	Fruit pulp	Quercetin	Anti-cancer activity by inducing apoptosis and arrested the cells at G0/G1, S, and G2/M in human lung carcinoma cells (A549).	Jalal et al. (2019)
		Heartwood	Artocarpin-enriched extract	UVB protection activity by stimulating matrix metalloproteinase-1 [in fibroblast], tumor necrosis factor-alpha (TNF-α) and interleukin-6 [in keratinocytes] production	Tiraravesit et al. (2015)
		Heartwood and cortex	Artocarpin	Anti-tyrosinase activity and reduced melanin production in B16F10 melanoma cells	Lan et al. (2013)
A. anisophyllus	Keledang babi/mentawa	Leaf and heartwood	Pyranocycloartobilo-xanthone A	Anti-tyrosinase activity (mushroom tyrosinase)	Lathiff et al. (2015)
A. communis	Sukun	–	Artocarpin	Wound healing activity as observed from the increasing level of myofibroblast (*in vitro*) and wound contraction in C57B/L mice (*in vivo*). *In vitro* study using human primary fibroblast cells (GM05386), human oral keratinocytes 1 (OK1), and human umbilical vein endothelial cells (HUVECs) demonstrated an increase in collagen synthesis, cell proliferation, and migration activities	Yeh et al. (2017), Berg et al. (2006)

Table 2.4, continued.

Species	Local name	Part(s)	Bioactive component(s)	Biological activity	Reference(s)
A. elasticus	Terap nasi	Root bark	Artonin E	Anti-cancer activity *via* apoptosis in MDA-MB 231 triple negative breast cancer cells	Etti et al. (2017)
		Wood	Artelastin	Anti-inflammatory activity by inhibition of NO production.	Cerqueira et al. (2008)
A. heterophyllus	Nangka	-	Moracin C	Anti-inflammatory activity by inhibiting mRNA and protein expression of inducible nitric oxide (iNOS), cyclooxygenase-2, pro-inflammatory cytokines and TNF-α	Yao et al. (2016)
		Fruit	Oxyresveratrol	Anti-tyrosinase activity (mushroom and cellular tyrosinase) and reduced melanin production in B16F10 melanoma cells (*in vitro*) and in *Caenorhabditis elegans* (*in vivo*)	Li et al. (2020)
		Fruit	Artocarheterones A–E, peucenin, peucenin-7-methylether, cnidimol A, cnidimol D, melanochromone, greveichromenol, and ficuformodiol B	Anti-viral activity by suppressing the cytopathic activity of human immunodeficiency virus (HIV-1) through the inhibition of HIV-1 reverse transcriptase enzyme activity	Fu et al. (2020)

Species	Local name	Part(s)	Bioactive component(s)	Biological activity	Reference(s)
		Leaf	2"-O-β-ᴅ-xylosylvitexin	Antioxidant activity in chemical [DPPH•, oxygen radical absorbance capacity (ORAC) and •OH scavenging activities] and cellular assays (Human HepG2 heptoma cancer cells)	Wen et al. (2017)
		Sapwood	3-prenyl luteolin	Anti-tyrosinase activity (mushroom tyrosinase) and reduced melanin production in B16F10 melanoma cells	Arung et al. (2010)
		Sapwood	Artocarpanone	Anti-tyrosinase activity (mushroom tyrosinase) and reduced melanin production in B16F10 melanoma cells	Arung et al. (2006)
		Seed	Seed oil	Antioxidant activity in chemical assays [DPPH•, ferric reducing antioxidant power (FRAP), reducing power assays and •OH scavenging activity]	Nagala et al. (2013)
		Skin, flesh and seed	Ethanolic and aqueous extracts	Anti-allergic activity by inhibiting β-hexosaminidase release in RBL-2H3 basophil cells	Tewtrakul et al. (2008)

Table 2.4, continued.

Species	Local name	Part(s)	Bioactive component(s)	Biological activity	Reference(s)
		Wood pulp	Artocarpin-rich wood extract	Anti-cancer activity by inhibiting cytochrome P450 CYP2C9 activity [*in vitro*, human], reduced tumor multiplicity [*in vivo*, C57BL/6 mice], and downregulated gene expression of pro-tumorigenic markers (*Pcna*, *Axin2*, *Vegf*, and *Myc*) and cytochrome P450 2C37 (*Cyp2c37*)	Morrison et al. (2021)
				Anti-inflammatory activity by reducing protein expression of proliferating cell nuclear antigen and gene expression of pro-inflammatory cytokines (*Il-6* and *Ifn-γ*)	
A. integer	Chempedak	Bark	Methoxycyclocommunol, heteroflavanone A, and cudraflavone C	Anti-inflammatory activity by inhibiting prostaglandin E_2 production in lipopolysaccharide-induced human whole blood using a radioimmunoassay method	Shah et al. (2016)
		Root	Artocarpanone	Anti-tyrosinase activity (mushroom tyrosinase)	Dej-adisai et al. (2014)
			Artocarpin and cudraflavone C	Antibacterial activity by inhibiting the growth of *Staphylococcus aureus*, *S. epidermidis* and *Propionibacterium acnes*	

Table 2.4, continued.

Species	Local name	Part(s)	Bioactive component(s)	Biological activity	Reference(s)
		Seed	Seed oil	Antioxidant activity in chemical assays (DPPH•, FRAP, reducing power assays and •OH scavenging activity)	Nagala et al. (2013)
A. kemando	Pudu	Fruit peel, flesh and seed	Methanolic extract	Antioxidant activity in chemical assays (DPPH•, FRAP and ABTS$^{+•}$ assays)	Bakar et al. (2015)
A. lakoocha	Tampang	Heartwood	Aqueous extract (oxyresveratrol)	Anti-tyrosinase activity (mushroom tyrosinase) and reduce melanin content *in vivo* using human volunteers	Tengamnuay et al. (2006), Sulaiman (2011)
A. lanceifolius	Keledang	Bark	Artoindonesianin Z-4, artoindonesianin Z-5, artonin E, artobiloxanthone and cycloartobiloxanthone	Cytotoxic against mouse luekemia P388 cells	Musthapa et al. (2009)
A. lowii	Miku	Leaf and heartwood	Flavonoids	Antibacterial activity by inhibiting the growth of gram positive (*S. aureus* and *Bacillus cereus*) and gram-negative bacteria (*Escherichia coli* and *Pseudomonas putida*)	Jamil et al. (2014)

41

Table 2.4, continued.

Species	Local name	Part(s)	Bioactive component(s)	Biological activity	Reference(s)
A. rigida	Temponek	Stem	Norartocarpetin, p-hydroxybenzoic acid and artocarmin G	Anti-tyrosinase activity (mushroom tyrosinase)	Nguyen et al. (2017), Sulaiman (2011)
A. rigidus	Temponek	Root bark	7-demethylartonol E, artonin F, cycloartobiloxanthone, artorigidusin, artonol B, and artoindonesianin C	Antibacterial activity by inhibiting the growth of *Mycobacterium tuberculosis*	Namdaung et al. (2006)
			7-demethylartonol E, artonin F, and cycloartobiloxanthone	Anti-parasitic activity by inhibiting the growth of *Plasmodium falciparum*	

2.5.1 The *A. altilis*

The *A. altilis* (synonyms: *A. communis* and *A. insicus*) is popularly known in Malaysia as "*sukun*" and commonly called as breadfruit tree in English due to the bread-like fruit texture (Lan et al., 2013). Breadfruit (Figure 2.18) can be roasted, baked, fried, or consumed directly. Besides that, breadfruit can be processed into snacks such as cookies and jelly (Lin et al., 2011). The tree can grow up to 35–40 m tall with buttresses, evergreen or deciduous. It has leafy twigs with slightly rough hairs at the joint (internodes). The leaves are coarse resembling leathery to papery texture (coriaceous to chartaceous) and covered with minutes hairs (Figure 2.19). The leaves are spirally arranged around the twigs with sizes range 20–100 cm length by 15–60 cm wide. Most leaves contain 1–5 pairs of lateral lobes or segments. Sometimes the lateral lobes can reach to 9 and up to 20 (Berg et al., 2006).

Figure 2.18: The tree of *A. altilis*. Photo by M. Sugumaran.

Figure 2.19: Leafy stem of *A. altilis*. Photo by M. Sugumaran.

Figure 2.20: Fruit of *A. altilis*.

2.5.2. The *A. heterophyllus*

The *A. heterophyllus* is commonly called as jackfruit in English and locally known as "*nangka*". The tree can grow up to 10–30 m tall, occasionally with short buttresses. The leaves are covered with minute white-creamy hairs and spirally arranged around the twigs (Figure 2.20). The leaves are somewhat leathery (subcoriaceous) and lobed (usually three lobed) when immature. The shape of the mature leaves are elliptic to somewhat narrower end at the base ((sub)obovate) with the size varies 4–15 cm length and 2–12 cm wide (Berg et al., 2006). The yield of *A. heterophyllus* fruits of a mature tree can range from 10–200 fruits. *A. heterophyllus* tree produces the largest fruit in the world as the weight of fruit can reach up to 45 kg (36" in length and 20" in diameter) (Baliga et al., 2011).

Figure 2.21: The tree of *A. heterophyllus* (red arrow). Photo by M. Sugumaran.

Figure 2.22: Leafy twigs of the *A. heterophyllus*. Photo by M. Sugumaran.

Figure 2.23: Fruit of *A. heterophyllus*. Photo by M. Sugumaran.

2.5.3   The *A. integer*

The *A. integer* (synonym: *A. champeden*) is locally called "*chempedak*". It is distributed through Thailand and Malesia which include Sumatra, Malay Peninsula, Borneo, Java, Celebes, Moluccas (Sula Islands, Ambon) and New Guinea (western). The tree can grow up to 30 m tall and evergreen. The leafy twigs are covered with fine hairs near the nodes and the leaves are spirally arranged (Figure 2.21). The leaves are subcoriaceous, covered with fine hairs and are lobed (usually three) when it is immature. The shape of the mature leaves are elliptic to (sub)obovate with the size varies 4–27 cm length by 1.5–12 cm wide (Berg et al., 2006). *A. integer* fruit (Figure 2.22) is similar with jackfruit, but the size is smaller and has softer flesh than jackfruit. The ripen flesh of *A. integer* can be eaten raw or as fritters (Buttara et al., 2014).

Figure 2.24: The tree of *A. integer*. Photo by M. Sugumaran.

Figure 2.25: Leafy branch of *A. integer.* Photo by M. Sugumaran.

Figure 2.26: Fruit of *A. integer.*

2.5.4   The *A. elasticus*

The *A. elasticus* (synonyms: *A. pubescens*, *A. blumei, A. kunstleri, A. scortechinii, A. corneri, A. jarrettiae*) is commonly called "*terap nasi*" in Malay (Figure 2.23). The tree is evergreen with buttresses and can reach up to 45–65 m tall. The leaves are spirally arranged, elliptic in shape (Figure 2.24) and range from being coriaceous to chartaceous in its texture. The size of leaves ranges from 13–60 cm length by 6–35 cm wide. The juvenile leaves have three to five lobes. The leaves are covered with very short fine hairs (Berg et al., 2006).
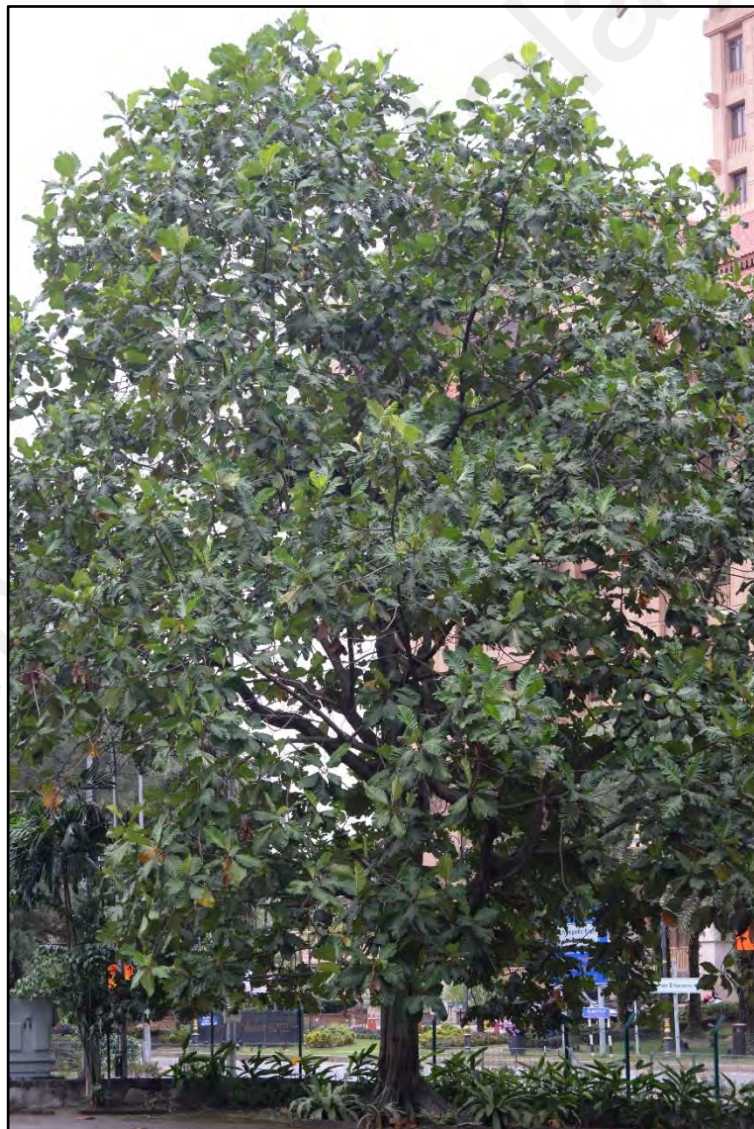
Figure 2.27: The tree of *A. elasticus*. Photo by M. Sugumaran.

Figure 2.28: Leafy twigs of *A. elasticus* with young fruit. Photo by M. Sugumaran.

Figure 2.29: Fruits of *A. elasticus*. Photo by M. Sugumaran.

2.5.5   The *A. rigidus*

The *A. rigidus* is distributed through Mynmar, Thailand, Sumatra, Peninsular Malaysia, Sabah, Java, and Lesser Sunda Islands. It is locally known as "*temponek*" (Figure 2.25) and can be found in evergreen forest at altitudes up to between 700 and 1,000 m above sea level. The tree is evergreen, buttressed and can reach up to 35 m tall. It has leafy twigs covered with thick and dense brown hairs. The hairy leaves are subcoriaceous, elliptic to (sub)obovate in its shape and are spirally arranged around the twig (Figure 2.26). The leaf size varies from 3–15 cm long and 1.5–15 cm wide and some leaves are lobed (Berg et al., 2006).

Figure 2.30: The tree of *A. rigidus*. Photo by M. Sugumaran.

Figure 2.31: Leafy branches of *A. rigidus*. Photo by M. Sugumaran.

Figure 2.32: Fruit of *A. rigidus*.

CHAPTER 3: MATERIALS AND METHODS

3.1 Chemicals and reagents

Kojic acid, tyrosinase from mushroom, dimethyl sulfoxide (DMSO), Dulbecco's Modified Eagle's Medium (DMEM), L-DOPA, phosphate buffered saline (PBS), fetal bovine serum (FBS), 4-(2-aminoethyl)benzenesulfonyl fluoride hydrochloride (AEBSF), α-melanocyte stimulating hormone (α-MSH), Triton X-100, penicillin-streptomycin, phenazine methosulfate (PMS), ABTS, DPPH, nitro blue tetrazolium (NBT), gallic acid, potassium peroxodisulfate, ascorbic acid, and NADH were acquired from Sigma-Aldrich Co. Louis, USA. The bicinchoninic acid protein assay kit was acquired from Thermo Fisher Scientific, USA. AlamarBlue® (Resazurin) was acquired from Bio-Rad Laboratories, Hercules, CA, USA. H_2O_2, chloroform, ethanol, hexanes, methanol and ether were acquired form Merck, Germany. ROS detection kit was acquired from Promokine, Heidelberg, Germany. The RNA isolation kit, microarray slides, and qPCR consumables were acquired from Agilent Tech. Inc., Santa Clara, CA, USA.

3.2 Plant materials and preparation of extracts

The location and date of sample collection of cultivated *A. altilis*, *A. heterophyllus*, *A. integer*, *A. elasticus*, and *A. rigidus* are shown in Table 3.1. All the plant materials were identified by Dr. Sugumaran Manickam, Rimba Ilmu Botanical Garden, Universiti Malaya Sustainability Development Centre, Level 6, Research and Innovation Management Complex, Universiti Malaya, Malaysia. Voucher specimens of the samples were deposited in the herbarium of the Institute of Biological Sciences, Faculty of Science, Universiti Malaya, Kuala Lumpur, Malaysia.

Briefly, the leaves and stem barks (Figure 3.1) of five *Artocarpus* species were air-dried at room temperature for five days while the peels (Figure 3.1) were freeze-dried to remove the water content. The dried plant materials were then ground into coarse powder (200 g) and extracted with ethanol (800 mL) for three days. The crude extracts were filtered, and then concentrated under vacuum at 40 °C using a rotary evaporator (BÜCHI Labortechnik AG, Switzerland) to obtain the ethanolic extracts. All the extracts were stored at −20 °C for less than two weeks prior to bioactivity evaluation.

Table 3.1: Sample collection of selected *Artocarpus* species.

Plant sample (Voucher specimen)	Part	Location of sample collection	Date of collection
A. altilis (KLU 49924)	Leaf	Rimba Ilmu Botanical Garden[a]	28th June 2018
	Stem bark		
	Peel	Local market[b]	30th July 2018
A. heterophyllus (KLU 49925)	Leaf	Rimba Ilmu Botanical Garden[a]	28th June 2018
	Stem bark		
	Peel	Local market[b]	30th July 2018
A. integer (KLU 49926)	Leaf	Rimba Ilmu Botanical Garden[a]	28th June 2018
	Stem bark		
	Peel	Local market[b]	30th July 2018
A. elasticus (KLU 49923)	Leaf	Rimba Ilmu Botanical Garden[a]	17th July 2018
	Stem bark		
	Peel		
A. rigidus (KLU 49922)	Leaf	Rimba Ilmu Botanical Garden[a]	17th July 2018
	Stem bark		
	Peel		

[a]Universiti Malaya Sustainability Development Centre, Level 6, Research and Innovation Management Complex, Universiti Malaya, Kuala Lumpur, Malaysia. [b]The sample was purchased from the local market of Petaling Jaya, Selangor, Malaysia.
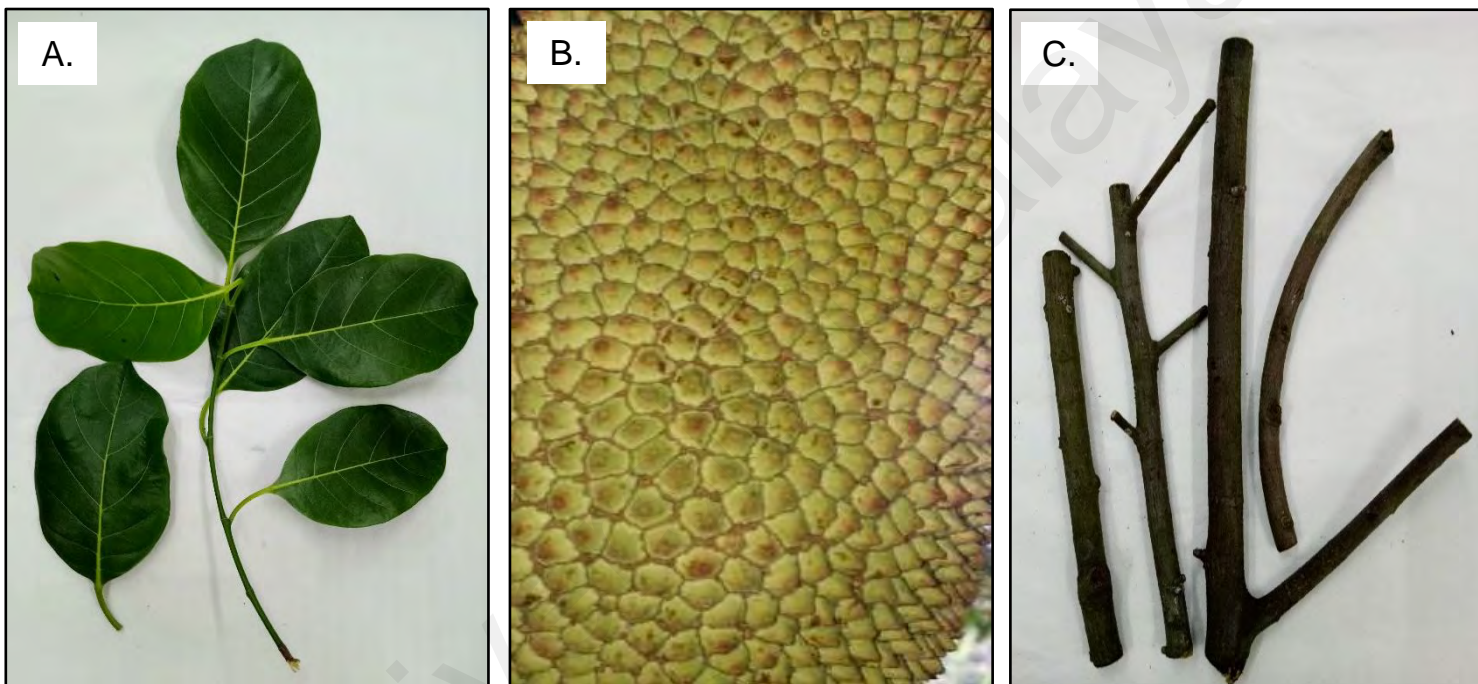
Figure 3.1: Parts of the samples used in the study. (A) Leaf. The individual leaf was taken apart from the stem. (B) Peel. The green-coloured skin was peeled from the fruit. (C) Stem bark. The bark was scraped off from the twigs, and the small stem was cut into small pieces.

3.3 Anti-melanogenesis activity evaluation

3.3.1 Mushroom tyrosinase assay

The non-cellular mushroom tyrosinase assay using L-DOPA as the substrate was carried out according to the method described by Alam et al. (2011) with minor modification on the incubation temperature. Into 96-well plate, 80 µL of sodium phosphate buffer (0.1 M, pH 6.8), 40 µL of *Artocarpus* extract (15.63–500.00 µg/mL), 40 µL of 60 units/mL tyrosinase in 0.1 M sodium phosphate buffer (pH 6.8), and 40 µL of 2.5 mM L-DOPA in 0.1 M sodium phosphate buffer (pH 6.8) were added into each well and incubated at room temperature in the dark for 10 minutes before the absorbance of dopachrome (product of L-DOPA) was measured at 475 nm using a Tecan M200 Infinite Pro microplate reader. Well containing all components except L-DOPA was employed as blank. For the untreated control, 40 µL of sodium phosphate buffer was added into the mixture instead of *Artocarpus* extracts. Kojic acid (15.63–500.00 µg/mL) was used as positive control. The percentage of tyrosinase inhibition was calculated using equation (3.1):

$$Tyrosinase\ inhibition\ (\%) = \left[\frac{(A_{control} - A_{sample})}{A_{control}}\right] \times 100\% \qquad (3.1)$$

Where, A_{sample} is the absorbance of mixture containing sample extract and $A_{control}$ is the absorbance from mixture containing buffer instead of sample extract.

3.3.2 Cell culture and cell viability assay

The B16F10 murine melanoma cells (CRL-6475™) were acquired from American Type Culture Collection (ATCC®, USA). The cells were cultured in DMEM supplemented with 10% FBS and 1% penicillin-streptomycin and incubated in an incubator (ESCO, Singapore) with a humidified atmosphere containing 5% carbon dioxide at 37 °C. The morphology of cells was observed regularly to avoid genetic drift.

The cells were detached using Accutase® and sub-cultured upon reaching 70–80% of confluency to maintain exponential growth of the cells.

The viability of B16F10 melanoma cells was performed using AlamarBlue® (Resazurin) assay as previously described by Beserra et al. (2018) with minor modifications on the number of seeded cells and the measured wavelength. Briefly, B16F10 melanoma cells were seeded at the density of 2×10^3 cells/well in 96-well plate and left to adhere overnight. Then, 200 μL of *Artocarpus* extract (1.56–50.00 μg/mL), *A. heterophyllus* stem bark sub-extracts (0.78–25.00 μg/mL), *A. heterophyllus* stem bark fractions, or H-3 liposomes (0.38–12.00 μg/mL) was added into each well and incubated for 48 hours. The wells containing cells and treatment-free media were regarded as the negative control. Kojic acid was used as positive control. The AlamarBlue® (20 μL) was added into all wells and further incubated for 6 hours at 37 °C. The absorbance of the reaction mixture in each well was measured using a Tecan M200 Infinite Pro microplate reader at 570 and 600 nm. Cells with culture medium without the addition of AlamarBlue® was used as background. The percentage difference of AlamarBlue® reduction was calculated using equation (3.2) which recommended by the manufacturer's:

$$Difference\ of\ AlamarBlue®reduction\ (\%) = \left\{\frac{[(O_2 \times A_1) - (O_1 \times A_2)]}{[(O_2 \times C_1) - (O_1 \times C_2)]}\right\} \times 100\% \quad (3.2)$$

Where, O_1 and O_2 are the constants representing the molar extinction coefficient of AlamarBlue® at 570 and 600 nm, respectively in oxidized state. A_1 and A_2 are the absorbance from the wells containing sample extract measured at 570 and 600 nm, respectively. C_1 and C_2 are the absorbance from well containing media without sample extract measured at 570 and 600 nm, respectively.

3.3.3 Intracellular melanin content assay

The intracellular melanin content was carried out as previously described by Saad et al. (2018) using B16F10 melanoma cells. Briefly, the cells were seeded with density 1×10^5/dish cells in 60-mm dish. After being incubated overnight, the cells were then exposed to varying concentrations of *Artocarpus* extract (1.56–50.00 μg/mL), *A. heterophyllus* stem bark sub-extracts (0.78–25.00 μg/mL), *A. heterophyllus* stem bark fractions, or H-3 liposomes (0.38–12.00 μg/mL) in the presence of α-MSH for 48 hours. Wells containing cells with media in the presence of α-MSH only were accounted as a negative control. After 48 hours, the cells were washed with PBS twice and the cell pellets were solubilized in 1 N sodium hydroxide at 80 °C for 1 hour. The melanin content was recorded by measuring the absorbance at 405 nm using Tecan M200 Infinite Pro Microplate Reader. Kojic acid was used as positive control. The percentage of melanin content was calculated using equation (3.3):

$$Melanin\ content\ (\%) = \left(\frac{A_{sample}}{A_{control}}\right) \times 100\% \tag{3.3}$$

Where, A_{sample} is the melanin content from the cells treated with sample extract and $A_{control}$ is the melanin content from the cell without sample extract.

3.3.4 Cellular tyrosinase assay

The cellular tyrosinase assay was performed based on the method previously described by Saad et al. (2018) using B16F10 melanoma cells. Briefly, the cells were seeded with density 1×10^5 cells/dish in 60-mm dish. After being incubated overnight, the cells were then exposed to varying concentrations of *Artocarpus heterophyllus* peel or stem bark extract (3.13–50.00 μg/mL) or H-3 (2.00–12.00 μg/mL) in the presence of α-MSH for 48 hours. Wells containing cells with media in the presence of α-MSH only were accounted as a negative control. The cells were washed with cold PBS twice and the detached cells were homogenized with cold lysis buffer consisting of 0.1 M sodium phosphate buffer at

pH 6.8, 1% Triton-X 100, and 0.2 mM of AEBSF for 30 minutes. The total protein was obtained by centrifugation at 13,000 rpm for 20 minutes at 4 °C. The quantification of protein was performed using a bicinchoninic acid protein assay kit. The protein (50 µg) was then mixed with 5 mM of L-DOPA (100 µL) in a 96-well plate and was incubated for 1 hour at 37 °C. Lastly, the dopachrome formation was measured based on the absorbance at 475 nm using Tecan M200 Infinite Pro Microplate Reader. Kojic acid was used as positive control. The percentage of tyrosinase activity was calculated as the following equation (3.4):

$$Tyrosinase\ activity\ (\%) = \left(\frac{A_{sample}}{A_{control}}\right) \times 100\% \tag{3.4}$$

Where, A_{sample} is the tyrosinase activity of total protein content with sample extract and $A_{control}$ is the tyrosinase activity of total protein content without sample extract.

3.4 Radical scavenging assays

3.4.1 DPPH radical scavenging assay

The scavenging activity of *Artocarpus* extracts on DPPH• was assessed according to the method described by Navanesan et al. (2015) with minor modification on the type of solvent used. Into 96-well plate, 50 µL of *Artocarpus* extract (15.63–500.00 µg/mL) was added into each well containing 150 µL DPPH• solution (0.3 mM). For the untreated control, 50 µL of methanol was added into DPPH• solution instead of the *Artocarpus* extract. After 30 minutes of incubation at room temperature in the dark, the absorbance of the reaction mixture in each well was measured at 515 nm using a Tecan M200 Infinite Pro microplate reader. Ascorbic acid (15.63–500.00 µg/mL) was used as positive control. The scavenging activity (%) of *Artocarpus* extracts on DPPH• was calculated according to equation (3.5):

$$Scavenging\ activity\ (\%) = \left[\frac{(A_{control} - A_{sample})}{A_{control}}\right] \times 100\% \tag{3.5}$$

Where, A_{sample} is the absorbance of mixture containing sample extract and $A_{control}$ is the absorbance of mixture containing methanol instead of the sample extract.

The antioxidant activity of the extracts was expressed in Antioxidant Activity Index (AAI), calculated according to equation (3.6) by Scherer and Godoy (2009):

$$AAI = \frac{Final\ cocentration\ of\ DPPH(mg/mL)}{IC_{50}(mg/mL)} \qquad (3.6)$$

3.4.2 ABTS cation radical scavenging assay

The ABTS$^{+\bullet}$ scavenging activity of *Artocarpus* extracts was performed using the method as described previously by Chatatikun and Chiabchalard (2017) with minor modifications on the ratio of ABTS$^{\bullet}$ and potassium peroxodisulfate and the type of solvent used in this experiment. The ABTS$^{+\bullet}$ solution was prepared by mixing an equal ratio of 7 mM ABTS$^{\bullet}$ and 2.45 mM of potassium peroxodisulfate and kept for 16–18 hours at room temperature in the dark. The ABTS$^{+\bullet}$ solution was diluted with methanol to an absorbance of 0.70 ± 0.02 at 734 nm. Each well was charged with 20 μL of *Artocarpus* extract (15.63–500.00 μg/mL) and 180 μL of the ABTS$^{+\bullet}$ solution. As for the untreated control, 20 μL of methanol was added to the ABTS$^{+\bullet}$ solution in place of the extract. The absorbance of the reaction mixture in each well was measured at 734 nm using a Tecan M200 Infinite Pro microplate reader after 20 minutes of incubation in the dark. Ascorbic acid (15.63–500.00 μg/mL) was used as positive control. The scavenging activity (%) of *Artocarpus* extracts on ABTS$^{+\bullet}$ was calculated according to the equation (3.5).

3.4.3 Superoxide anion radical scavenging assay

The $O_2^{-\bullet}$ scavenging activity of *Artocarpus* extracts was determined using NADH-PMS-NBT system according to the method by Vargas et al. (2016) with minor modifications on the NADH and NBT concentration. Tris-hydrochloric acid (HCl) buffer (16 mM, pH 8.0) was used as the solution for this assay. The reaction mixture which contained 40 µL of *Artocarpus* extract (15.63–500.00 µg/mL), 80 µL of NADH (195 µM), 80 µL of NBT (63 µM), and 80 µL of PMS (10 µM) was incubated at room temperature in the dark for 5 minutes before the absorbance of the reaction mixture in each well was measured at 560 nm using a Tecan M200 Infinite Pro microplate reader. For the untreated control, 40 µL of Tris-HCl buffer was added into the well instead of *Artocarpus* extract. Gallic acid (15.63–500.00 µg/mL) was used as positive control. The scavenging activity (%) of *Artocarpus* extracts on $O_2^{-\bullet}$ was calculated by using the equation (3.7):

$$Scavenging\ activity\ (\%) = \left[\frac{(A_{control} - A_{sample})}{A_{control}}\right] \times 100\% \qquad (3.7)$$

Where, A_{sample} is the absorbance of the mixture containing sample extract and $A_{control}$ is the absorbance of the mixture containing Tris-HCl buffer instead of sample extract.

3.5 UV absorption analysis

The assay was conducted based on the method described by Lee et al. (2013) and Kaur and Saraf (2010). Briefly, the *Artocarpus* extracts were dissolved in ethanol at the concentration of 1000 µg/mL and further diluted to 50 µg/mL. The UV absorption spectra (200–400 nm) of *Artocarpus* extracts were determined using a Shimadzu UV-1600 series spectrophotometer in 1 cm path length standard quartz cuvette. The *in vitro* Sun Protection Factor (SPF) of *Artocarpus* extracts was calculated according to equation (3.8) by observing the absorbance values within the range of 290–320 nm at 5 nm interval:

$$SPF_{spectrophotometric} = CF \times \sum_{290}^{320} EE(\lambda) \times I(\lambda) Abs(\lambda) \qquad (3.8)$$

Where, *CF* is correction factor (10); *EE (λ)* is erythemal effect spectrum; *I (λ)* is solar intensity spectrum; *Abs (λ)* is spectrometric absorbance values at wavelength *λ*. The values of *EE × I* are previously determined constants (Sayre et al., 1979).

3.6 Pesticide residue testing

The identification of pesticide components from *A. heterophyllus* stem bark extract (the bioactive extract in anti-melanogenesis activity) was performed at Alpha Testing Labs, Malaysia using Bruker Scion 456 Gas Chromatography (GC) with a triple quadrupole mass spectrometer (MS) equipped with MEGA-5MS fused silica capillary column (length: 30 m, inner diameter: 0.25 mm, film thickness: 0.25 mm). The carrier gas used was hydrogen with a flow rate of 1 mL/minute. The injection was conducted in splitless mode at a temperature of 250 °C. The initial GC column temperature was 50 °C and then was raised to 320 °C at the rate of 10 °C/minute. The MS was operated in the electron ionization mode at 70 Ev. The ion source temperature for MS was 250 °C with a transfer line temperature of 300 °C. The mass spectra scan mode was range from 45–450 m/z. The peaks were identified by comparing with their mass fragmentation pattern from the National Institute of Standards and Technology 17 library.

3.7 Proximate composition

The proximate analysis of *A. heterophyllus* stem bark extract was performed at Alpha Testing Labs, Malaysia. In accordance with Pearson (1976), the carbohydrate content was determined by differential summation of combined protein, fat, ash, crude fiber, and moisture. Fat content was determined using Soxhlet extraction, followed by gravimetric quantification of the extract and protein content was determined using the Kjeldahl method for total nitrogen multiply by a factor of 6.25.

3.8   Bioassay-guided fractionation

The overall bioassay-guided fractionation is demonstrated in Figure 3.2. Briefly, *A. heterophyllus* ethanolic stem bark extract (6.63 g) which was previously obtained (Section 3.2 and 4.1) was partitioned with water and chloroform to yield water (1.46 g) and chloroform (2.67 g) sub-extracts. The sub-extracts were then assessed with cell viability and melanin content assay (Section 3.3.2 and 3.3.3) using B16F10 melanoma cells at a treatment concentration of 0.78–25.00 µg/mL. The chloroform sub-extract, being the more active sub-extract was subjected to flash column chromatography (silica gel, 230–400 mesh) that eluted using hexanes with increasing chloroform gradient (10–80%), chloroform, chloroform with increasing methanol gradient (1–20%), followed by ethanol to furnish 12 semi-pure fractions (fractions A–L). The bioactivity assessments were conducted on these fractions by performing the above-mentioned assays at the same treatment concentration, and fraction H was then identified as the bioactive fraction. Fraction H (0.75 g) was therefore further purified using preparative radial chromatography (silica gel 60 PF_{254}) and eluted using hexanes with increasing ether gradient (60–90%), ether, ether with increasing methanol gradient (3–12%), followed by ethanol to yield five fractions (H-1–H-5). Aside from the cell viability and melanin content assays, additional assays were performed on these fractions at a treatment concentration of 0.38–12.00 µg/mL.
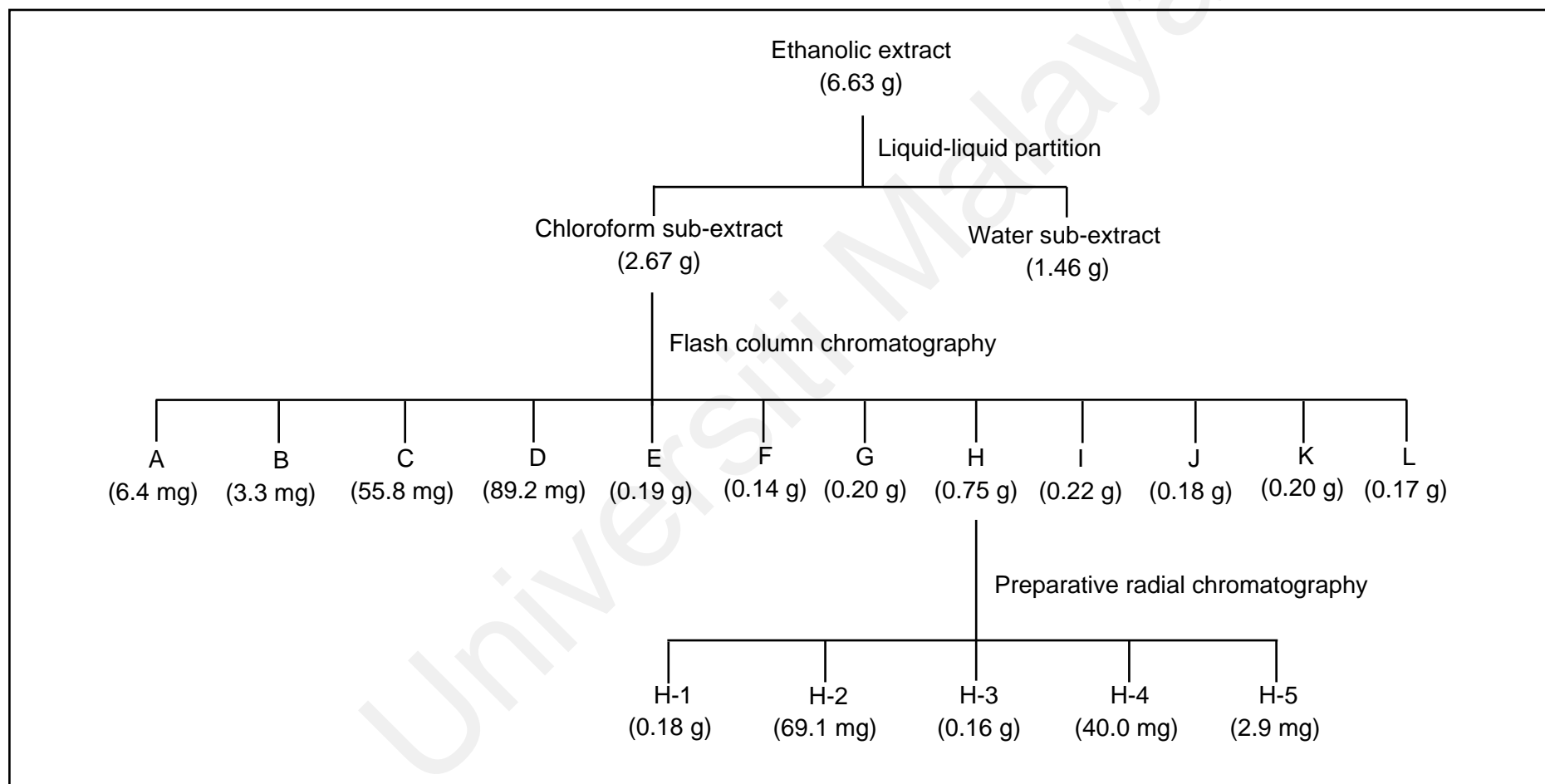
Figure 3.2: Fractionation of stem bark extract of *A. heterophyllus*.

3.9   Liquid chromatography-mass spectrometry (LCMS) analysis

The phytochemical analysis of H-3 was performed using Agilent 1290 Infinity LC system coupled to Agilent 6520 Accurate-Mass Quadrupole Time-of-Flight (Q-TOF) MS with dual electrospray ionization (ESI) source (Agilent Tech. Inc., CA, USA) which was done by Monash University Malaysia. The chromatographic separation was carried out using Agilent Eclipse XDB-C18 narrow-bore column (150mm x 2.1mm, 3.5 μm). The temperature of the column was set at 25 °C throughout the run. The sample was injected using an autosampler with an injection volume of 1 μL. The mobile phase consisted of 0.1% formic acid in water (A) and 0.1% formic acid in acetonitrile (B) with a flow rate of 0.5 mL/minute. The mass spectrometry was performed in the ESI positive mode under the following conditions: capillary voltage of 4000 V, fragmentor voltage of 125 V, skimmer of 65 V, gas temperature of 300 °C, drying gas flow rate 10 L/minute, and nebulizer gas pressure of 45 psi. The mass spectrum was scan from 100 *m/z* to 3200 *m/z*. The reference ions (121.0508 and 922.0097 *m/z*) used were used in order to verify the high resolution of mass spectrometry.

The data obtained were processed with Agilent MassHunter Qualitative Analysis B.07.00 software. The molecular feature extraction was set to a small molecule algorithm. Compound identification was performed by matching the obtained MS spectra with the Metlin Metabolite Personal Compound Database and Library. The molecular formula generator algorithm was used by the software when the compound does not appear in the database. Compound with score > 90% with deviation of ±2 in Metlin database or molecular formula generator algorithm was reported as the identified compound.

3.10   Measurement of intracellular ROS

The intracellular ROS level in B16F10 melanoma cells was measured using flow cytometry according to the protocol outlined by Promokine ROS Detection Assay Kit, which utilized 2'7'-dichlorodihydrofluorescin diacetate (H$_2$DCFDA) as the fluorescence probe. In brief, cells were seeded with a density of 1×10^5 cells/dish in a 60-mm cell culture dish. After incubated overnight, the cells were exposed to H$_2$O$_2$ (20 mM) for 1 hour, following by treatment with H-3 (12 µg/mL) in the presence of α-MSH (100 nM) for 24 and 48 hours. Wells containing cells and α-MSH without treatment were accounted as negative control, while those incubated with H$_2$O$_2$ for 1 hour and α-MSH without treatment were used as positive control. After the designated treatment periods, the cells were washed with PBS twice, harvested, and resuspended in assay buffer provided by the kit at concentration of 1×10^6 cells/mL, followed by incubation with H$_2$DCFDA in the dark for 30 minutes at 37 °C. The fluorescence intensity of DCF was measured by a BD FACS Canto II flow cytometer and analysed using a FACSDiva software. A total of 1×10^4 events was collected.

3.11   Mechanistic analysis

3.11.1 Total RNA extraction and quality control

The total RNA from treated (H-3, 12 µg/mL) and untreated B16F10 melanoma cells were extracted using Agilent Total RNA Isolation Mini Kit according to the manufacturer's protocol. The concentration of RNA was determined using a Thermo Scientific NanoDrop 2000c spectrophotometer, and the quality of RNA was analysed using Agilent Bioanalyzer. The RNA samples with a ratio of UV absorbance at 260 and 280 nm (i.e., A260/A280) ~ 1.70–2.00 and RNA integrity number (RIN) > 7 were selected for the microarray analysis.

3.11.2 Microarray analysis

Gene expression in B16F10 melanoma cells was analysed using an Agilent SurePrint G3 Mouse Gene Expression Microarray v3, 8 × 60K (design ID: 072363) which was performed by Neoscience Sdn. Bhd., Malaysia. The total RNA extracted was transcribed into double-stranded cDNA and synthesized into cRNA. The cRNA was then labeled with Canine-3 (Cy3) using One-Colour Low Input Quick Amp Labelling Kit (Agilent Tech. Inc., CA, USA) according to the manufacturer's instructions. The Cy3 labeled cRNA was purified by RNeasy Mini Kit (Qiagen, Valencia, CA). Dye incorporation and cRNA yield were determined using a NanoVue™ Plus spectrophotometer (GE Healthcare, UK). The cRNA was fragmented at 60 °C for 30 minutes and was hybridized for 17 hours at 65 °C in a rotating Agilent microarray hybridization oven. Then, the microarray was washed with Agilent GE wash buffer and immediately scanned using Agilent SureScan Microarray Scanner (G4900DA). Analysis was performed using Agilent GeneSpring Analysis Software (version 14.9.1) to identify the differentially expressed genes (DEGs) based on the statistical significance (p-value ≤ 0.05 and fold change ≥ 2.0). Gene Ontology (GO) analysis was performed to determine the roles of DEGs. The data obtained were subjected to the Benjamini-Hochberg correction and the cut-off were set at p-value ≤ 0.05 and False Discovery Rate (FDR) ≤ 25%.

3.11.3 Real-time polymerase chain reaction (qPCR) analysis

The total RNA was subjected to reverse transcription using AffinityScript qPCR cDNA Synthesis Kit (Agilent Tech. Inc, CA, USA) to form cDNA. The primers were designed by Primer3Plus (http://www.bioinformatics.nl/cgi-bin/primer3plus/primer3plus.cgi) and their specificity was determined using Primer-BLAST (https://www.ncbi.nlm.nih.gov/tools/primer-blast/index.cgi). The sequence of the primers and their amplicon sizes are displayed in Table 3.2. A total volume of 10 µL of the reaction mixture for the qPCR experiment was prepared, which contained 5 µL of SYBR® Green Master mix (Brilliant III Ultra-Fast SYBR® QPCR Master Mix, Agilent Tech. Inc., CA, USA), 4 µL of cDNA (10 ng), and 1 µL of primers (833 nM) of the tested gene. The qPCR analysis was performed in 7500 Fast Real-time PCR System (Applied Biosystems, MA, USA) using the following thermo cycle profile: 95 °C for 6 minutes, followed by 40 cycles of 95 °C for 5 seconds and 60 °C for 30 seconds. *Gapdh* was used as a reference gene for normalization. The qPCR amplification for all genes was performed in triplicates. The relative mRNA expression levels were calculated using the $2^{-\Delta\Delta Cq}$ method. The qPCR experiments were carried out according to the Minimum Information for Publication of Quantitative Real-Time PCR Experiments (MIQE) guidelines (Bustin et al., 2009).

Table 3.2: Primers of selected genes for qPCR analysis.

Genes	Primer sequence	Amplicon size (base pair)	Reference
Creb3l2	F: 5′-GACTCTGAGGGCAGCTTGAG-3′	111	-
	R: 5′-AGATGTGGACAAGGCAGAGG-3′		
Creb3l3	F: 5′-CTGACCCCAGCTCTCCATTA-3′	95	-
	R: 5′-ACTACGAGGAGGGGTGTCCT-3′		
Map3k20	F: 5′-ACACACATGTCCTTGGTTGG-3′	77	-
	R: 5′-CAGGTTTCAGACACAGGGAGA-3′		
Mapk14	F: 5′-GGACCTGAACAACATCGTGA -3′	79	-
	R: 5′-CCCTCGGAGGATCTGGTAGA-3′		
Mitf	F: 5′-GTATGAACACGCACTCTCGA-3′	135	Oskoueian et al. (2020)
	R: 5′-GTAACGTATTTGCCATTTGC-3′		
Tyr	F: 5′-CGCCCTCTTTTGGAAGTTTA-3′	84	-
	R: 5′-GAGCGGTATGAAAGGAACCA-3′		
Tyrp1	F: 5′-CTTTCTCCCTTCCTTACTGG-3′	163	Sangkaew and Yompakdee (2020)
	R: 5′-TCGTACTCTTCCAAGGATTC-3′		
Dct	F: 5′-TTATATCCTTCGAAACCAGGA-3′	176	Oskoueian et al. (2020)
	R: 5′-GGGAATGGATATTCCGTCTTA-3′		
Gapdh	F: 5'-TTGGCATTGTGGAAGGGCTC-3'	134	Seo et al. (2019)
	R: 5′-ACCAGTGGATGCAGGGATGA-3′		

3.12   Encapsulation

3.12.1 Preparation of liposomes

The H-3 liposomes was prepared through the thin-film hydration method by mixing 2.0 mg of lecithin, 1.7 mg oleic acid, and 0.5 mg of H-3 in a minimal volume of chloroform. The mixture was then being concentrated using a rotary evaporator until a thin layer formed at the bottom of the round bottom flask. The thin layer was rehydrated with a warm PBS (50 °C) at pH 8.6 containing 1% DMSO followed by sonication in an ultrasonic sonicator for 20 minutes. The pH of the H-3 liposomal dispersion was then being readjusted to pH 7.4 and stored at 4 °C until further analysis.

3.12.2 Particle size and zeta potential

The particle sizes, polydispersity index (PDI), and zeta potential of H-3 liposomes were determined using a Malvern Nano series Zetasiser (Malvern Instrument, UK). The measurement was performed at 25 °C by aliquoting 800 µL of H-3 liposomes into the disposable folded capillary cell DTS 1070.

3.12.3 Encapsulation efficiency

The amount of encapsulated H-3 was determined by UV spectrophotometry analysis. Approximately 5 mL of H-3 liposomes was aliquoted into Vivaspin® 6 (Sartorius Stedim Biotech, Germany) and the solution was centrifuged at 1,400 × g for 10 minutes. The concentration of encapsulated and free H-3 was determined by measuring the UV absorbance at 411 nm. Equal volume of absolute ethanol was added into the H-3 liposomes prior UV spectrophotometry analysis. From this measurement, the total weight of encapsulated and free H-3 was calculated. The percentage of encapsulation efficiency was calculated using the following equation (3.9):

$$Encapsulation\ efficiency\ (\%) = \left(\frac{Weight\ of\ encapsulated\ H\text{-}3}{Total\ weight\ of\ H\text{-}3}\right) \times 100\% \qquad (3.9)$$

3.12.4 *In vitro* release study

The *in vitro* release of H-3 from liposomes was performed using sample and separate method as described by Bahreini et al. (2014) with modifications. Several 1.5 mL tubes were prepared, and each tube was filled with 500 µL of H-3 liposomes dispersion and 500 µL of PBS. All tubes were then being incubated at 37 °C. Each tube was removed at predetermined time (1, 2, 3, 4, 6, 8, 24, 48, and 72 hours) and followed by centrifugation at 16,000 × g for 1 hour. The collected supernatant was then subjected to UV Vis spectrophotometry analysis. The cumulative H-3 released from the liposomes was calculated based on the following equation (3.10):

$$Cumulative\ H\text{-}3\ release\ (\%) = \left(\frac{Concentration\ of\ H\text{-}3\ in\ supernatant}{Initial\ concentration\ of\ H\text{-}3}\right) \times 100\% \ (3.10)$$

3.13 Statistical analysis

The results were presented as the mean ± standard deviation of three independent experiments. The means of different groups were compared using one-way ANOVA followed by the Tukey's post hoc test. Single comparison between the means of two groups were analysed using Student's t test. The IC_{50} values and the statistical analysis were obtained using the GraphPad Prism 7.0 Software (GraphPad Software Inc., CA, USA). The values are considered statistically significant when $p < 0.05$.

CHAPTER 4: RESULTS

4.1   Extraction yield of *Artocarpus* extracts

The yield of extracts from the leaf, peel, and stem bark of five selected *Artocarpus* species is presented in Table 4.1. The results showed that the percentage of yield for each extract varies from 1.17–27.58% and *A. rigidus* peel recorded the highest percentage of yield (27.58%), followed by *A. integer* peel (26.14%), and *A. elasticus* peel (20.42%). The percentage yield of extracts from three different parts used in the current study was in the sequence of peel, leaf, and stem bark (except for *A. heterophyllus*).

Table 4.1: Yield of fifteen *Artocarpus* extracts.

Plant	Part	Initial weight (g)[a]	Final weight (g)[b]	Percentage of yield (%)[c]
A. altilis	Leaf	200	15.94	7.97
	Peel	200	18.26	9.13
	Stem bark	200	5.49	2.75
A. heterophyllus	Leaf	200	2.33	1.17
	Peel	200	3.22	1.61
	Stem bark	200	8.22	4.11
A. integer	Leaf	200	33.28	16.64
	Peel	200	52.28	26.14
	Stem bark	200	10.81	5.40
A. elasticus	Leaf	200	22.17	11.09
	Peel	200	40.83	20.42
	Stem bark	200	14.90	7.45
A. rigidus	Leaf	200	22.30	11.15
	Peel	200	55.16	27.58
	Stem bark	200	14.84	7.42

[a]The dry weight of sample (coarse powder form); [b]The weight of extract; [c]The percentage of yield was calculated based on the initial weight of *Artocarpus* samples.

4.2 Anti-melanogenesis activity of *Artocarpus* extracts

4.2.1 Effect of *Artocarpus* extracts on mushroom tyrosinase activity

The effect of fifteen *Artocarpus* extracts on cell-free mushroom tyrosinase activity was investigated and the results are presented in Figure 4.1 as IC_{50} (the concentration of extract that inhibited 50% of mushroom tyrosinase activity). Both *A. integer* peel and *A. altilis* stem bark extracts exhibited strong mushroom tyrosinase inhibitory activity with IC_{50} 0.234 ± 0.026 and 0.242 ± 0.023 mg/mL, respectively. The other extract that exhibited a significant inhibitory effect on mushroom tyrosinase activity was *A. rigidus* stem bark with IC_{50} value of 0.314 ± 0.12 mg/mL.
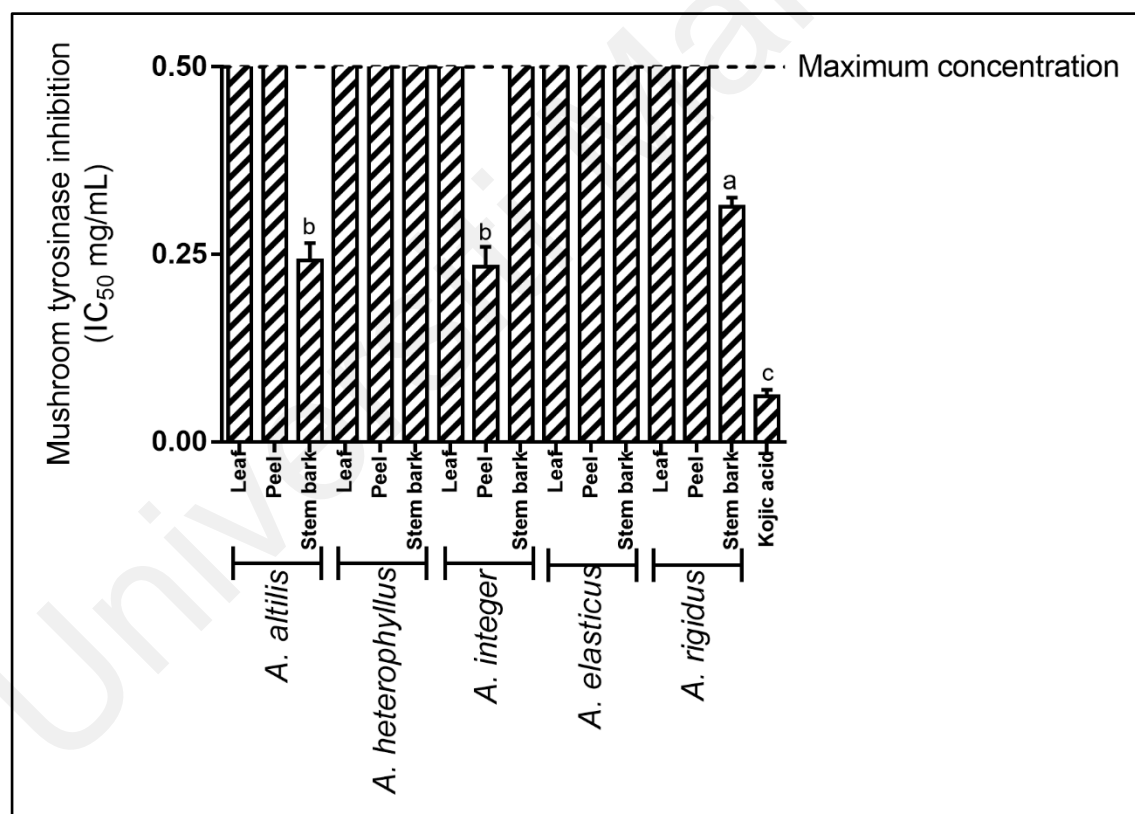
Figure 4.1: Effect of fifteen *Artocarpus* extracts on mushroom tyrosinase activity. Data are expressed as the mean ± standard deviation of three independent experiments. Means with different letter in each column means significantly different ($p < 0.05$, ANOVA).

4.2.2 Effect of *Artocarpus* extracts on viability of B16F10 melanoma cell

The cell viability assay was carried out as the toxicity of active ingredients is a crucial parameter that needs to be investigated preceding to the analysis of the cosmeceutical applications. Based on the results summarized in Figure 4.2, all *Artocarpus* extracts were non-cytotoxic, i.e., cell viability > 50% at the highest concentration tested (50 µg/mL), except the *A. altilis* leaf (30.69 ± 6.04%), *A. altilis* stem bark (3.66 ± 1.91%), *A. integer* stem bark (42.55 ± 5.73%), and *A. rigidus* stem bark (4.33 ± 1.70%) extracts. Chan et al. (2011) has cited that an effective skin-lightening agent should inhibit melanogenesis with a minimum cytotoxicity on the melanoma cells. Hence, the concentrations of *Artocarpus* extracts which showed viability ≥ 50% were selected for the following cellular assay.
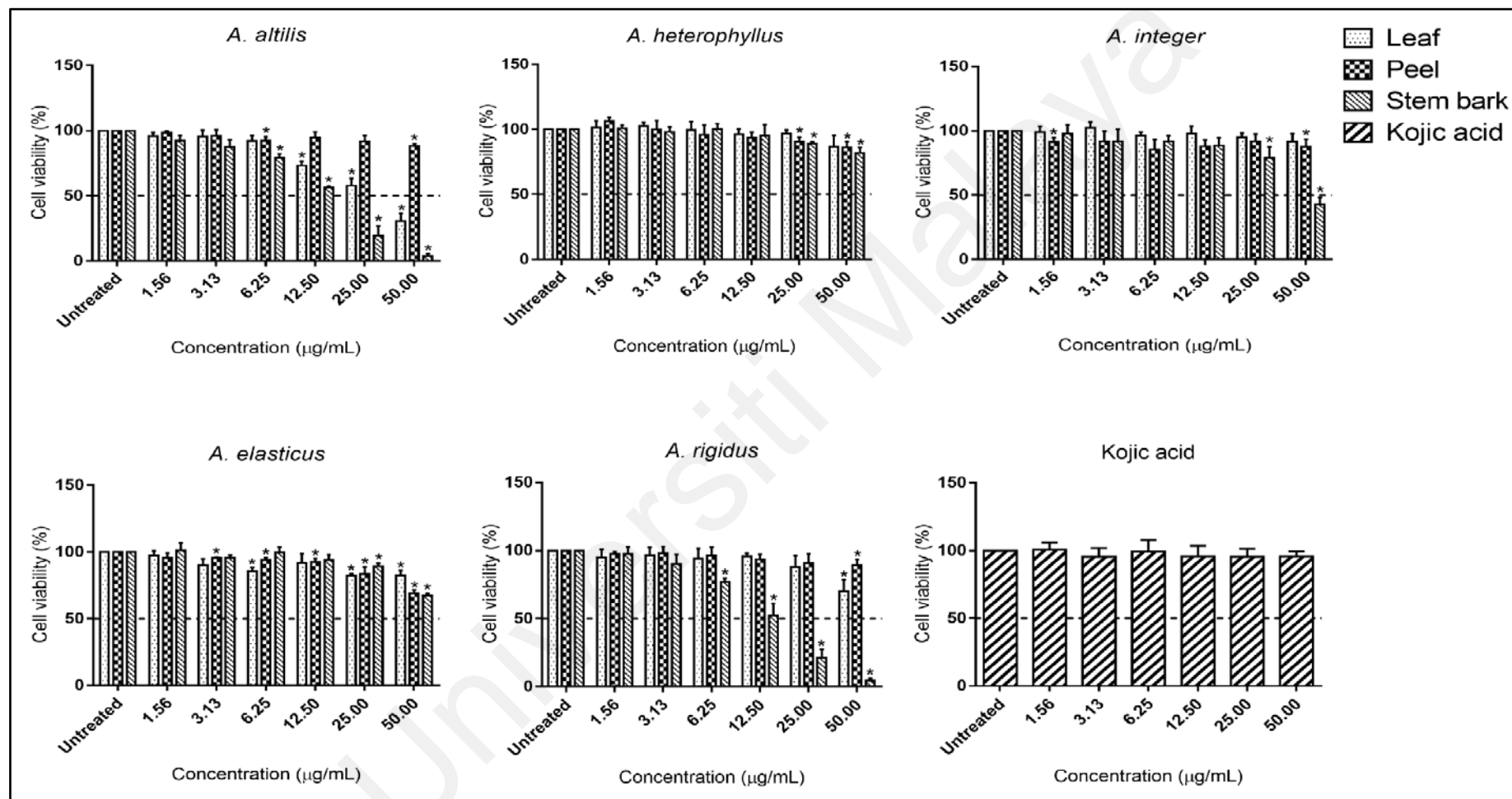
Figure 4.2: The viability of B16F10 melanoma cell after treatment with *Artocarpus* extracts for 48 hours. Kojic acid was used as positive control. Values are expressed as the mean ± standard deviation of three independent experiments. *$p < 0.05$ indicates significant different from untreated group.

4.2.3 Effect of *Artocarpus* extracts on melanin content in B16F10 melanoma cells

The effect of *Artocarpus* extracts on melanin content in B16F10 melanoma cells is displayed in Figure 4.3. At the highest concentration tested (50.00 µg/mL), cells treated with *A. elasticus* peel extract recorded the lowest intracellular melanin content (21.91 ± 1.80%), followed by *A. heterophyllus* stem bark (23.62 ± 0.69%) and *A. heterophyllus* peel (24.10 ± 3.96%) extracts. Kojic acid was used as positive control in the current study. Interestingly, the intracellular melanin content upon kojic acid treatment was 82.41 ± 7.15% at the highest concentration tested (50.00 µg/mL).

Due to their low toxicity and substantial intracellular melanin content reduction effects, both *A. heterophyllus* peel and stem bark extracts were then selected for the cellular tyrosinase assay. Despite having the lowest melanin content, *A. elasticus* peel extract was excluded from the cellular tyrosinase assay due to mild toxicity (cell viability 69.13 ± 2.35%, Figure 4.2) at the highest concentration tested (50.00 µg/mL).
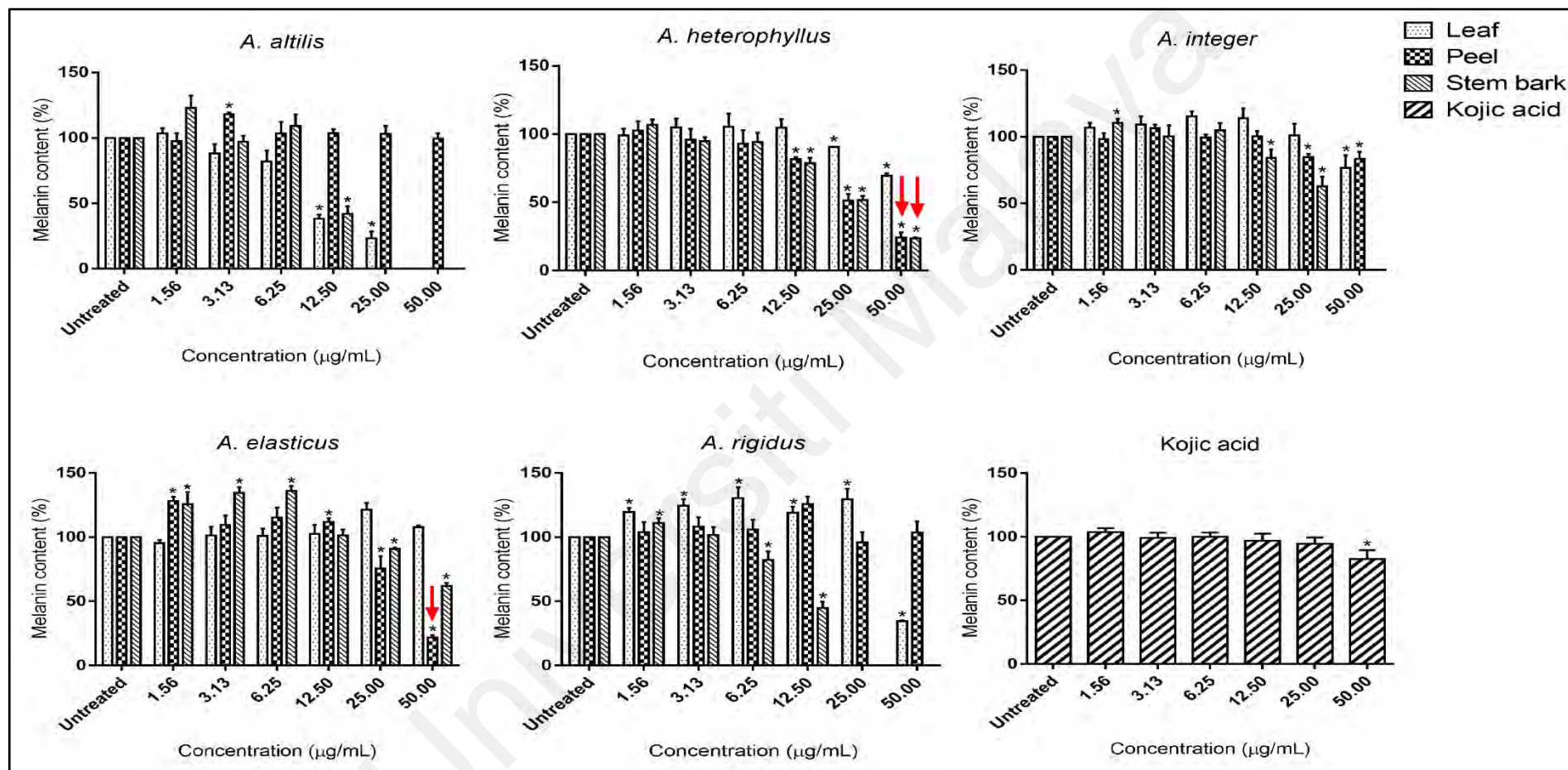
Figure 4.3: Effect of fifteen *Artocarpus* extracts on melanin content in B16F10 melanoma cells. The concentrations of *Artocarpus* extracts that reduced ≥ 50% cell viability (Figure 4.2) were excluded from melanin content assay. The red arrows indicate the extracts that showed substantial melanin reduction effect in B16F10 melanoma cells at 50 μg/mL. Kojic acid was used as positive control. Values are expressed as the mean ± standard deviation of three independent experiments. *$p < 0.05$ indicates significant different from untreated group.

4.2.4 Effect of *Artocarpus* extracts on cellular tyrosinase activity

The cellular tyrosinase assay was conducted on *A. heterophyllus* peel and stem bark extracts by extracting total protein from B16F10 melanoma cells after treatment. In this assay, extract that recorded a lower percentage of cellular tyrosinase activity indicating a stronger anti-melanogenesis effect. As shown in Figure 4.4, *A. heterophyllus* peel extract treatment (3.13–50.00 µg/mL) reduced cellular tyrosinase activity from 79.00 to 73.26% in a concentration-dependent manner, and its activity was higher than kojic acid at concentration of 6.25–50.00 µg/mL. As for *A. heterophyllus* stem bark extract treatment (3.13–25.00 µg/mL), the cellular tyrosinase activity recorded was only 92.02–90.42%, but the treatment abruptly reduced the activity to $56.09 \pm 8.27\%$ at 50.00 µg/mL, surpassing the inhibitory effect of showed by *A. heterophyllus* peel extract at 50.0 µg/mL $(72.36 \pm 4.86\%)$. Therefore, it is suggested that 50.00 µg/mL is a threshold concentration for *A. heterophyllus* stem bark extract in order to exhibit a significant cellular tyrosinase inhibitory effect.
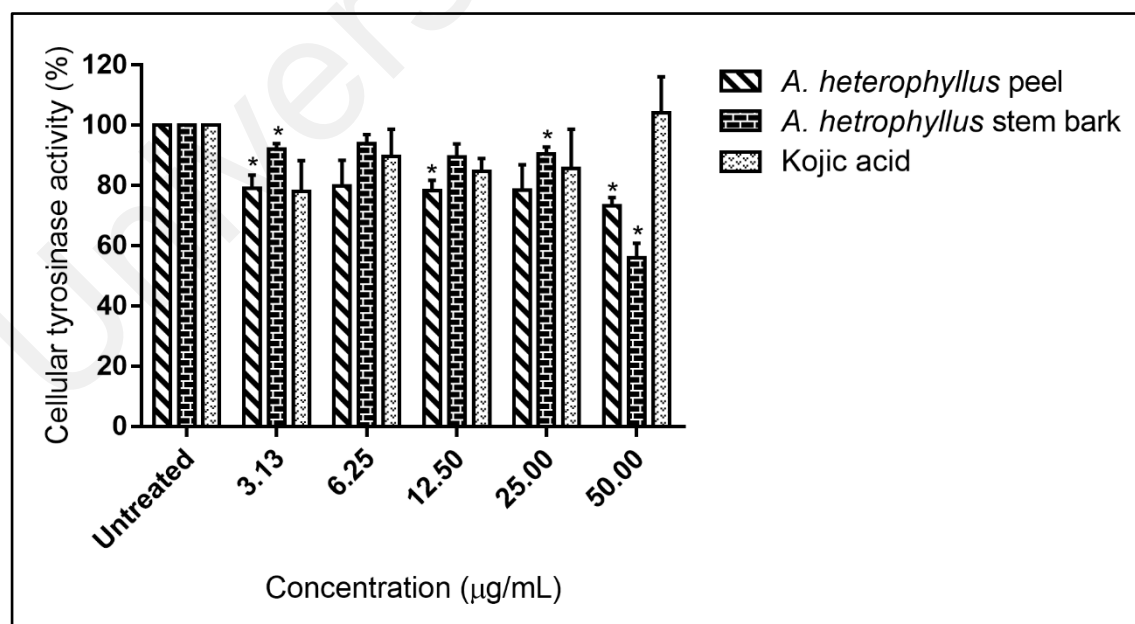
Figure 4.4: Effect of *A. heterophyllus* peel and stem bark extracts on cellular tyrosinase activity. Kojic acid was used as positive control. Data is represented as the mean ± standard deviation of three independent experiments. *$p < 0.05$ indicates significant different from untreated group.

4.3   Radical scavenging activity of *Artocarpus* extracts

The results of the radical scavenging activity of *Artocarpus* extracts are displayed in Figure 4.5 as IC_{50} (the concentrations of extracts that inhibited 50% of radical formation). *A. elasticus* peel extract presented the strongest radical scavenging activity for all three assays carried out with IC_{50} value of 0.017 ± 0.004 mg/mL for DPPH•, 0.007 ± 0.001 mg/mL for $ABTS^{+•}$ and 0.078 ± 0.010 mg/L for $O_2^{-•}$. The other *Artocarpus* extracts tested in this current study possessed a substantial antioxidant activity (AAI between 0.55–1.77), except for *A. altilis* peel and *A. heterophyllus* peel extracts (AAI < 0.5).
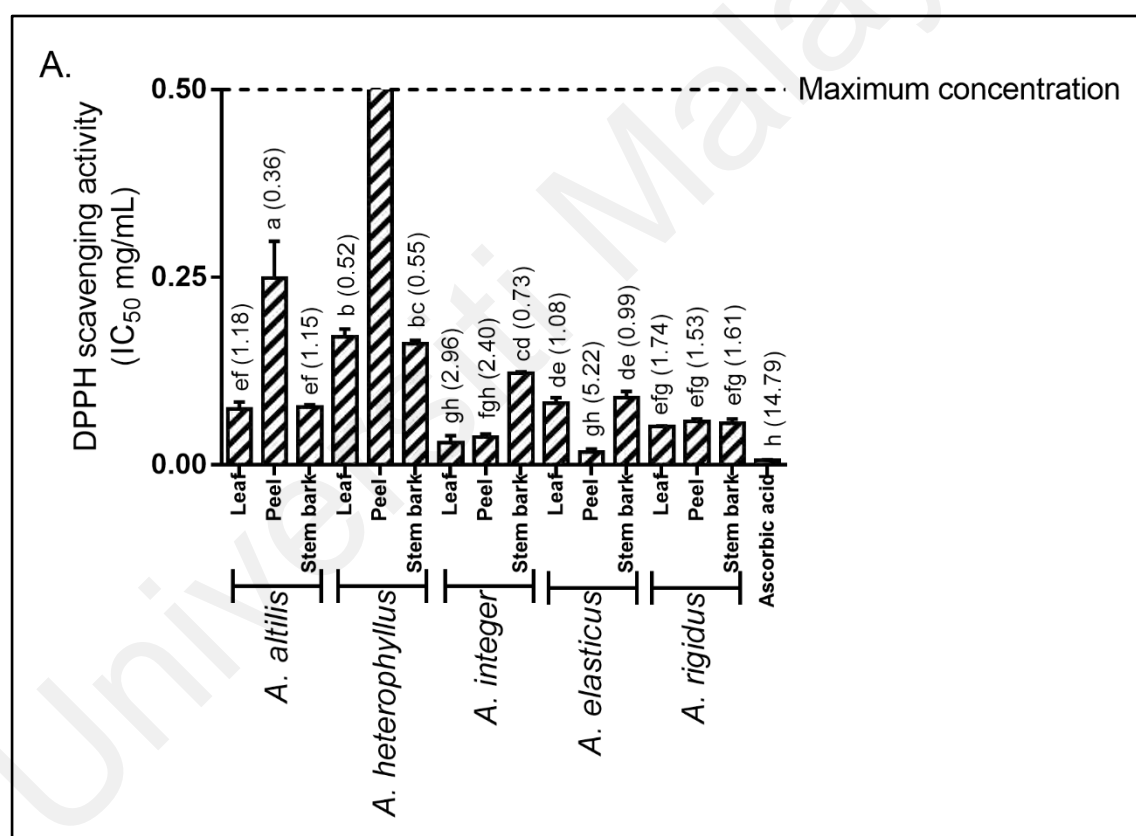
Figure 4.5: Radical scavenging activities of fifteen *Artocarpus* extracts. A) DPPH scavenging activity, where AAI values were shown in bracket, B) $ABTS^{+•}$ scavenging activity C) $O_2^{-•}$ scavenging activity. Data are expressed as the mean ± standard deviation of three independent experiments. Means with same letter in each column means not significantly different ($p < 0.05$, ANOVA).
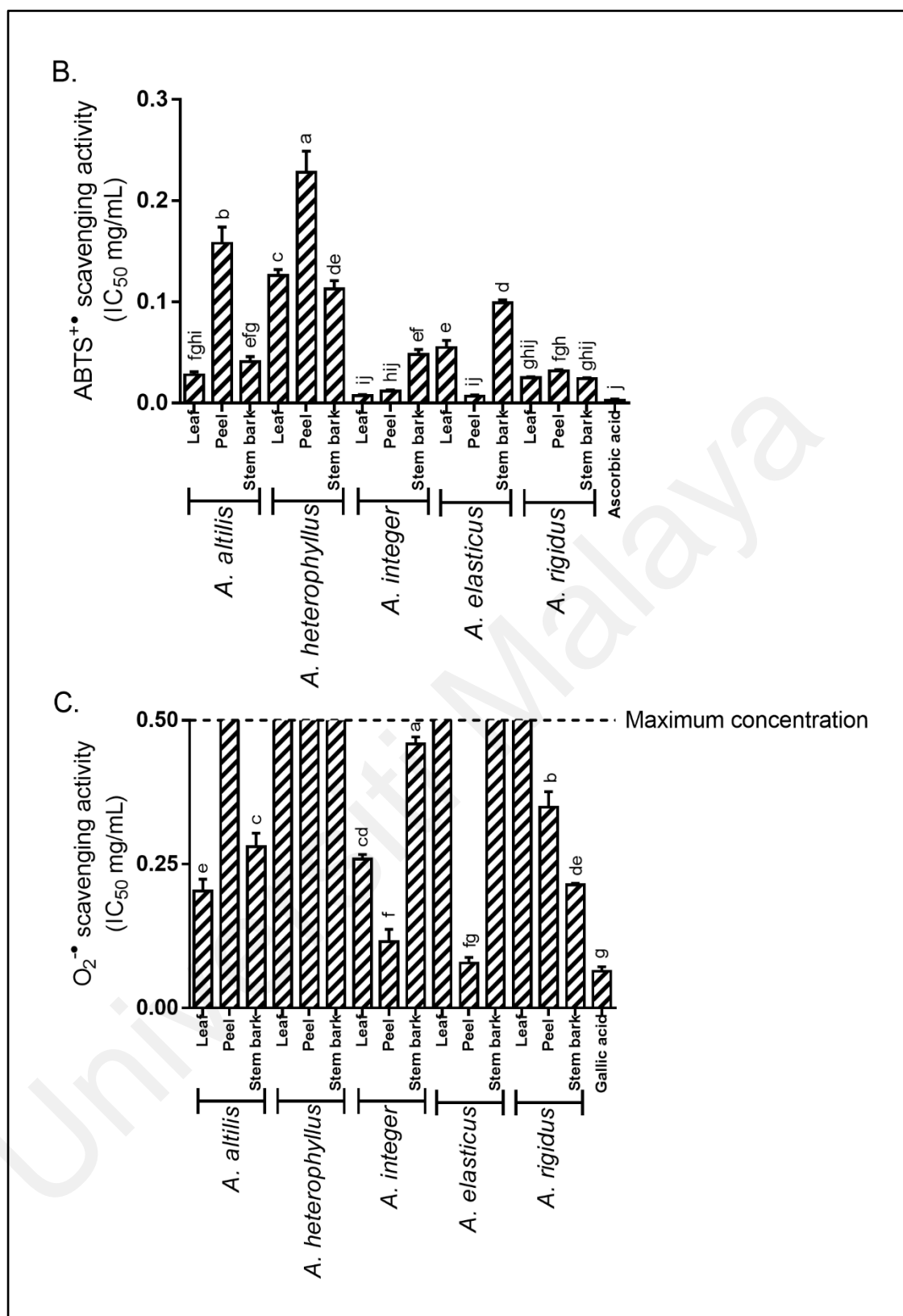
Figure 4.5, continued.

4.4   UV absorption pattern of *Artocarpus* extracts

The UV absorption spectra of the *Artocarpus* extracts are shown in the Figure 4.6 and it was evident that all *Artocarpus* extracts absorbed UV radiation strongly at UVC region, but weakly at UVB and UVA regions. Only *A. altilis* leaf extract substantially absorbed UVB radiation. The calculated SPF of all *Artocarpus* extracts were in the range of 0.30–5.84 (Figure 4.6).
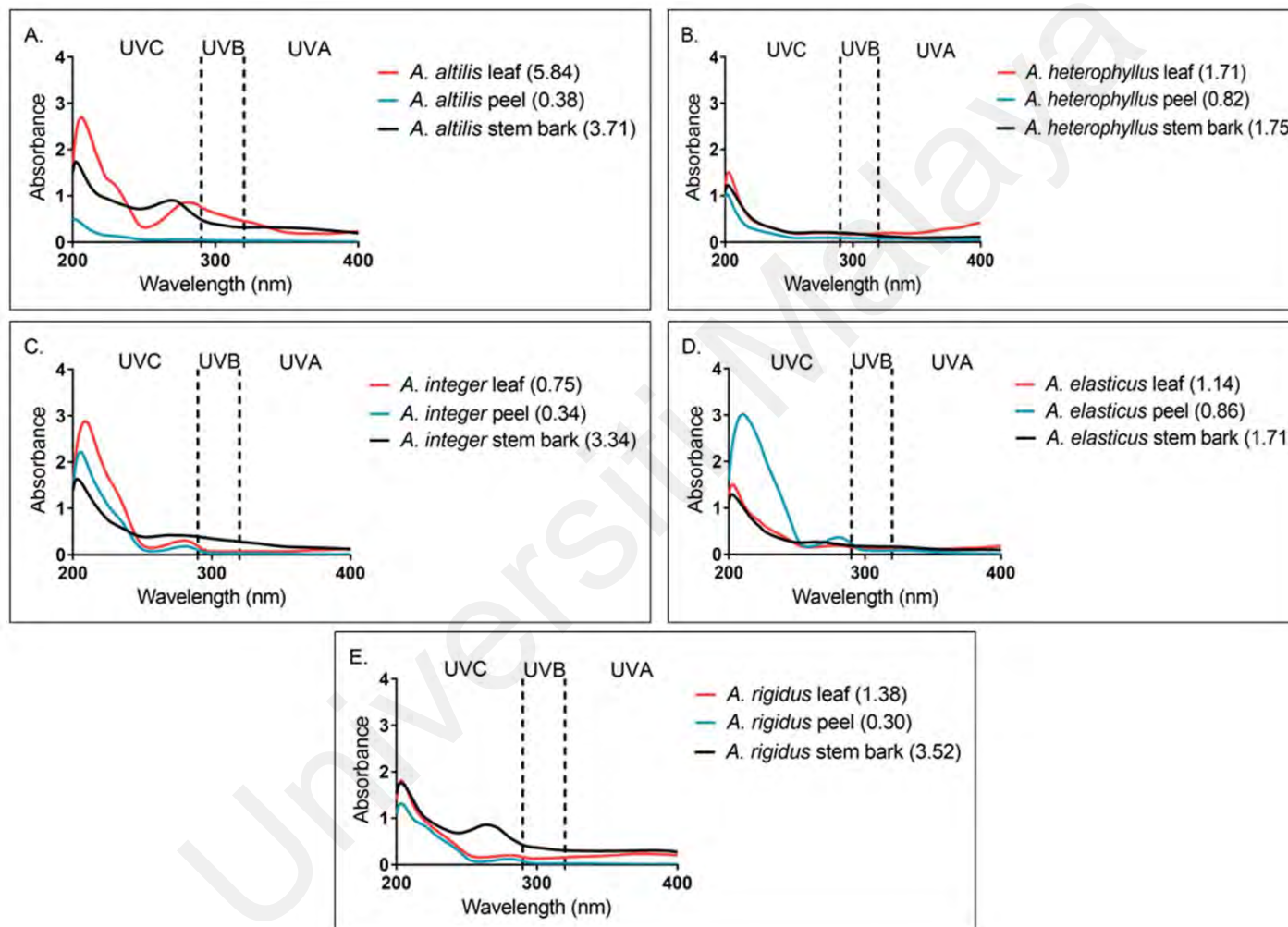
Figure 4.6: UV absorption analysis of *Artocarpus* species (200–400 nm). A) *A. altilis*, B) *A. heterophyllus*, C) *A. integer*, D) *A. elasticus*, and E) *A. rigidus*. All data were presented as the mean of triplicate readings. The SPF of *Artocarpus* extracts was indicated in bracket at the legend.

4.5   Pesticide residue analysis and biomass composition of *A. heterophyllus* stem bark extract

A. heterophyllus stem bark was selected as the bioactive extract, presenting an excellent melanin reduction effect in B16F10 melanoma cells without cytotoxicity. In addition, this bioactive extract also showed a potent inhibitory effect on cellular tyrosinase activity at 50 µg/mL. Therefore, *A. heterophyllus* stem bark extract was selected for subsequent investigation, including pesticide residue analysis and biomass composition.

Based on the GC/MS analysis, the pesticide components including insecticides, herbicides, fungicides, acaricides, and rodenticides were not detected in *A. heterophyllus* stem bark (results are presented as Appendix A). The proximate composition has been carried out and it was found that *A. heterophyllus* stem bark extract contains a high amount of crude fiber (41.20%) and carbohydrate (33.20%), while protein (2.20%) and crude fat (0.20%) are present in residual amount.

4.6   Bioassay-guided fractionation of *A. heterophyllus* stem bark extract

The effect of water and chloroform sub-extracts (Figure 3.2) on cell viability and melanin content in B16F10 melanoma cells were examined and the results are presented in Figure 4.7. Chloroform sub-extract exerted a higher anti-melanogenic activity compared to water sub-extract as evident from a lower melanin content ($36.67 \pm 7.75\%$) at a concentration of 25.00 µg/mL without appreciable cytotoxicity (cell viability > 50%).
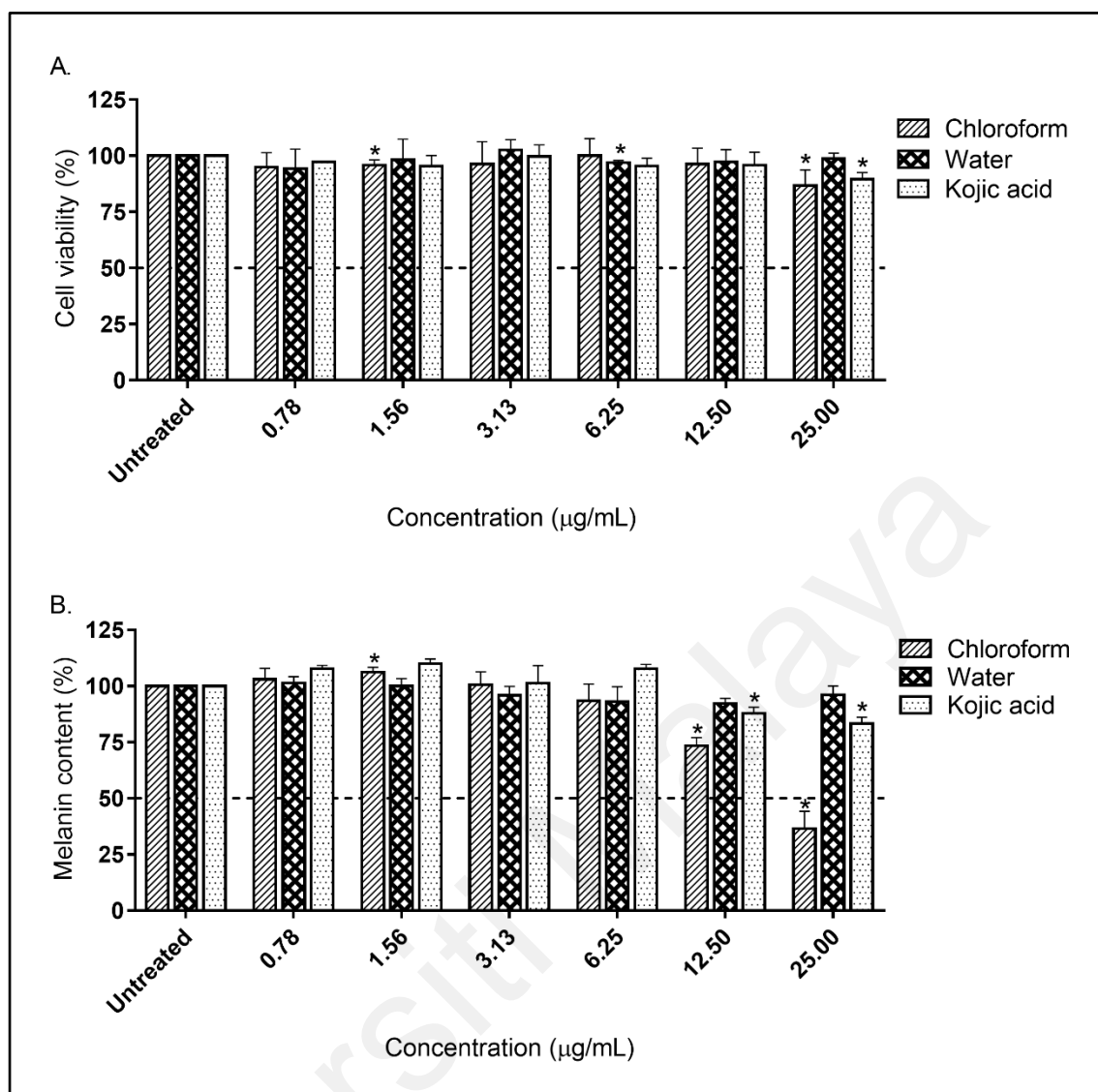
Figure 4.7: Viability (A) and melanin content (B) of B16F10 melanoma cells after treatment with *A. heterophyllus* stem bark sub-extracts for 48 hours. Kojic acid was used as positive control. Values are expressed as the mean ± standard deviation of three independent experiments. *p < 0.05 indicates significant different from untreated group.

Thus, the chloroform sub-extract was selected for further fractionation using silica gel flash column chromatography and produced 12 semi-pure fractions (A–L; Figure 3.2). Owing to a minute amount of fraction A (6.4 mg) and B (3.3 mg), these fractions were not tested in bioassays. The anti-proliferative and anti-melanogenic activities of fractions C–L were investigated using the same assays, and the results of active fractions (H, I, and J) are presented in Figure 4.8, whereas the non-active fractions (C, D, E, F, G, K, and L)

are presented in Appendix B. All fractions were not cytotoxic (cell viability > 50%),

except for the fraction H (11.21 ± 7.85%) and I (44.56 ± 3.79%) at the highest

concentration tested (25.00 µg/mL). In the melanin content assay, fraction H recorded the

lowest melanin content (27.49 ± 0.52%) at a non-cytotoxic concentration of 12.50 µg/mL,

and it was therefore selected for further purification using preparative radial

chromatography to obtain another five fractions (H-1–H-5; Figure 3.2).
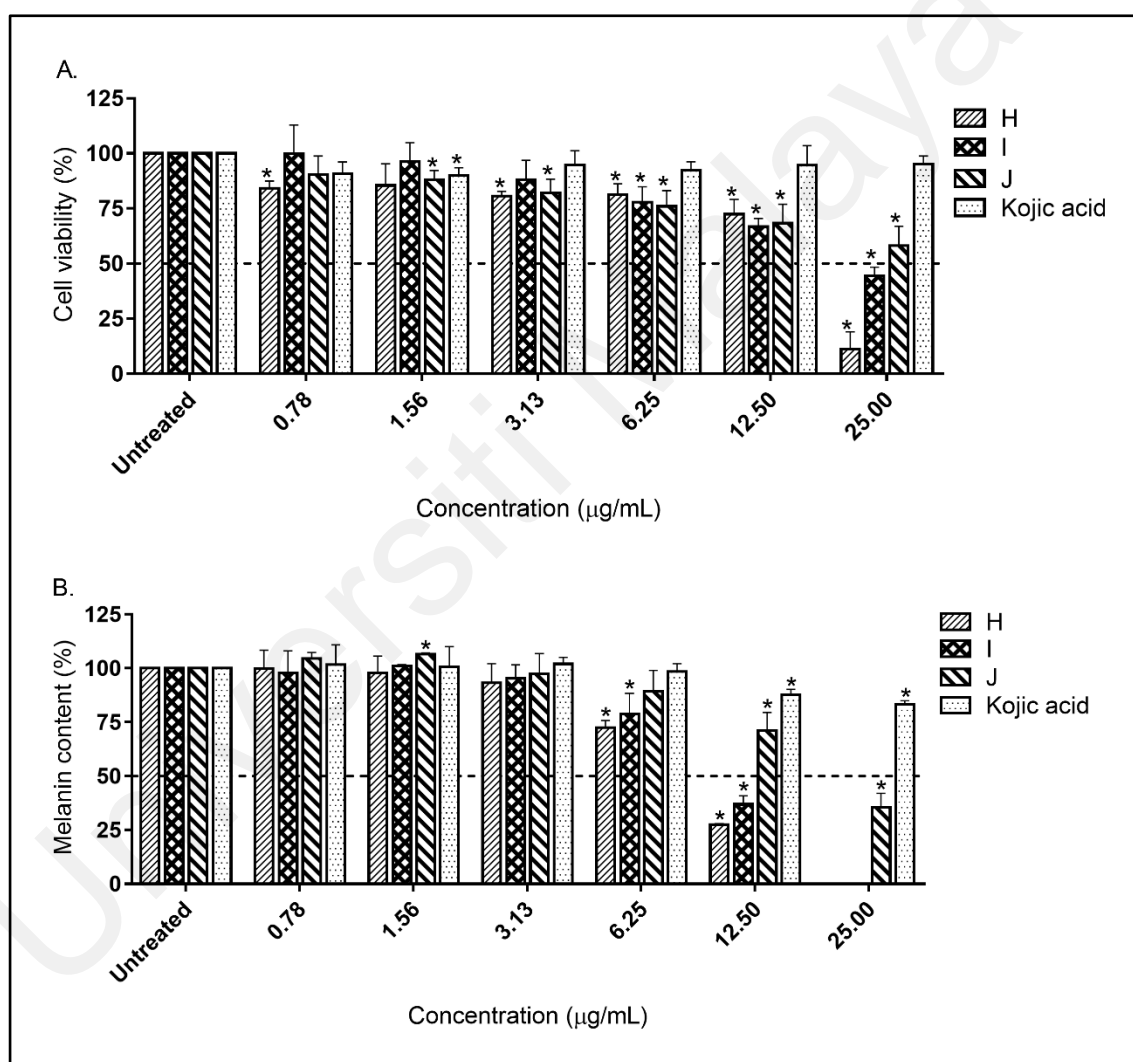
Figure 4.8: Viability (A) and melanin content (B) of B16F10 melanoma cells after treatment with _A. heterophyllus_ stem bark fractions (H–J) for 48 hours. The concentrations of fractions that reduced ≥ 50% cell viability (A) were excluded from melanin content assay (B). Kojic acid was used as positive control. Values are expressed as the mean ± standard deviation of three independent experiments. *$p <$ 0.05 indicates significant different from untreated group.

The yield of five fractions obtained were as follow: H-1 (0.18 g), H-2 (69.1 mg), H-3 (0.16 g), H-4 (40.0 mg), and H-5 (2.9 mg). Fraction H-5 was not tested in biological assays due to its extremely low yield. The anti-proliferative and anti-melanogenic effects of fraction H-1–H-4 were assessed, and the results are illustrated in Figure 4.9. All fractions H-1–H-4 were not cytotoxic, with fraction H-3 recorded the lowest melanin content (22.86 ± 2.90%) at the highest concentration tested (12.00 µg/mL) and it was 4-fold better than kojic acid (93.26 ± 3.23%). Hence, fraction H-3 was selected for subsequent investigation.
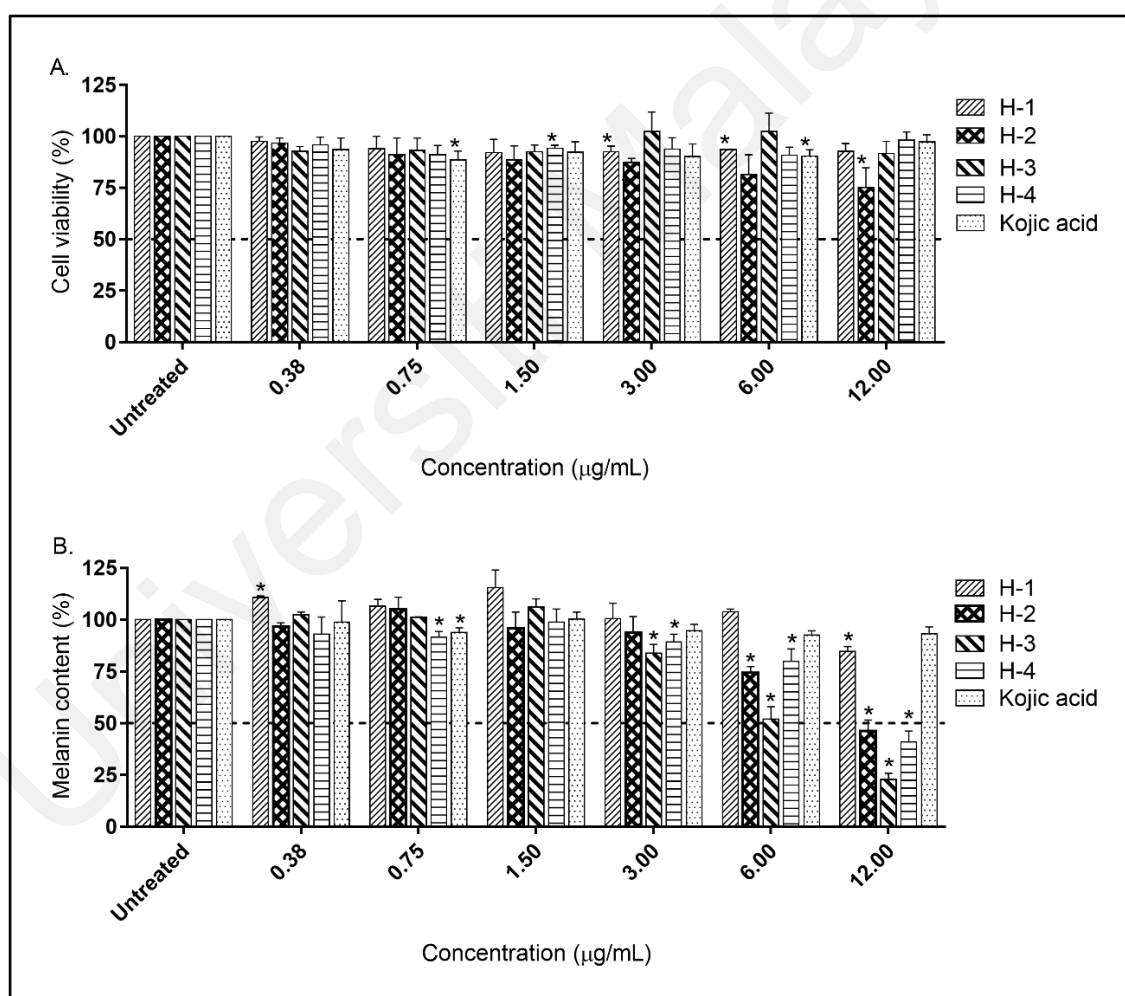
Figure 4.9: Viability (A) and melanin content (B) of B16F10 melanoma cells after treatment with *A. heterophyllus* stem bark fractions (H-1–H-4) for 48 hours. Fraction H-5 was excluded in biological assessment due to its low yield. Kojic acid was used as positive control. Values are expressed as the mean ± standard deviation of three independent experiments. *$p < 0.05$ indicates significant different from untreated group.

4.7 Identification of chemical constituents present in H-3

The LCMS analysis of H-3 has identified six chemical constituents based on Metlin database or molecular formula generator algorithm with a score of > 90% (±2). Two of the identified chemical constituents are fatty acids (N-palmitoyl serine and palmitic amide) and four are flavonoids (artonin B, cudraflavone A, cyclomorusin, and polystachin). Table 4.2 summarized the identified chemical constituents from H-3 through LCMS analysis with reported bioactivities from literature.

Table 4.2: List of chemical constituents present in H-3 based on LCMS analysis
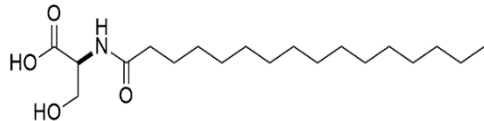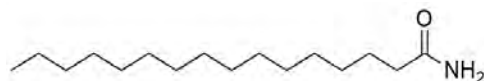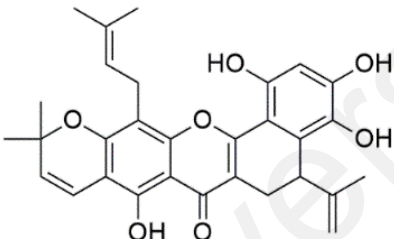
Class	Compound	Chemical structure	m/z [M+H]$^+$	Mass	Biological activity	Reference
Fatty acid	N-palmitoyl serine ($C_{19}H_{37}NO_4$)		344.2797	343.2718	Not reported	-
	Palmitic amide ($C_{16}H_{33}NO$)		256.2637	255.256	Not reported	-
Flavonoid	Artonin B ($C_{30}H_{30}O_7$)		503.2077	502.2008	Anti-inflammatory activity by inhibiting $O_2^{-\bullet}$ generation in rat neutrophil cells	Wei et al. (2005)
					Cytotoxic against human CCRF-CEM leukemia cells by inducing apoptosis	Lee et al. (2006)
					Radical scavenging activity by inhibiting iron-induced lipid peroxidation in rat brain homogenate and copper-catalysed oxidation of human low-density lipoprotein. Scavenged DPPH•	Ko et al. (1998)

Table 4.2, continued.
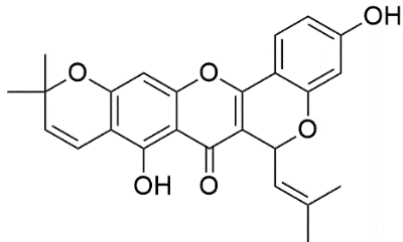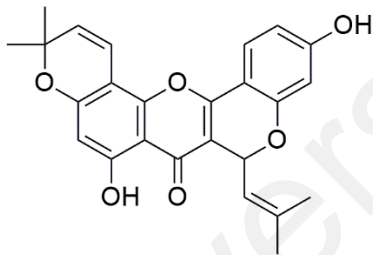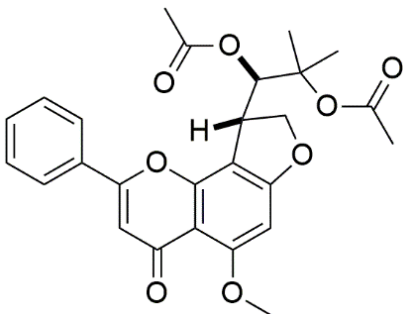
Class	Compound	Chemical structure	m/z [M+H]$^+$	Mass	Biological activity	Reference
Flavonoid	Cudraflavone A ($C_{25}H_{22}O_6$)		419.1485	418.1415	Anti-inflammatory activity by inducing $O_2^{-\bullet}$ generation in rat neutrophil cells	Wei et al. (2005)
	Cyclomorusin ($C_{25}H_{22}O_6$)		419.1485	418.1415	Anti-inflammatory activity by inducing $O_2^{-\bullet}$ generation in rat neutrophil cells	Wei et al. (2005)
					Anti-platelet activities in rabbit blood suspension	Chun-Nan et al. (1993)
					Anti-tyrosinase activity (mushroom tyrosinase)	Ryu et al. (2008)
					Inhibited human phosphodiesterase-4 activity	Guo et al. (2018)

Table 4.2, continued.

Class	Compound	Chemical structure	m/z [M+H]$^+$	Mass	Biological activity	Reference
Flavonoid	Polystachin ($C_{26}H_{26}O_8$)		467.1705	466.1634	Not reported	-

4.8   Effect of H-3 on cellular tyrosinase activity

Based on the results displayed in Figure 4.10, H-3 exerted significant inhibition on cellular tyrosinase activity in a dose-dependent manner, from $74.47 \pm 3.78\%$ at treatment concentration of 6.00 μg/mL to $40.41 \pm 4.89\%$ at 12.00 μg/mL. Interestingly, the inhibition of cellular tyrosinase activity by H-3 at 12.00 μg/mL was similar to that of kojic acid ($37.55 \pm 8.43\%$) at 400 μg/mL, indicating that the former reduced cellular tyrosinase activity at a treatment concentration of 33-folds lower than kojic acid.
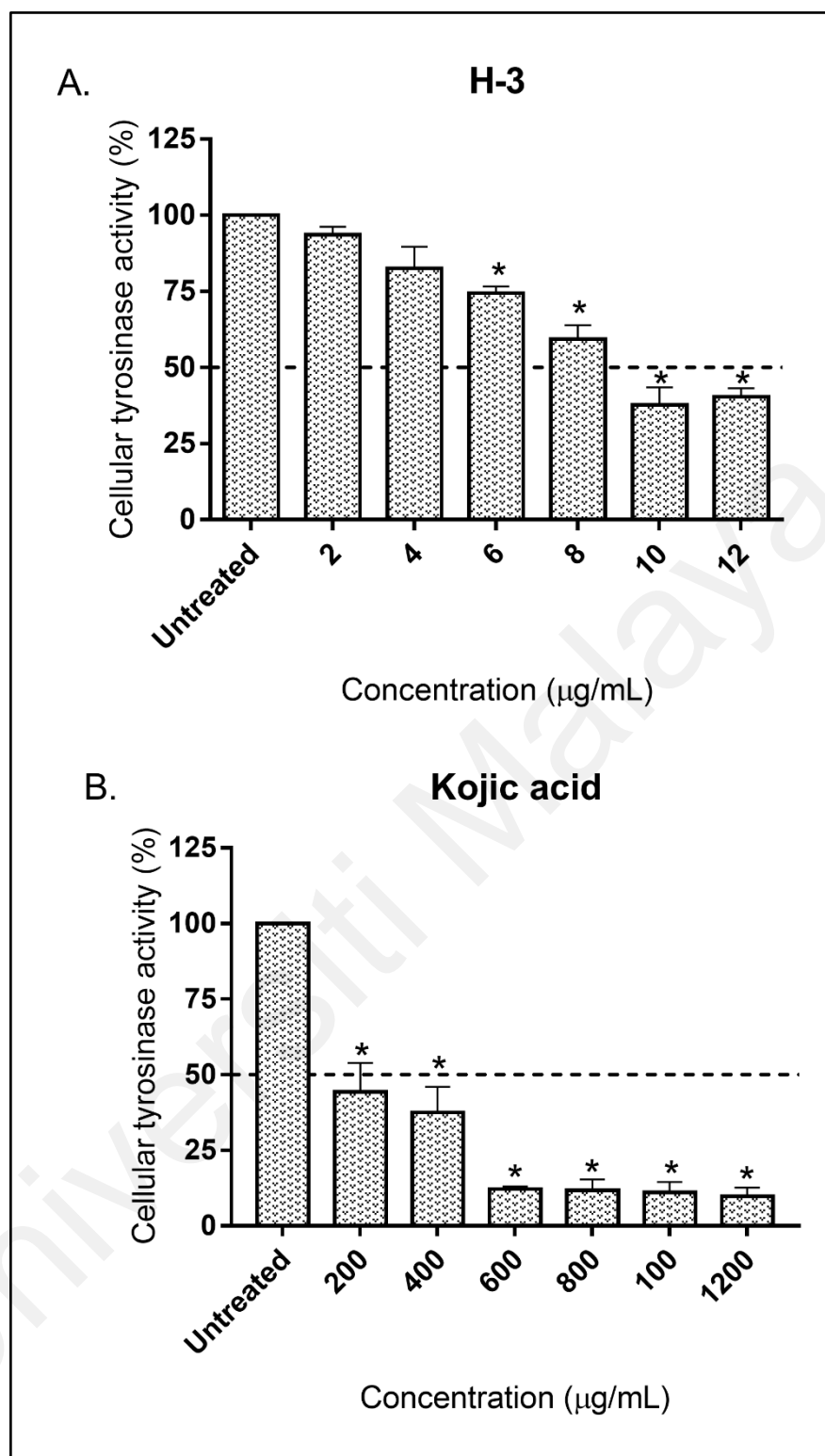
Figure 4.10: Effect of H-3 (A) and kojic acid (B) on cellular tyrosinase activity. Kojic acid was used as a positive control. Data represented as the mean ± standard deviation of three independent experiments. *$p < 0.05$ indicates significant different from untreated group.

4.9   Effect of H-3 on intracellular ROS level

The ROS scavenging effect of H-3 in B16F10 melanoma cells was measured using flow cytometry upon staining with H_2DCFDA and the results are presented in Figure 4.11. Treatment with either α-MSH or H-3 individually did not affect the ROS level in the cells (ROS level < 1%). The generation of ROS in the cells was induced by pre-incubation with H_2O_2 for 1 hour prior to the treatment with H-3 for 24 and 48 hours. The results showed that H-3 slightly reduced the intracellular ROS level from 2.5 to 1.8% after 24 hours treatment. On the extension of the treatment to 48 hours, H-3 further reduced the ROS level from 8.1 to 4.4%, indicative of a substantial ROS scavenging activity of H-3.
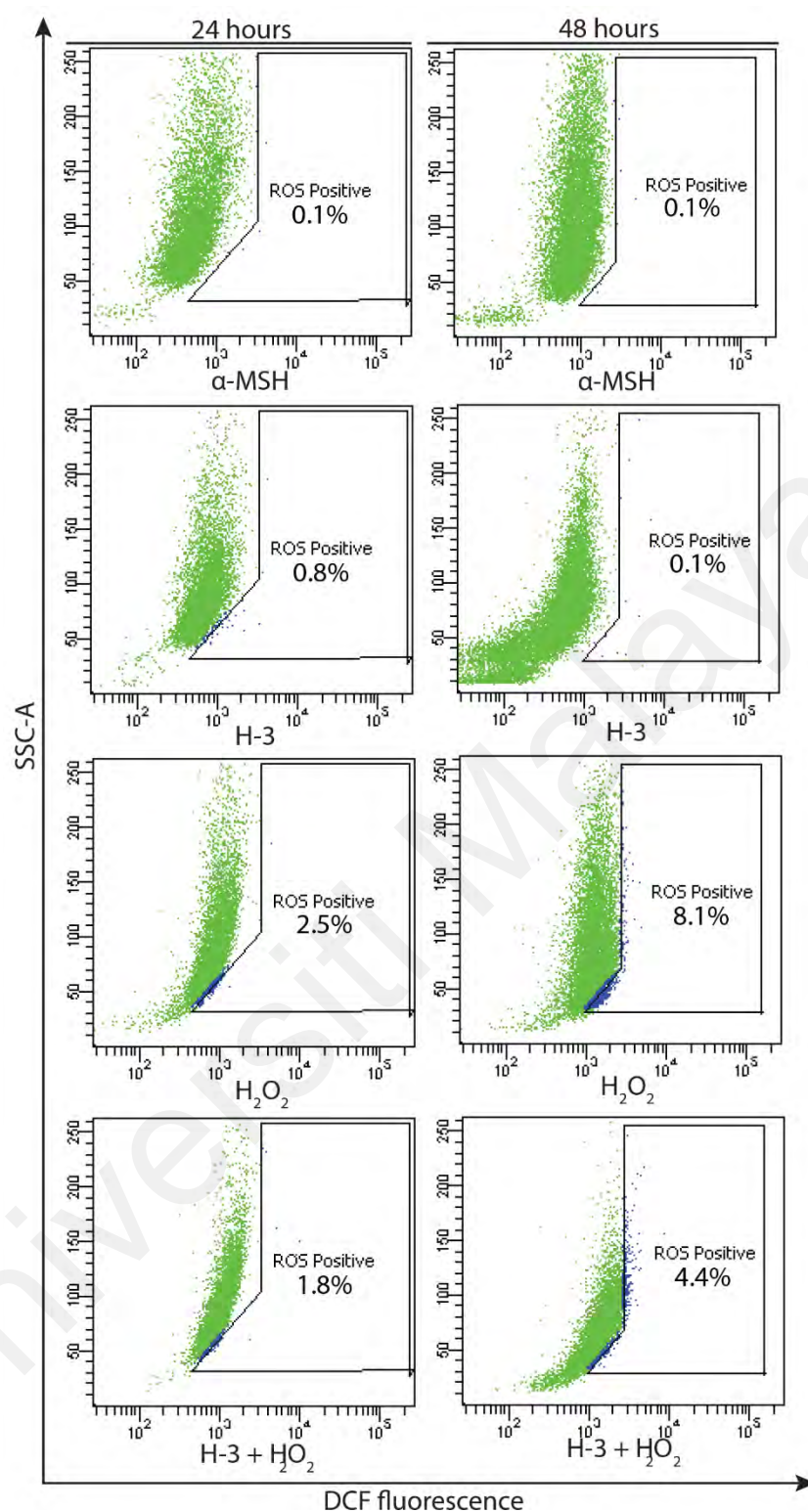
Figure 4.11: Effect of H-3 (12 µg/mL) on intracellular ROS level in B16F10 melanoma cells for 24 and 48 hours. The cells treated with media containing α-MSH only was regarded as negative control, while those incubated with H_2O_2 (20 mM) and α-MSH were regarded as a positive control.

4.10   Effect of H-3 on transcriptome in B16F10 melanoma cells

H-3 treatment on B16F10 melanoma cells at 12 µg/mL for 48 hours produced 4633 (14.62%) DEGs out of 31700 that are present in the microarray (Figure 4.12A). Among these DEGs, 1729 (5.45%) of them were upregulated, ranging from 2.00- to 16.95-folds, while 2904 (9.16%) of them were downregulated, ranging from 2.00- to 61.37-folds. Through GO analysis, these DEGs can be grouped into three domains, namely biological process, cellular component, and molecular function (Figure 4.12B). The specific cellular events taken part by these DEGs in each domain were further elaborated and are presented in Figure 4.13A–C. Particularly, the DEGs involved in biological process were subjected to further analysis, whereupon 29 genes that are related to melanogenesis were identified and are listed in Table 4.3. Among these genes, the expression of a master regulator of melanogenesis (*Mitf*), a rate-limiting enzyme in melanogenesis (*Tyr*), and a melanosome transport-associated gene (*Mlph*) were significantly downregulated by 2.69–6.78-fold. In addition, the markers of autophagy (involved in melanogenesis) were also significantly upregulated, such as *Sqstm1* and *Ulk1* (2.24-fold for both genes). The genes related to the cAMP signaling pathway, such as *Creb3l1*, *Creb3l2*, *Creb3l3*, and *Atf1* were downregulated by 2.10–3.58-fold. Furthermore, the genes involved in the MAPK signaling pathway, i.e., *Map3k20* and *Mapk14* were upregulated by 4.10- and 2.01-fold, respectively.
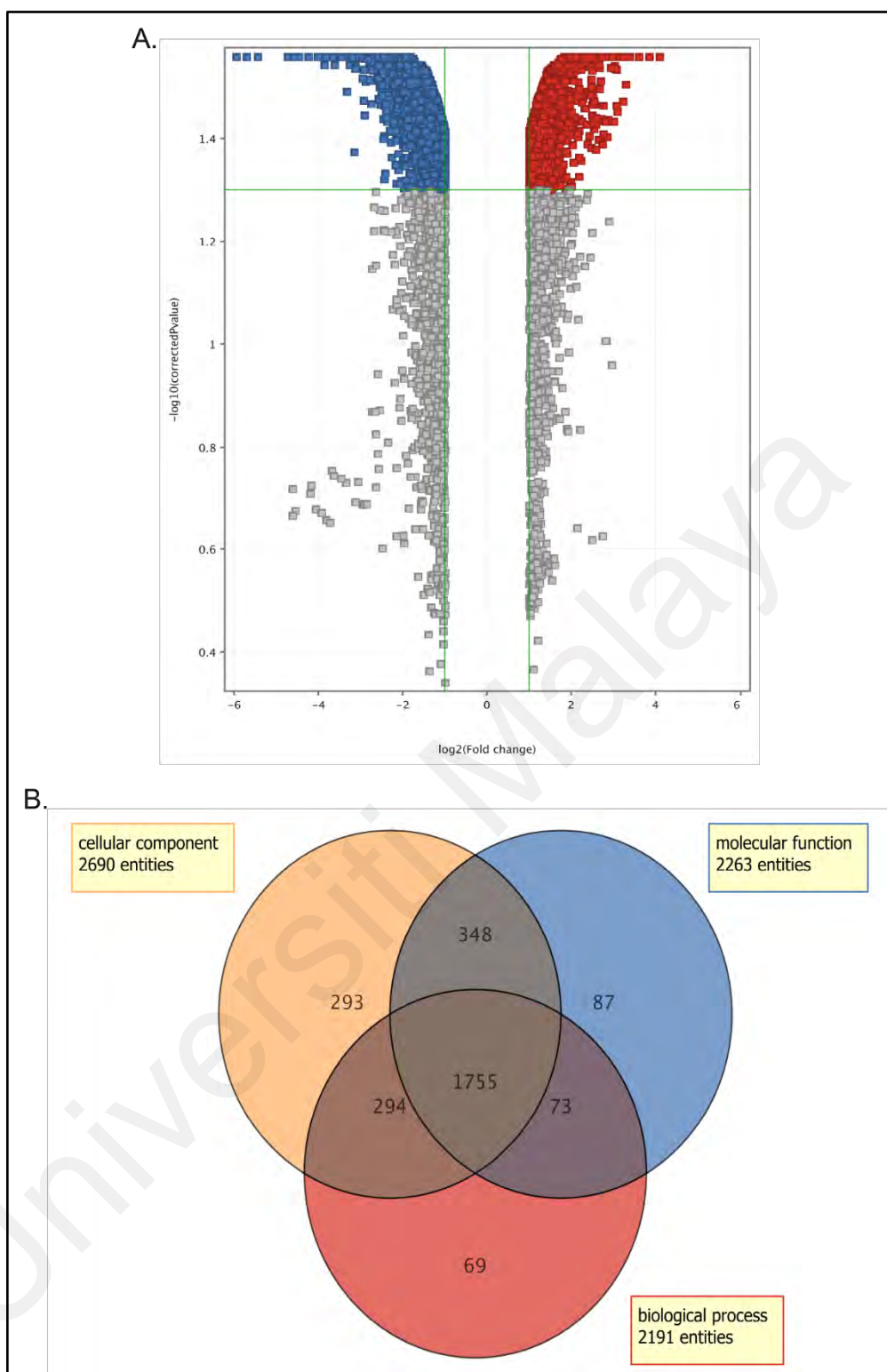
Figure 4.12: Microarray analysis of B16F10 melanoma cells treated with H-3 (12 μg/mL) for 48 hours. (A) Volcano plot of DEGs after treatment with H-3. Each dot represents a gene. The red field represents the upregulated genes, and the blue field represents the downregulated genes with fold change > 2.0 and *p* < 0.05. The grey coloured field represents the genes that do not meet the selection criteria, and they are non-DEGs. (B) Venn diagram shows the number of DEGs and their biological roles are classified into the biological process, cellular component, and molecular function.
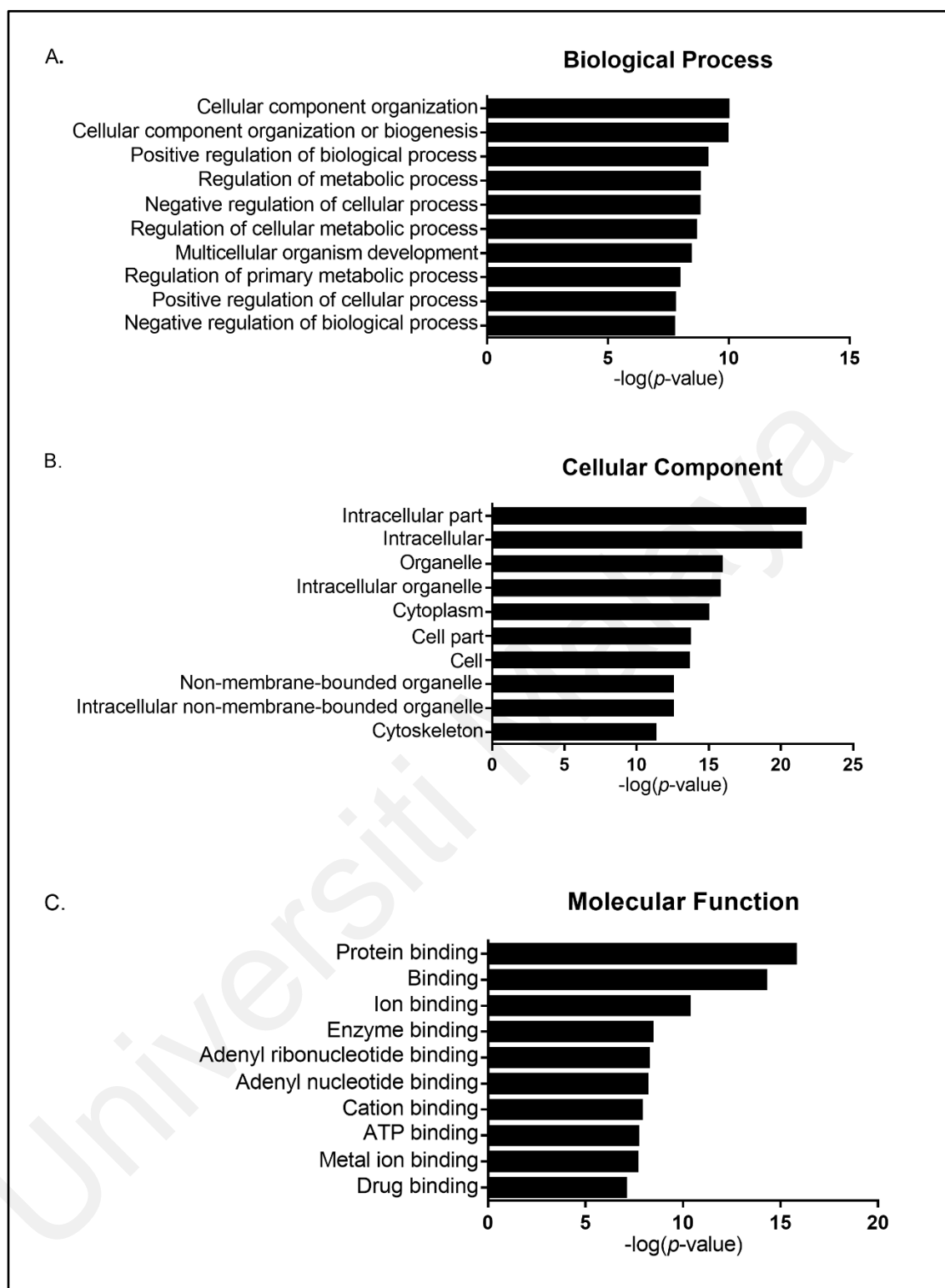
Figure 4.13: Cellular events in B16F10 melanoma cells affected by H-3 treatment at 12 μg/mL based on GO analysis. (A) Ten most significant biological process affected by H-3 treatment. (B) Ten most significant cellular component affected by H-3 treatment. (C) Ten most significant molecular function affected by H-3 treatment.

Table 4.3: List up- and down-regulated genes in B16F10 melanoma cells treated with H-3 (12 µg/mL).

Gene symbol	Gene name	Biological process	Log$_{10}$ (FC)[a]	Reference(s)
Il6st	Interleukin 6 signal transducer	Cell differentiation, cell population proliferation, homeostasis, immune system, protein and lipid metabolic process, response to stimulus, signaling, system development	2.05	Bult et al. (2019); Kumari et al. (2018)
Map3k20	Mitogen-activated protein kinase kinase kinase 20	Cell death, cellular component organization, protein metabolic process, respond to stimulus, signaling	2.04	Bult et al. (2019); Gotoh et al. (2001); The UniProt (2019)
Csnk2a2	Casein kinase 2, alpha prime polypeptide	Cell death, protein metabolic process, response to stimulus, signaling	1.49	Bult et al. (2019); Villareal et al. (2012); The UniProt (2019)
Tpr	Translocated promoter region	Cellular component organization, establishment of localization, nucleic acid-templated transcription, protein metabolic process, response to stimulus, signaling	1.45	Bult et al. (2019); Makbal et al. (2020)
Gnao	Guanine nucleotide binding protein, alpha O	Establishment of localization, response to stimulus, signaling	1.23	Bult et al. (2019); Kanehisa and Goto (2000)
Mtfr2	Mitochondrial fission regulator 2	Cellular component organization	1.20	Bult et al. (2019); Kumari et al. (2018)

[a]The value is presented as log$_{10}$ fold change of treated versus untreated group; FC: Fold change.

Table 4.3, continued.

Gene symbol	Gene name	Biological process	$\log_{10}$ (FC)[a]	Reference(s)
Sqstm1	Sequestosome 1	Cell death, cell differentiation, cell population proliferation, cellular component organization, establishment of localization, homeostasis, immune system process, nucleic acid-templated transcription, protein metabolic process, response to stimulus, signaling	1.16	Bult et al. (2019); Jeong et al. (2020); Liu et al. (2016)
Ulk1	Unc-51 like kinase 1	Cell death, cell differentiation, cellular component organization, establishment of localization, protein metabolic process, response to stimulus, signaling, system development	1.16	Bult et al. (2019); Jeong et al. (2020)
Uchl1os	Ubiquitin carboxy-terminal hydrolase L1, opposite strand	Protein metabolic process, response to stimulus	1.15	Seo et al. (2017); Bult et al. (2019)
Csnk1a1	Casein kinase 1, alpha 1	Protein metabolic process, and response to stimulus, signaling	1.10	Bult et al. (2019); Villareal et al. (2012)
Foxo3	Forkhead box O3	Cell death, cell differentiation, cell population proliferation, homeostasis, immune system, nucleic acid-templated transcription, protein metabolic process, response to stimulus, signaling, system development	1.10	Bult et al. (2019); Kim et al. (2014a)

[a]The value is presented as $\log_{10}$ fold change of treated versus untreated group; FC: Fold change.

Table 4.3, continued.

Gene symbol	Gene name	Biological process	Log$_{10}$ (FC)^a	Reference(s)
Mapk14	Mitogen-activated protein kinase 14	Cell death, cell population proliferation, cell differentiation, cellular component organization, establishment of localization, homeostasis, immune system, nucleic acid-templated transcription, protein and lipid metabolic process, response to stimulus, signaling, system development	1.01	Bult et al. (2019); Keshet and Seger (2010); The UniProt (2019)
Creb3l1	cAMP responsive element binding protein 3-like 1	Cell death, cell differentiation, cellular component organization, establishment of localization, nucleic acid-templated transcription, response to stimulus, signaling, system development	−1.07	Bult et al. (2019); Greenwood et al. (2017); Kanehisa and Goto (2000)
Fzd3	Frizzled class receptor 3	Cell death, cell population proliferation, cell differentiation, cellular components organization, response to stimulus, signaling, system development	−1.07	Bult et al. (2019); Carlson et al. (2007); Kanehisa and Goto (2000)
Gpr143	G protein-coupled receptor 143	Melanosome organization, melanosome localization, melanosome transport, response to stimulus, signaling	−1.14	Bult et al. (2019); Makbal et al. (2020)

^{a}The value is presented as log$_{10}$ fold change of treated versus untreated group; FC: Fold change.

Table 4.3, continued.

Gene symbol	Gene name	Biological process	Log$_{10}$ (FC)[a]	Reference(s)
Prkca	Protein kinase C, alpha	Cell death, cell differentiation, cell population proliferation, cellular component organization, establishment of localization, homeostasis, immune system, protein metabolic process, response to stimulus, signaling, system development	−1.23	Bult et al. (2019); Kanehisa and Goto (2000)
Creb3l2	cAMP responsive element binding protein 3-like 2	Cell differentiation, cellular component organization, establishment of localization, nucleic acid-templated transcription, response to stimulus, signaling, system development	−1.29	Bult et al. (2019); Kanehisa and Goto (2000); Villareal et al. (2012)
Sorbs3	Sorbin and SH3 domain containing 3	Cellular component organization, nucleic acid-templated transcription, response to stimulus, signaling	−1.29	Bult et al. (2019); Villareal et al. (2012)
Creb3l3	cAMP responsive element binding protein 3-like 3	Nucleic acid-templated transcription, response to stimulus, signaling	−1.33	Bult et al. (2019); Glick et al. (2010); Kanehisa and Goto (2000)
Calm1	Calmodulin-1	Establishment of localization, homeostasis, protein metabolic process, response to stimulus	−1.42	Bult et al. (2019); Kanehisa and Goto (2000)
Tyr	Tyrosinase	Cell population proliferation, immune system process, respond to stimulus, system development, melanin biosynthesis, pigmentation	−1.43	Bult et al. (2019); The UniProt (2019);

[a]The value is presented as log$_{10}$ fold change of treated versus untreated group; FC: Fold change.

Gene symbol	Gene name	Biological process	$\log_{10}$ (FC)[a]	Reference(s)
Trpm1	Transient receptor potential cation channel subfamily M, member 1	Cell differentiation, cellular component organization, establishment of localization, homeostasis, response to stimulus, signaling, system development	−1.64	Bult et al. (2019); Ma et al. (2017)
Kif6	Kinesin family member 6	Microtubule-based movement	−1.65	Miki et al. (2001); The UniProt (2019)
Plcb1	Phospholipase C, beta 1	Carbohydrate derivative metabolism, cell differentiation, cellular component organization, establishment of localization, homeostasis, immune system, nucleic acid-templated transcription, protein and lipid metabolic process, response to stimulus, signaling, system development	−1.70	Bult et al. (2019); Kanehisa and Goto (2000)
Mitf	Melanogenesis associated transcription factor	Cell death, cell population proliferation, cell differentiation, melanocyte differentiation, pigmentation, cellular component organization, immune system, nucleic acid-templated transcription, response to stimulus, signaling, system development	−1.77	Bult et al. (2019); Makbal et al. (2020); Villareal et al. (2012)
Atp7b	ATPase, Cu^{++} transporting, beta polypeptide	Establishment of localization, homeostasis, protein metabolic process, respond to stimulus, system development	−1.78	Bult et al. (2019); Matsui et al. (2015)

[a]The value is presented as $\log_{10}$ fold change of treated versus untreated group; FC: Fold change.

Table 4.3, continued.

Gene symbol	Gene name	Biological process	Log$_{10}$ (FC)[a]	Reference(s)
Atf1	Activating transcription factor 1	Cell differentiation, cellular component organization, nucleic acid-templated transcription, system development	−1.84	Bult et al. (2019); Kawakami and Fisher (2017); Roh et al. (2014)
Fzd6	Frizzled class receptor 6	Cell population proliferation, nucleic acid-templated transcription, response to stimulus, signaling, system development	−2.26	Bult et al. (2019); Carlson et al. (2007); Kanehisa and Goto (2000)
Mlph	Melanophilin	Melanocyte differentiation, melanosome localization, pigmentation, protein targeting	−2.76	Lee et al. (2018); The UniProt (2019)

[a]The value is presented as log$_{10}$ fold change of treated versus untreated group; FC: Fold change.

The expression of selected DEGs involved in melanogenesis was validated using qPCR analysis and the results are shown in Figure 4.14. Treatment with H-3 for 48 hours significantly downregulated *Creb3l2*, *Creb3l3*, *Mitf*, *Tyr*, *Tyrp1*, and *Dct*, while *Map3k20* and *Mapk14* presented a significant increment in the expression level. The results of the qPCR analysis were therefore consistent with the microarray profile (Table 4.3). Based on the microarray and qPCR analysis, the possible involvement of H-3 in the signaling pathway related to reduction melanogenesis in B16F10 melanoma cells are summarized in Figure 4.15.
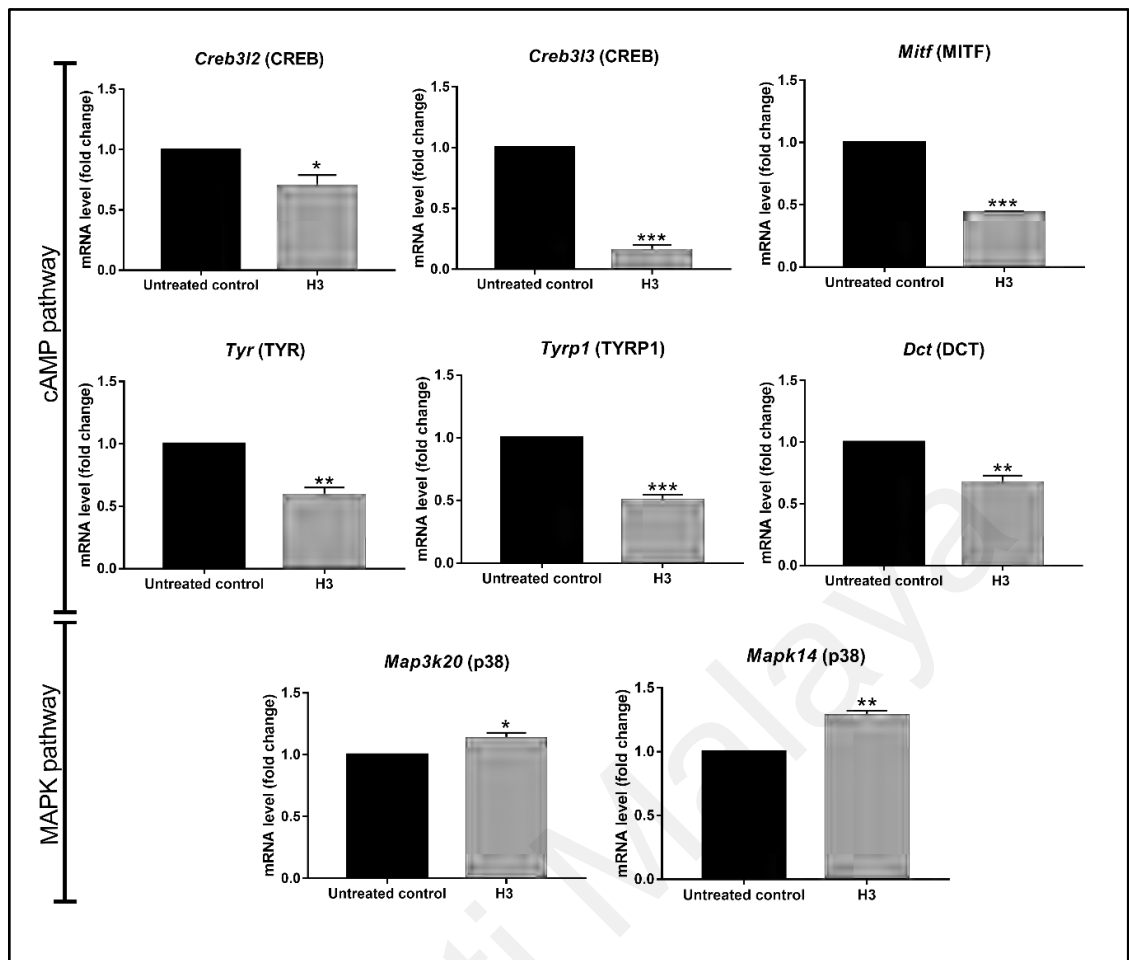
Figure 4.14: mRNA level of selected genes related to melanogenesis in B16F10 melanoma cells. mRNA level was examined using qPCR. The $2^{-\Delta\Delta Cq}$ method was employed to quantify the changes in expression level between the untreated control and H-3 (12 µg/mL) cells and was based on the normalisation with *Gapdh* (reference gene). The data are presented as the mean ± standard deviation of three experimental observations (*$p < 0.05$, **$p < 0.005$, ***$p < 0.0005$, multiple *t*-test).
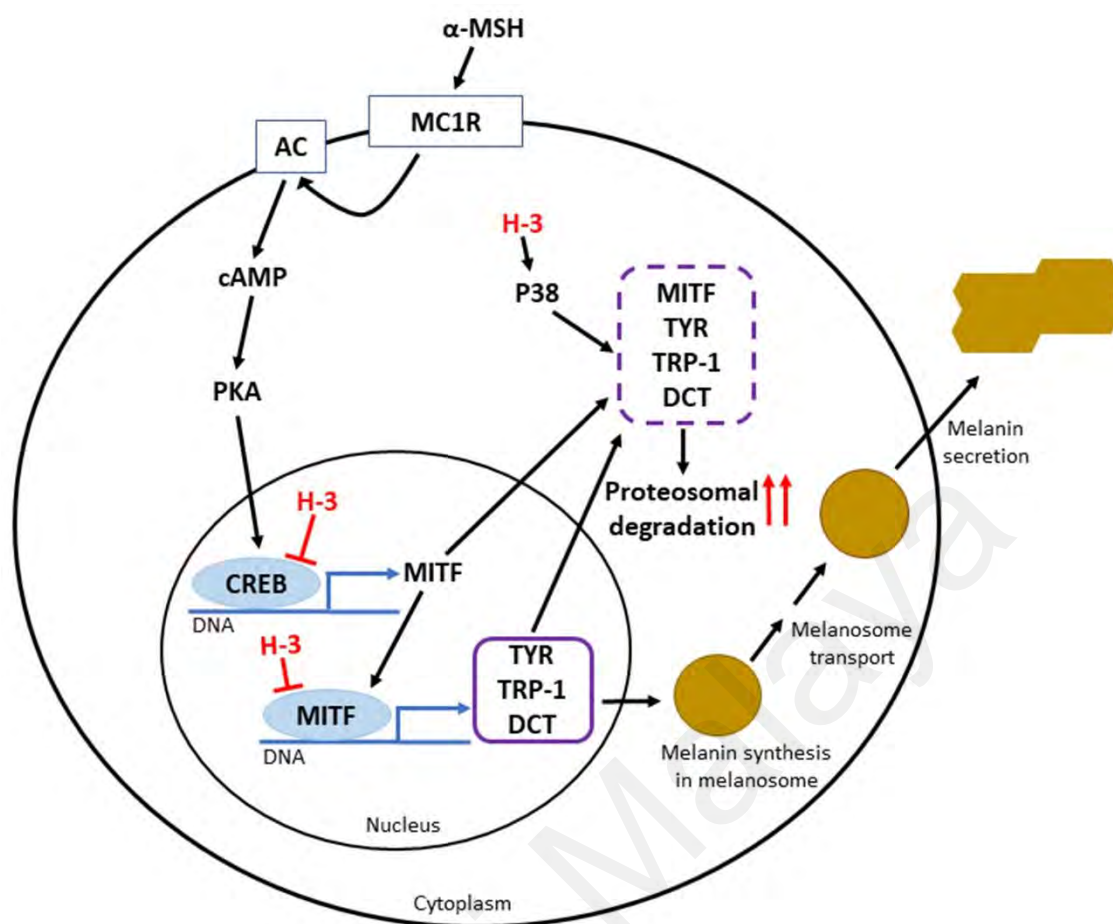
Figure 4.15: Putative anti-melanogenesis mechanisms of H-3 in B16F10 melanoma cells.

4.11   Physicochemical characteristics and *in vitro* release profile of prepared liposomes

The physicochemical characteristics of blank and H-3 liposomes have been analysed and the results is listed in Table 4.4. The average size of the blank and H-3 liposomes was 183.47 ± 10.95 and 185.17 ± 4.41 nm, respectively. The PDI value of blank liposomes was 0.35 ± 0.02 whereas H-3 liposomes recorded a PDI value of 0.38 ± 0.07. Both blank and H-3 liposomes had a negative zeta potential, with an average value of -38 mV. The encapsulation efficiency for H-3 liposomes was $78.54 \pm 2.76\%$. The *in vitro* release of H-3 depicted a biphasic release pattern, with an initial burst release at first hour (39.09 ± 4.01 %) and followed by prolonged and sustained release ($\sim 70\%$) for over 72 hours (Figure 4.16).

Table 4.4: Physicochemical characterization of prepared liposomes.

Liposomes	Size (nm)	PDI	Zp (mV)	EE (%)
Blank	183.47 ± 10.95	0.35 ± 0.02	-37.58 ± 2.03	NA
H-3	185.17 ± 4.41	0.38 ± 0.07	-37.93 ± 2.57	78.54 ± 2.76

Zp: zeta potential; EE: encapsulation efficiency; NA: not applicable.
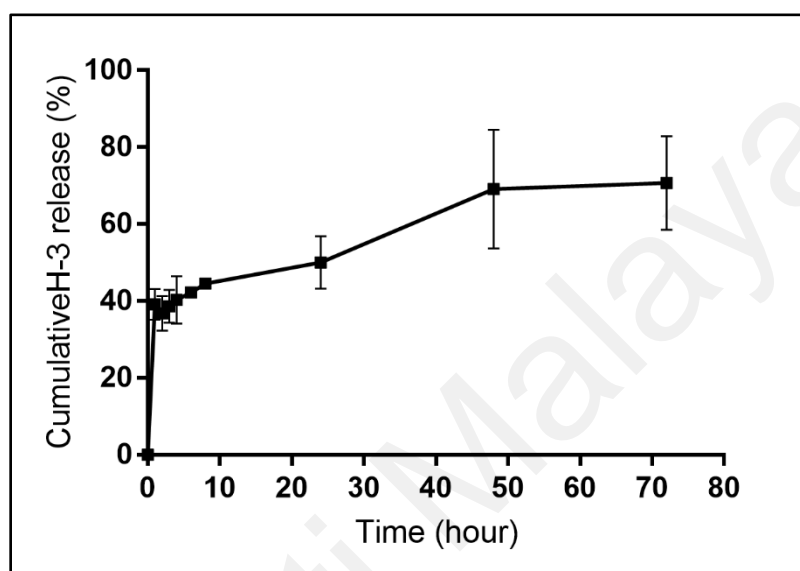
Figure 4.16: *In vitro* release profile of H-3.

4.12 Effect of liposomes on cell viability and melanin content

The effect of blank and H-3 liposomes on cell viability and melanin content in B16F10 melanoma cells was investigated and the results is displayed in Figure 4.17. As shown in Figure 4.17 (A), both blank and H-3 liposomes were not cytotoxic on B16F10 melanoma cells with cell viability of 99.12 ± 7.84 and $82.50 \pm 6.57\%$ at 12 µg/mL, respectively. The percentage of melanin content presented by blank liposomes at 12 µg/mL was $78.78 \pm 3.56\%$ whereas H-3 liposomes reduce the melanin content to $27.78 \pm 2.69\%$ at the same concentration (Figure 4.17 (B)).
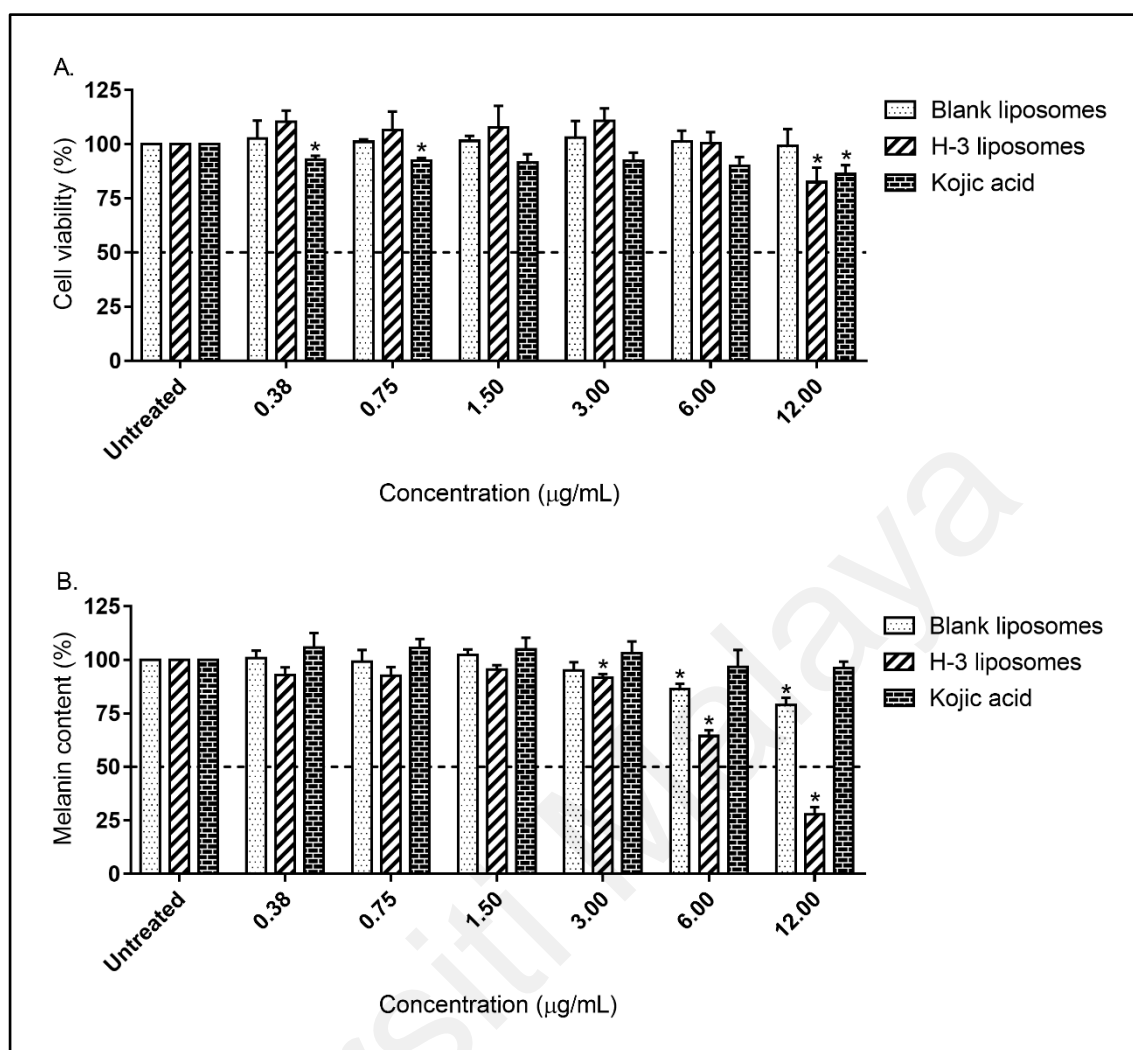
Figure 4.17: Viability (A) and melanin content (B) of B16F10 melanoma cells after treatment with blank and H-3 liposomes for 48 hours. Values are expressed as the mean ± standard deviation of three independent experiments. *$p < 0.05$ indicates significant different from untreated group.

CHAPTER 5: DISCUSSION

In the effort to study the anti-melanogenesis effects of *Artocarpus* species, fifteen *Artocarpus* extracts were firstly screened in a cell-free assay using tyrosinase from mushroom which are commercially available and cost effective. The obtained results demonstrated that both *A. integer* peel and *A. altilis* stem bark extracts exerted strong mushroom tyrosinase inhibitory activity (Figure 4.1) and it was reported that the *A. altilis* stem bark extract comprised of prenylated flavones with 4-substituted resorcinol moiety such as morusin, artocarpin, and hydroxyartocarpin (Shamaun et al., 2010) which exhibited strong anti-tyrosinase activity (Jiménez & García-Carmona, 1997). Hence, the high inhibitory effect on mushroom tyrosinase activity by *A. altilis* stem bark extract as evident from its low IC$_{50}$ could possibly be attributed by these chemical constituents. The stem bark and leaf extracts of *A. altilis*, *A. heterophyllus*, and *A. integer* possessed a notably lower activity when compared with previous studies conducted by Dej-adisai et al. (2014) and Liyanaarachchi et al. (2018) in Thailand and Sri Lanka, suggesting that the biological activity of the extracts may be affected by the variations in the phytochemical composition of the samples taken from two distinct geographical locations (Nguyen et al., 2012; Zheng et al., 2008).

The anti-melanogenesis assessment was continued with cellular assays using B16F10 melanoma cells where the pigmentation and cytotoxicity mechanism are similar to the normal melanocytes as well as rapid growth rate (Chaikul et al., 2017; Cheng et al., 2018). It was observed that all *Artocarpus* extracts were non-cytotoxic except for the *A. altilis* leaf, *A. altilis* stem bark, *A. integer* stem bark, and *A. rigidus* stem bark extracts (Figure 4.2). In melanin content assay, *A. elasticus* peel and *A. heterophylllus* stem bark & peel presented the best inhibitory effect, which was four folds better than positive control, kojic acid that is a well-known cosmeceutical ingredient for hyperpigmentation treatment

(Tetali et al., 2020) (Figure 4.3). The *A. heterophyllus* peel and stem bark extracts were then selected for the cellular tyrosinase assay due to their low toxicity and potent intracellular melanin content reducing effect. Although *A. elasticus* peel extract treatment produced a marked intracellular melanin content reducing effect, this extract was excluded in cellular tyrosinase assay due to its moderate toxicity (cell viability $69.13 \pm 2.35\%$, Figure 4.2) at the highest concentration tested (50.00 µg/mL).

In cellular tyrosinase assay, both *A. heterophyllus* peel and stem bark extracts reduced cellular tyrosinase activity with 1.42 and 1.85 folds stronger than kojic acid at 50 µg/mL (Figure 4.4). Interestingly, both *A. heterophyllus* peel and stem bark extracts presented a weak mushroom tyrosinase inhibitory activity ($IC_{50} > 0.5$ mg/mL, Figure 4.1) despite of a potent cellular tyrosinase inhibitory effect (Figure 4.4). Such variation of results suggested that the inhibitory effect of *A. heterophyllus* peel and stem bark extracts are highly specific to the enzyme structure, whereby they interact more readily with cellular tyrosinase (membrane bound monomer enzyme) rather than the mushroom tyrosinase (soluble tetramer enzyme) (Chang, 2009; Nishioka, 1978; Parvez et al., 2007). Besides that, the active components of *A. heterophyllus* peel and stem bark extracts may be the pro-drugs which become active during intracellular biotransformation (Kim et al., 2012). On that account, *A. heterophyllus* peel and stem bark extracts may be considered as a strong anti-melanogenesis agent based on the result from cellular tyrosinase assay instead of that in mushroom tyrosinase assay, since cellular tyrosinase resemble more to mammalian melanocytes system than the mushroom tyrosinase.

The radical scavenging activity of *Artocarpus* extracts was determined for indirect anti-melanogenesis evaluation. Three radical scavenging assays were performed which include DPPH•, $ABTS^+$•, and $O2^-$• assays. Botanical samples are known to comprise complex chemical constituents, hence multiple radical scavenging assays need to be carried out in order to verify the antioxidant capacity of the *Artocarpus* extracts (Huang

et al., 2005). The results generally showed that all *Artocarpus* extracts exhibited a relatively strong ability to scavenge $ABTS^{+\bullet}$ than those of $DPPH\bullet$ and $O2^{-\bullet}$, suggesting the extracts are more capable of scavenging cationic radicals rather than the neutral or anionic radicals. *A. elasticus* peel extract exhibited the most prominent radical scavenging ability in all three assays ($IC_{50} < 0.5$ mg/mL) and is classified as a very strong antioxidant (AAI 5.22) (Scherer & Godoy, 2009). This observation is in agreement with the previous study by Lin et al. (2009) on *A. elasticus* root extract that comprises of prenylated flavonoids such as artonol A, cycloartelastoxanthone, cycloartobiloxanthone, and artelastoheterol with a strong $DPPH\bullet$ scavenging activity (IC_{50} 18.70–42.20 µM).

The other assay that has been performed for indirect anti-melanogenesis evaluation of *Artocarpus* extracts was UV absorption analysis. UV light is known to cause hyperpigmentation-related disorders such as melasma, solar lentigines, and ephelides (Passeron & Picardo, 2018; Plensdorf & Martinez, 2009). An effective sunscreen substance is able to protect the skin from tanning, sunburn, and skin damages through its ability absorb UVB and UVA lights (Fonseca & Rafaela, 2013; Lee et al., 2013). All *Artocarpus* extract possessed weak sun screening effect with SPF value below than 10 (Figure 4.6) with only *A. altilis* leaf extract (SPF 5.84) possessed a considerable sun screening effect on black and dark brown skin type V and VI (Fitzpatrick classification of , Table 2.1) (Fonseca & Rafaela, 2013).

Anti-melanogenesis evaluation of *Artocarpus* extracts highlighted that *A. heterophyllus* peel and stem bark extracts exhibited a pronounced inhibitory effect on melanin production and cellular tyrosinase activity in B16F10 melanoma cells without significant cytotoxicity (Figure 4.2, 4.3, and 4.4). However, only *A. heterophyllus* stem bark extract was subjected for further anti-melanogenesis study as this extract demonstrated a slightly higher anti-melanogenesis activity (Figure 4.3 and 4.4) compared

to *A. heterophyllus* peel extract at 50 µg/mL. Moreover, the weight of *A. heterophyllus* stem bark extract (Table 4.1) was adequate for further analysis.

The bioassay-guided fractionation of *A. heterophyllus* stem bark extract ultimately yielded a semi-pure fraction H-3 (Figure 3.2), which potently reduced melanin content and inhibited cellular tyrosinase activity in B16F10 melanoma cells at concentration of 12 µg/mL (Figure 4.9 and 4.10). Based on the LCMS analysis, three prenylated flavonoids which include artonin B, cudraflavone A, and cyclomorusin, and a flavone (polystachin) have been identified in H-3. In addition, these prenylated flavonoids have been reported to be present in the Moraceae family. Moreover, cyclomorusin was reported to have various biological activities such as anti-tyrosinase, anti-inflammatory, anti-platelet, and anti-phosphodiesterase activities (Chun-Nan et al., 1993; Guo et al., 2018; Ryu et al., 2008; Wei et al., 2005). Besides that, artonin B was shown to have potent anti-inflammatory, radical scavenging activities, and cytotoxic against human leukemia cells by inducing apoptosis (Ko et al., 1998; Lee et al., 2006; Wei et al., 2005). Hence, it was tentatively suggested that chemical constituents which presented in H-3, especially cyclomorusin with intense anti-tyrosinase activity, artonin B with excellent radical scavenging capabilities, and the synergistic effects from all chemical constituents might be contributed to the strong anti-melanogenic effect in B16F10 melanoma cells.

To further understand the anti-melanogenic mechanisms of H-3 in B16F10 melanoma cells, microarray profiling and qPCR analysis were performed. With all the gene expression results (Table 4.3 and Figure 4.12, 4.13, and 4.14), the probable mechanisms of H-3 in B16F10 melanoma cells are outlined in Figure 4.15. Notably, H-3 treatment downregulated the expression of *Mitf*, a dimeric transcription factor that functions as a master regulator of melanogenesis, as well as a regulator of survival and differentiation of melanocytes (Bino et al., 2018; Levy et al., 2006). This indicated that H-3 could have directly decreased the expression of *Mitf* gene that subsequently downregulated three

crucial genes for melanogenesis, viz., *Tyr*, *Tyrp1*, and *Dct* (Sun et al., 2020) (Figure 4.15), leading to a decreased melanin content and inhibition of cellular tyrosinase activity in B16F10 melanoma cells.

The expression of MITF protein can be regulated transcriptionally through the cAMP signaling pathway (Price et al., 1998). As shown in Figure 4.15, the activation of the cAMP signaling pathway starts with the binding of α-MSH to MC1R, which in turn activates PKA through cAMP induction. The ensuing activated PKA translocates into the nucleus and thereby phosphorylates the CREB protein, ultimately initiating the transcription of MITF (Pillaiyar et al., 2017a; Wu et al., 2019). Since the current study showed that H-3 treatment also decreased the expression of *Creb3l1*, *Creb3l2*, and *Creb3l3* genes (CREB), it is suggested that H-3 could have downregulated the *Mitf* gene in B16F10 melanoma cells through the inhibition of the cAMP/PKA signaling pathway. In addition, *Atf1* gene (cAMP dependent transcription factor, ATF-1) was downregulated upon H-3 treatment. ATF-1 is a crucial component in the cAMP signaling pathway, where the binding of this protein will activate CREB (Kawakami & Fisher, 2017). The decreased *Atf1* gene expression and the subsequent inhibition of the cAMP/PKA signaling pathway have been observed in our studies, which are in accordance with those conducted by Roh et al. (2014), thus providing further verification that H-3 exhibited anti-melanogenic activity through the inhibition of this pathway.

Since treatment with H-3 has also significantly increased the expression of *Map3k20* and *Mapk14* genes (p38) (Table 4.3, Figure 4.12, and 4.13), another hypothesized mechanism of H-3 is through the post-translational modification of MITF *via* ubiquitination (Alam et al., 2017; Wu et al., 2000), which involved the activation of the MAPK signaling pathway (Hsiao & Fisher, 2014). P38 is a stress-regulated protein kinase belonging to the MAPK superfamily, whereby it can be activated by several stimuli, such as ultraviolet light, irradiation, heat shock, osmotic stress, and pro-inflammatory

cytokines (Bellei et al., 2010). Studies conducted by Ko et al. (2019) and Ko et al. (2014) reported that eupafolin and *Annona squamosa* leaves extract have increased the expression of p38, subsequently leading to the manifestation of their anti-melanogenic activities. In addition to *Map3k20* and *Mapk14* genes (p38), H-3 also upregulated the expression *Uchl1os* gene (ubiquitin carboxyl-terminal hydrolase isozyme L1), indicating that H-3 reduced melanogenesis in B16F10 melanoma cells through the activation of the MAPK pathway, subsequently ubiquitinating the proteins involved in melanogenesis, such as MITF, tyrosinase, TYRP-1, and DCT in a proteasome-dependent mechanism (Figure 4.15) (Alam et al., 2018; Bellei et al., 2010).

The synthesized melanin in the melanosome will be transported to neighboring keratinocytes to distribute the melanin (Tsatmali et al., 2002). Aside from reducing melanin synthesis, H-3 could have interfered the melanosome transport, as downregulation of the genes involved in melanosome transport was detected, such as *Mlph* (Lee et al., 2018; Taira et al., 2018) and *Gpr143* (Makbal et al., 2020) (Table 4.3). It has been reported that autophagy plays an important role in regulating melanogenesis by inducing melanosome degradation through autophagosomes (Jeong et al., 2020; Kim et al., 2020). In accordance with this, the markers for autophagy, such as *Sqstm1* (p62) and *Ulk1* (ULK1) were upregulated upon H-3 treatment for 48 hours (Table 4.3), suggesting that H-3 have probably activated autophagy and carried out melanosome degradation.

Reactive oxygen species (ROS) is a signaling molecule in the activation of the melanogenic pathway, hence, it is reasonable to suggest that scavenging ROS could be an effective approach to inhibit melanogenesis (Ochiai et al., 2008). The effect of H-3 on intracellular ROS was analysed using flow cytometry and the results showed that H-3 reduced ROS level in B16F10 melanoma cells that was previously elevated by H_2O_2 (Figure 4.11). Kim et al. (2014b) have shown that radical scavengers, such as vitamin C,

N-acetylcysteine, and Trolox potently inhibited melanogenesis in melanoma cells by activating Forkhead Box O3 transcription factor (FOXO3a), a regulator that involved in the antioxidative response in skin cells and other cell types (Kim et al., 2014b). Additionally, Kwon et al. (2017) reported that resveratrol, an anti-melanogenic agent exhibited ROS scavenging effect and induced the expression of FOXO3a protein in melanoma cells. In line with these studies, our microarray profile revealed that H-3 significantly upregulated the expression of the *Foxo3* gene (Table 4.3). Therefore, it can be hypothesized that the ROS scavenging ability of H-3 could be one of its anti-melanogenic mechanisms in B16F10 melanoma cells whereby the reduction of ROS concentration will lead to the increment of the *Foxo3* gene expression and subsequently decrease in melanin production.

Studies have shown that topical application liposomal formulation facilitates the penetration of active substances into the stratum corneum, the epidermis's topmost layer (Yoo et al., 2008). Due to the promising anti-melanogenic effect, the bioactive fraction (H-3) was incorporated into the liposomes with the addition of oleic acid as a skin penetration enhancer. The encapsulation of H-3 in liposomes yields vesicles with a size of 185 nm and a PDI value of 0.3 (Table 4.4), showing that H-3 liposomes have a moderate polydisperse distribution (Banna et al., 2018). In addition, with a zeta potential of > -30 mV, H-3 showed good physical stability in the colloidal system (Table 4.4). As a result, particle aggregation is unlikely to develop due to the electrostatic repulsion (Teeranachaideekul et al., 2007). In comparison to the neutral and positively charged liposomes, negatively charged liposomes also had a greater flux across the negatively charged epidermis (Gillet et al., 2011; Sinico et al., 2005). The release pattern of H-3 from liposomes was observed through *in vitro* release assay and it was discovered that H-3 liposomes had a biphasic release pattern (Figure 4.16). The initial burst release of H-3 will facilitate the permeation of H-3 into the skin by providing a sufficient

concentration gradient, while the sustained release will maintain the local concentration in the targeted area. The slow-release of H-3 from the liposomes over an extended time highlighted an optimal aspect of this delivery system, resulting a prolonged anti-melanogenesis effect in the skin (Al-Amin et al., 2016; Banna et al., 2018). In the anti-melanogenesis assessment using B16F10 melanoma cells, H-3 liposomes at 12 μg/mL presented an excellent melanin reduction effect without cytotoxicity which is similar to the free H-3 at the same concentration (Figure 4.9 and 4.17). Since liposomes are composed of a component similar to the cell membrane (phospholipids), it enables the cells to recognize the lipid vesicles and initiates the fusion of the lipid vesicles into the cells. Subsequently, H-3 contained in the lipid vesicles will be delivered directly into the B16F10 melanoma cells (Singpanna et al., 2021). These results imply that the liposomes formulation used in this study was an effective delivery strategy for H-3, resulting in an outstanding anti-melanogenesis activity in B16F10 melanoma cells.

CHAPTER 6: CONCLUSION AND RECOMMENDATIONS

The preliminary cosmeceutical evaluation of *Artocarpus* extracts revealed that *A. heterophyllus* peel and stem bark extracts are two candidates with strong anti-melanogenesis activity with substantial melanin content reduction ability and potent cellular tyrosinase inhibitory activity without toxicity, whereby all these activities are better than the positive control, kojic acid. On the other hand, *A. elasticus* peel extract exhibited a remarkable radical scavenging ability which shed some light on the potentiality of this extract to be used as an anti-aging or naturally additive ingredients to prevent oxidation in cosmeceutical. However, the concentration of the extract should be handled carefully to avoid dose-limited toxicity.

The in-depth anti-melanogenesis study involving bioassay-guided fractionation of *A. heterophyllus* stem bark yielded H-3, the bioactive fraction in suppressing melanogenesis in B16F10 melanoma cells by reducing melanin content and inhibiting cellular tyrosinase activity at a non-cytotoxic concentration (12 µg/mL). The molecular analyses showed that H-3 exhibited multifunctional inhibitory activity against melanogenesis by direct suppression of *Mitf*, inhibition of the cAMP pathway, activation of the MAPK signaling pathways, melanosome degradation, as well as scavenging the ROS in B16F10 melanoma cells.

The encapsulation of H-3 in liposomes resulted in a good anti-melanogenesis effect in B16F10 melanoma cells without noticeable cytotoxicity. The results depicted that the encapsulation did not affect the intrinsic anti-melanogenesis activity of H-3 and possessed a high potential to be developed for cosmeceutical application.

This study has proved the potential of *A. heterophyllus* stem bark in skin lightening application by highlighting the signaling pathways involved by bioactive fraction H-3 in its anti-melanogenesis effect. Furthermore, these findings showed that bioactive fraction H-3 possessed a versatile mechanism that targeted several anti-melanogenesis markers and signaling pathways. It is hoped that when the skin permeation, skin irritation, *in vivo* studies of H-3 liposomes are clarified, the attractiveness and potential of H-3 from *A. heterophyllus* stem bark as active ingredients in skin-lightening cosmeceutical for the treatment of hyperpigmentation disorders can be substantially enhanced.

REFERENCES

Abd, E., Roberts, M. S., & Grice, J. E. (2016). A comparison of the penetration and permeation of caffeine into and through human epidermis after application in various vesicle formulations. *Skin Pharmacology and Physiology*, *29*(1), 24-30.

Al-Amin, M., Cao, J., Naeem, M., Banna, H., Kim, M.-S., Jung, Y., . . . Yoo, J.-W. (2016). Increased therapeutic efficacy of a newly synthesized tyrosinase inhibitor by solid lipid nanoparticles in the topical treatment of hyperpigmentation. *Drug Design, Development and Therapy*, *10*, 3947-3957.

Alam, M. B., Ahmed, A., Motin, M. A., Kim, S., & Lee, S.-H. (2018). Attenuation of melanogenesis by *Nymphaea nouchali* (Burm. f) flower extract through the regulation of cAMP/CREB/MAPKs/MITF and proteasomal degradation of tyrosinase. *Scientific Reports*, *8*(1), Article#13928.

Alam, M. B., Bajpai, V. K., Lee, J., Zhao, P., Byeon, J.-H., Ra, J.-S., . . . Lee, S.-H. (2017). Inhibition of melanogenesis by jineol from *Scolopendra subspinipes mutilans* via MAP-Kinase mediated MITF downregulation and the proteasomal degradation of tyrosinase. *Scientific Reports*, *7*(1), Article#45858.

Alam, N., Yoon, K. N., & Lee, T. S. (2011). Evaluation of the antioxidant and antityrosinase activities of three extracts from *Pleurotus nebrodensis* fruiting bodies. *African Journal of Biotechnology*, *10*(15), 2978-2986.

Ali, S. A., Choudhary, R. K., Naaz, I., & Ali, A. S. (2015). Understanding the challenges of melanogenesis: key role of bioactive compounds in the treatment of hyperpigmentory disorders. *Journal of Pigmentary Disorders*, *2*, Article#1000223.

Alves, A., Sousa, E., Kijjoa, A., & Pinto, M. (2020). Marine-derived compounds with potential use as cosmeceuticals and nutricosmetics. *Molecules*, *25*(11), Article#2536.

Ammala, A. (2013). Biodegradable polymers as encapsulation materials for cosmetics and personal care markets. *International Journal of Cosmetic Science*, *35*(2), 113-124.

Arda, O., Göksügür, N., & Tüzün, Y. (2014). Basic histological structure and functions of facial skin. *Clinics in Dermatology*, *32*(1), 3-13.

Arung, E. T., Shimizu, K., & Kondo, R. (2006). Inhibitory effect of artocarpanone from *Artocarpus heterophyllus* on melanin biosynthesis. *Biological and Pharmaceutical Bulletin*, *29*(9), 1966-1969.

Arung, E. T., Shimizu, K., Tanaka, H., & Kondo, R. (2010). 3-Prenyl luteolin, a new prenylated flavone with melanin biosynthesis inhibitory activity from wood of *Artocarpus heterophyllus*. *Fitoterapia*, *81*(6), 640-643.

Atefi, N., Dalvand, B., Ghassemi, M., Mehran, G., & Heydarian, A. (2017). Therapeutic effects of topical tranexamic acid in comparison with hydroquinone in treatment of women with melasma. *Dermatology and Therapy*, *7*(3), 417-424.

Aust, D. T., Ross, M. A., Wilmott, J. M., & Hayward, J. A. (2001). *Stabilizing vitamin A derivatives by encapsulation in lipid vesicles formed with alkylammonium fatty acid salts* (United States Patent No. 6,183,774 B1).

Bahreini, E., Aghaiypour, K., Abbasalipourkabir, R., Mokarram, A. R., Goodarzi, M. T., & Saidijam, M. (2014). Preparation and nanoencapsulation of l-asparaginase II in chitosan-tripolyphosphate nanoparticles and i*n vitro* release study. *Nanoscale Research Letters*, *9*(1), Article#340.

Bakar, M. F. A., Karim, F. A., & Perisamy, E. (2015). Comparison of phytochemicals and antioxidant properties of different fruit parts of selected *Artocarpus* species from Sabah, Malaysia. *Sains Malaysiana*, *44*(3), 355-363.

Baker, L. B. (2019). Physiology of sweat gland function: the roles of sweating and sweat composition in human health. *Temperature*, *6*(3), 211-259.

Baliga, M. S., Shivashankara, A. R., Haniadka, R., Dsouza, J., & Bhat, H. P. (2011). Phytochemistry, nutritional and pharmacological properties of *Artocarpus heterophyllus* Lam (jackfruit): a review. *Food Research International*, *44*(7), 1800-1811.

Banna, H., Hasan, N., Lee, J., Kim, J., Cao, J., Lee, E. H., . . . Yoo, J.-W. (2018). *In vitro* and *in vivo* evaluation of MHY908-loaded nanostructured lipid carriers for the topical treatment of hyperpigmentation. *Journal of Drug Delivery Science and Technology*, *48*, 457-465.

Baroni, A., Buommino, E., De Gregorio, V., Ruocco, E., Ruocco, V., & Wolf, R. (2012). Structure and function of the epidermis related to barrier properties. *Clinics in Dermatology*, *30*(3), 257-262.

Bastiaens, M., Hoefnagel, J., Westendorp, R., Vermeer, B.-J., & Bouwes Bavinck, J. N. (2004). Solar Lentigines are strongly related to sun exposure in contrast to ephelides. *Pigment Cell Research*, *17*(3), 225-229.

Bellei, B., Maresca, V., Flori, E., Pitisci, A., Larue, L., & Picardo, M. (2010). p38 regulates pigmentation via proteasomal degradation of tyrosinase. *Journal of Biological Chemistry*, *285*(10), 7288-7299.

Bellei, B., Pitisci, A., Izzo, E., & Picardo, M. (2012). Inhibition of melanogenesis by the pyridinyl imidazole class of compounds: possible involvement of the Wnt/β-catenin signaling pathway. *PLoS One*, *7*(3), Article#e33021.

Berg, C. C., Corner, E. J. H., & Jarrett, F. (2006). Moraceae genera other than *Ficus*. *Flora Malesiana-Series 1, Spermatophyta*, *17*(1), 1-152.

Beserra, A. M. S. E. S., Vilegas, W., Tangerina, M. M. P., Ascêncio, S. D., Soares, I. M., Pavan, E., . . . Martins, D. T. D. O. (2018). Chemical characterisation and toxicity assessment *in vitro* and *in vivo* of the hydroethanolic extract of *Terminalia argentea* Mart. leaves. *Journal of Ethnopharmacology*, *227*, 56-68.

Bino, S. D., Duval, C., & Bernerd, F. (2018). Clinical and biological characterization of skin pigmentation diversity and its consequences on UV impact. *International Journal of Molecular Sciences*, *19*(9), Article#2668.

Bondurand, N., Pingault, V., Goerich, D. E., Lemort, N., Sock, E., Caignec, C. L., . . . Goossens, M. (2000). Interaction among SOX10, PAX3 and MITF, three genes altered in Waardenburg syndrome. *Human Molecular Genetics*, *9*(13), 1907-1917.

Brody, I. (1960). The ultrastructure of the tonofibrils in the keratinization process of normal human epidermis. *Journal of Ultrastructure Research*, *4*(3), 264-297.

Bult, C. J., Blake, J. A., Smith, C. L., Kadin, J. A., Richardson, J. E., & The Mouse Genome Database Group. (2019). Mouse genome database (MGD) 2019. *Nucleic Acids Research*, *47*(D1), D801-D806.

Busca, R., & Ballotti, R. (2000). Cyclic AMP a key messenger in the regulation of skin pigmentation. *Pigment Cell Research*, *13*(2), 60-69.

Bustin, S. A., Benes, V., Garson, J. A., Hellemans, J., Huggett, J., Kubista, M., . . . Wittwer, C. T. (2009). The MIQE guidelines: minimum information for publication of quantitative real-time PCR experiments. *Clinical Chemistry*, *55*(4), 611-622.

Buttara, M., Intarapichet, K. O., & Cadwallader, K. R. (2014). Characterization of potent odorants in Thai chempedak fruit (*Artocarpus integer* Merr.), an exotic fruit of Southeast Asia. *Food Research International*, *66*, 388-395.

Caddeo, C., Teskač, K., Sinico, C., & Kristl, J. (2008). Effect of resveratrol incorporated in liposomes on proliferation and UV-B protection of cells. *International Journal of Pharmaceutics*, *363*(1), 183-191.

Callender, V. D., St. Surin-Lord, S., Davis, E. C., & Maclin, M. (2011). Postinflammatory hyperpigmentation. *American Journal of Clinical Dermatology*, *12*(2), 87-99.

Carlson, J. A., Linette, G. P., Aplin, A., Ng, B., & Slominski, A. (2007). Melanocyte receptors: clinical implications and therapeutic relevance. *Dermatologic Clinics*, *25*(4), 541-557.

Casanova, F., & Santos, L. (2016). Encapsulation of cosmetic active ingredients for topical application–a review. *Journal of Microencapsulation*, *33*(1), 1-17.

Cerqueira, F., Cidade, H., Van Ufford, L., Beukelman, C., Kijjoa, A., & Nascimento, M. (2008). The natural prenylated flavone artelastin is an inhibitor of ROS and NO production. *International Immunopharmacology*, *8*(4), 597-602.

Chaikul, P., Lourith, N., & Kanlayavattanakul, M. (2017). Antimelanogenesis and cellular antioxidant activities of rubber (*Hevea brasiliensis*) seed oil for cosmetics. *Industrial Crops and Products*, *108*, 56-62.

Chan, Y., Kim, K., & Cheah, S. (2011). Inhibitory effects of *Sargassum polycystum* on tyrosinase activity and melanin formation in B16F10 murine melanoma cells. *Journal of Ethnopharmacology*, *137*(3), 1183-1188.

Chang, T.-S. (2009). An updated review of tyrosinase inhibitors. *International Journal of Molecular Sciences*, *10*(6), 2440-2475.

Chang, T.-S. (2012). Natural melanogenesis inhibitors acting through the down-regulation of tyrosinase activity. *Materials*, *5*(9), 1661-1685.

Charles Dorni, A. I., Amalraj, A., Gopi, S., Varma, K., & Anjana, S. N. (2017). Novel cosmeceuticals from plants—an industry guided review. *Journal of Applied Research on Medicinal and Aromatic Plants*, *7*, 1-26.

Chatatikun, M., & Chiabchalard, A. (2017). Thai plants with high antioxidant levels, free radical scavenging activity, anti-tyrosinase and anti-collagenase activity. *BMC Complementary and Alternative Medicine*, *17*, Article#487.

Cheng, M. C., Lee, T. H., Chu, Y. T., Syu, L. L., Hsu, S. J., Cheng, C. H., . . . Lee, C. K. (2018). Melanogenesis inhibitors from the rhizoma of *Ligusticum sinense* in B16-F10 melanoma cells *in vitro* and zebrafish *in vivo*. *International Journal of Molecular Sciences*, *19*(12), Article#3994.

Chun-Nan, L., Wen-Liang, S., Feng-Nien, K., & Che-Ming, T. (1993). Antiplatelet activity of some prenylflavonoids. *Biochemical pharmacology*, *45*(2), 509-512.

Chung, J. Y., Lee, J. H., & Lee, J. H. (2016). Topical tranexamic acid as an adjuvant treatment in melasma: side-by-side comparison clinical study. *Journal of Dermatological Treatment*, *27*(4), 373-377.

Davis, E. C., & Callender, V. D. (2010). Postinflammatory hyperpigmentation: a review of the epidemiology, clinical features, and treatment options in skin of color. *The Journal of Clinical and Aesthetic Dermatology*, *3*(7), 20-31.

Deb, P. K., Al-Attraqchi, O., Chandrasekaran, B., Paradkar, A., & Tekade, R. K. (2019). Chapter 16 - Protein/peptide drug delivery systems: practical considerations in pharmaceutical product development. In R. K. Tekade (Ed.), *Basic Fundamentals of Drug Delivery* (pp. 651-684). Academic Press.

Dej-adisai, S., Meechai, I., Puripattanavong, J., & Kummee, S. (2014). Antityrosinase and antimicrobial activities from Thai medicinal plants. *Archives of Pharmacal Research*, *37*(4), 473-483.

Draelos, Z. D., Elewski, B. E., Harper, J. C., Sand, M., Staedtler, G., Nkulikiyinka, R., . . . Shakery, K. (2015). A phase 3 randomized, double-blind, vehicle-controlled trial of azelaic acid foam 15% in the treatment of papulopustular rosacea. *Cutis*, *96*(1), 54-61.

Elias, P. M. (2005). Stratum corneum defensive functions: an integrated view. *Journal of Investigative Dermatology*, *125*(2), 183-200.

Ephrem, E., Elaissari, H., & Greige-Gerges, H. (2017). Improvement of skin whitening agents efficiency through encapsulation: current state of knowledge. *International Journal of Pharmaceutics*, *526*(1), 50-68.

Esposito, E., Menegatti, E., & Cortesi, R. (2004). Ethosomes and liposomes as topical vehicles for azelaic acid: a preformulation study. *International Journal of Cosmetic Science*, *26*(5), 270-271.

Etti, I. C., Abdullah, R., Kadir, A., Hashim, N. M., Yeap, S. K., Imam, M. U., . . . Etti, U. (2017). The molecular mechanism of the anticancer effect of artonin E in MDA-MB 231 triple negative breast cancer cells. *PLoS One*, *12*(8), Article#e0182357.

Fitzpatrick, T. B. (1988). The validity and practicality of sun-reactive skin types I through VI. *Archives of Dermatology*, *124*(6), 869-871.

Fonseca, A., & Rafaela, N. (2013). Determination of sun protection factor by UV-vis spectrophotometry. *Health Care: Current Reviews*, *1*(1), Article#1000108.

Fowler Jr, J. F., Woolery-Lloyd, H., Waldorf, H., & Saini, R. (2010). Innovations in natural ingredients and their use in skin care. *Journal of Drugs in Dermatology*, *9*(6), s72-s81.

Fu, Y.-H., Guo, J.-M., Xie, Y.-T., Yu, X.-M., Su, Q.-T., Qiang, L., . . . Liu, Y.-P. (2020). Prenylated chromones from the fruits of *Artocarpus heterophyllus* and their potential anti-HIV-1 activities. *Journal of Agricultural and Food Chemistry*, *68*(7), 2024-2030.

Gillet, A., Compère, P., Lecomte, F., Hubert, P., Ducat, E., Evrard, B., . . . Piel, G. (2011). Liposome surface charge influence on skin penetration behaviour. *International Journal of Pharmaceutics*, *411*(1), 223-231.

Glen Alvin, M., Nino Catambay, M., Ailynne Vergara, M., & Jamora, M. (2011). A comparative study of the safety and efficacy of 75% mulberry (*Morus alba*) extract oil versus placebo as a topical treatment for melasma: a randomized, single-blind, placebo-controlled trial. *Journal of Drugs in Dermatology*, *10*(9), 1025-1031.

Glick, D., Barth, S., & Macleod, K. F. (2010). Autophagy: cellular and molecular mechanisms. *The Journal of Pathology*, *221*(1), 3-12.

Gotoh, I., Adachi, M., & Nishida, E. (2001). Identification and characterization of a novel MAP kinase kinase kinase, MLTK. *Journal of Biological Chemistry*, *276*(6), 4276-4286.

Greenwood, M. P., Greenwood, M., Gillard, B. T., Chitra Devi, R., & Murphy, D. (2017). Regulation of cAMP responsive element binding protein 3-Like 1 (Creb3l1) expression by orphan nuclear receptor Nr4a1. *Frontiers in Molecular Neuroscience*, *10*, 413.

Gu, Y., Han, J., Jiang, C., & Zhang, Y. (2020). Biomarkers, oxidative stress and autophagy in skin aging. *Ageing Research Reviews*, *59*, Article#101036.

Guo, Y.-Q., Tang, G.-H., Lou, L.-L., Li, W., Zhang, B., Liu, B., . . . Yin, S. (2018). Prenylated flavonoids as potent phosphodiesterase-4 inhibitors from *Morus alba*: isolation, modification, and structure-activity relationship study. *European Journal of Medicinal Chemistry*, *144*, 758-766.

Gupta, V., & Sharma, V. K. (2019). Skin typing: Fitzpatrick grading and others. *Clinics in Dermatology*, *37*(5), 430-436.

Halaban, R., Patton, R. S., Cheng, E., Svedine, S., Trombetta, E. S., Wahl, M. L., . . . Hebert, D. N. (2002). Abnormal acidification of melanoma cells induces tyrosinase retention in the early secretory pathway. *Journal of Biological Chemistry*, *277*(17), 14821-14828.

Han, S. M., Kim, J. M., & Pak, S. C. (2015). Anti-melanogenic properties of honeybee (*Apis mellifera* L.) venom in α-MSH-stimulated B16F1 cells. *Food and Agricultural Immunology*, *26*(3), 451-462.

Hara, M., Yaar, M., Byers, H. R., Goukassian, D., Gonsalves, J., Gilchrest, B. A., . . . Fine, R. E. (2000). Kinesin participates in melanosomal movement along melanocyte dendrites. *Journal of Investigative Dermatology*, *114*(3), 438-443.

Harding, C. R. (2004). The stratum corneum: structure and function in health and disease. *Dermatologic Therapy*, *17*(s1), 6-15.

Ho, B. K., & Robinson, J. K. (2015). Color bar tool for skin type self-identification: a cross-sectional study. *Journal of the American Academy of Dermatology*, *73*(2), 312-313.

Hodge, B. D., Sanvictores, T., & Brodell, R. T. (2018). Anatomy, skin sweat glands. In *StatPearls [Internet]*. Treasure Island (FL): StatPearls Publishing. https://www.ncbi.nlm.nih.gov/books/NBK482278/

Hoover, E., Aslam, S., & Krishnamurthy, K. (2020). Physiology, sebaceous glands. In *StatPearls [Internet]*. Treasure Island (FL): StatPearls Publishing. https://www.ncbi.nlm.nih.gov/books/NBK499819/

Hsiao, J. J., & Fisher, D. E. (2014). The roles of microphthalmia-associated transcription factor and pigmentation in melanoma. *Archives of Biochemistry and Biophysics*, *563*, 28-34.

Huang, D., Ou, B., & Prior, R. L. (2005). The chemistry behind antioxidant capacity assays. *Journal of Agricultural and Food Chemistry*, *53*(6), 1841-1856.

Huang, H.-C., Hsieh, W.-Y., Niu, Y.-L., & Chang, T.-M. (2012). Inhibition of melanogenesis and antioxidant properties of *Magnolia grandiflora* L. flower extract. *BMC Complementary and Alternative Medicine*, *12*(1), 1-9, Article#72.

Hume, A. N., Collinson, L. M., Hopkins, C. R., Strom, M., Barral, D. C., Bossi, G., . . . Seabra, M. C. (2002). The leaden gene product is required with Rab27a to recruit myosin Va to melanosomes in melanocytes. *Traffic*, *3*(3), 193-202.

Jagtap, U., & Bapat, V. (2010). *Artocarpus*: a review of its traditional uses, phytochemistry and pharmacology. *Journal of Ethnopharmacology*, *129*(2), 142-166.

Jalal, T. K., Khan, A. a. Y. F., Natto, H. A., Abdull Rasad, M. S. B., Arifin Kaderi, M., Mohammad, M., . . . Abdul Wahab, R. (2019). Identification and quantification of quercetin, a major constituent of *Artocarpus altilis* by targeting related genes of apoptosis and cell cycle: *in vitro* cytotoxic activity against human lung carcinoma cell lines. *Nutrition and Cancer*, *71*(5), 792-805.

Jamil, S., Lathiff, S. M. A., Abdullah, S. A., Jemaon, N., & Sirat, H. M. (2014). Antimicrobial flavonoids from *Artocarpus Anisophyllus* miq. and *Artocarpus lowii* King. *Jurnal Teknologi*, *71*(1), 95-99.

Jang, K. A., Chung, E. C., Choi, J. H., Sung, K. J., Moon, K. C., & Koh, J. K. (2000). Successful removal of freckles in Asian skin with a Q‑switched alexandrite laser. *Dermatologic surgery*, *26*(3), 231-234.

Jegasothy, S. M., Zabolotniaia, V., & Bielfeldt, S. (2014). Efficacy of a new topical nano-hyaluronic acid in humans. *The Journal of Clinical and Aesthetic Dermatology*, *7*(3), 27-29.

Jeong, D., Park, S. H., Kim, M.-H., Lee, S., Cho, Y. K., Kim, Y. A., . . . Cho, J. Y. (2020). Anti-melanogenic effects of ethanol extracts of the leaves and roots of *Patrinia villosa* (Thunb.) juss through their inhibition of CREB and induction of ERK and autophagy. *Molecules*, *25*(22), Article#5375.

Jiménez, M., & García-Carmona, F. (1997). 4-Substituted resorcinols (sulfite alternatives) as slow-binding inhibitors of tyrosinase catecholase activity. *Journal of Agricultural and Food Chemistry*, *45*(6), 2061-2065.

Kammeyer, A., & Luiten, R. M. (2015). Oxidation events and skin aging. *Ageing Research Reviews*, *21*, 16-29.

Kanehisa, M., & Goto, S. (2000). KEGG: kyoto encyclopedia of genes and genomes. *Nucleic Acids Research*, *28*(1), 27-30.

Kanitakis, J. (2002). Anatomy, histology and immunohistochemistry of normal human skin. *European Journal of Dermatology*, *12*(4), 390-401.

Kaufman, B. P., Aman, T., & Alexis, A. F. (2018). Postinflammatory hyperpigmentation: epidemiology, clinical presentation, pathogenesis and treatment. *American Journal of Clinical Dermatology*, *19*(4), 489-503.

Kaur, C. D., & Saraf, S. (2010). *In vitro* sun protection factor determination of herbal oils used in cosmetics. *Pharmacognosy Research*, *2*(1), 22-25.

Kawada, A., Konishi, N., Momma, T., Oiso, N., & Kawara, S. (2009). Evaluation of anti-wrinkle effects of a novel cosmetic containing retinol using the guideline of the Japan Cosmetic Industry Association. *The Journal of Dermatology*, *36*(11), 583-586.

Kawakami, A., & Fisher, D. E. (2017). The master role of microphthalmia-associated transcription factor in melanocyte and melanoma biology. *Laboratory Investigation*, *97*(6), 649-656.

Keshet, Y., & Seger, R. (2010). *The MAP kinase signaling cascades: a system of hundreds of components regulates a diverse array of physiological functions* (R. Seger, Ed. Vol. 661). Humana Press.

Khaled, M., Larribere, L., Bille, K., Aberdam, E., Ortonne, J.-P., Ballotti, R., . . . Bertolotto, C. (2002). Glycogen synthase kinase 3β is activated by cAMP and plays an active role in the regulation of melanogenesis. *Journal of Biological Chemistry*, *277*(37), 33690-33697.

Kim, D.-S., Hwang, E.-S., Lee, J.-E., Kim, S.-Y., Kwon, S.-B., & Park, K.-C. (2003). Sphingosine-1-phosphate decreases melanin synthesis via sustained ERK activation and subsequent MITF degradation. *Journal of Cell Science*, *116*(9), 1699-1706.

Kim, E. S., Park, S. J., Goh, M.-J., Na, Y.-J., Jo, D. S., Jo, Y. K., . . . Cho, D.-H. (2014a). Mitochondrial dynamics regulate melanogenesis through proteasomal degradation of MITF via ROS-ERK activation. *Pigment Cell & Melanoma Research*, *27*(6), 1051-1062.

Kim, H., Kim, N., Jung, S., Mun, J., Kim, J., Kim, B., . . . Jung, H. (2010). Improvement in skin wrinkles from the use of photostable retinyl retinoate: a randomized controlled trial. *British Journal of Dermatology*, *162*(3), 497-502.

Kim, H. J., Kim, J. S., Woo, J.-T., Lee, I.-S., & Cha, B.-Y. (2015). Hyperpigmentation mechanism of methyl 3,5-di-caffeoylquinate through activation of p38 and MITF induction of tyrosinase. *Acta Biochimica et Biophysica Sinica*, *47*(7), 548-556.

Kim, J.-K., Park, K.-T., Lee, H.-S., Kim, M., & Lim, Y.-H. (2012). Evaluation of the inhibition of mushroom tyrosinase and cellular tyrosinase activities of oxyresveratrol: comparison with mulberroside A. *Journal of Enzyme Inhibition and Medicinal Chemistry*, *27*(4), 495-503.

Kim, J., Choi, H., Cho, E.-G., & Lee, T. R. (2014b). FoxO3a is an antimelanogenic factor that mediates antioxidant-induced depigmentation. *Journal of Investigative Dermatology*, *134*(5), 1378-1388.

Kim, J. Y., Kim, J., Ahn, Y., Lee, E. J., Hwang, S., Almurayshid, A., . . . Oh, S. H. (2020). Autophagy induction can regulate skin pigmentation by causing melanosome degradation in keratinocytes and melanocytes. *Pigment Cell & Melanoma Research*, *33*(3), 403-415.

Ko, F. N., Cheng, Z. J., Lin, C. N., & Teng, C. M. (1998). Scavenger and antioxidant properties of prenylflavones isolated From *Artocarpus heterophyllus*. *Free Radical Biology and Medicine*, *25*(2), 160-168.

Ko, G.-A., Kang, H. R., Moon, J. Y., Ediriweera, M. K., Eum, S., Bach, T. T., . . . Cho, S. K. (2019). *Annona squamosa* L. leaves inhibit alpha-melanocyte-stimulating hormone (α-MSH) stimulated melanogenesis via p38 signaling pathway in B16F10 melanoma cells. *Journal of Cosmetic Dermatology*, *19*(7), 1785-1792.

Ko, H.-H., Chiang, Y.-C., Tsai, M.-H., Liang, C.-J., Hsu, L.-F., Li, S.-Y., . . . Lee, C.-W. (2014). Eupafolin, a skin whitening flavonoid isolated from *Phyla nodiflora*, downregulated melanogenesis: role of MAPK and Akt pathways. *Journal of Ethnopharmacology*, *151*(1), 386-393.

Kumari, S., Thng, S. T. G., Verma, N. K., & Gautam, H. K. (2018). Melanogenesis inhibitors. *Acta Dermato-Venereologica*, *98*(9-10), 924-931.

Kwon, H. S., Lee, J. H., Kim, G. M., & Bae, J. M. (2018). Efficacy and safety of retinaldehyde 0.1% and 0.05% creams used to treat photoaged skin: a randomized double-blind controlled trial. *Journal of Cosmetic Dermatology*, *17*(3), 471-476.

Kwon, S.-H., Choi, H.-R., Kang, Y.-A., & Park, K.-C. (2017). Depigmenting effect of resveratrol is dependent on FOXO3a activation without SIRT1 activation. *International Journal of Molecular Sciences*, *18*(6), Article#1213.

Kwon, S.-H., Hwang, Y.-J., Lee, S.-K., & Park, K.-C. (2016). Heterogeneous pathology of melasma and its clinical implications. *International Journal of Molecular Sciences*, *17*(6), Article#824.

Lan, W.-C., Tzeng, C.-W., Lin, C.-C., Yen, F.-L., & Ko, H.-H. (2013). Prenylated flavonoids from *Artocarpus altilis*: antioxidant activities and inhibitory effects on melanin production. *Phytochemistry*, *89*, 78-88.

Lane, M. E. (2013). Skin penetration enhancers. *International Journal of Pharmaceutics*, *447*(1), 12-21.

Latha, M., Martis, J., Shobha, V., Shinde, R. S., Bangera, S., Krishnankutty, B., . . . Kumar, B. N. (2013). Sunscreening agents: a review. *The Journal of Clinical and Aesthetic Dermatology*, *6*(1), 16-26.

Lathiff, S. M. A., Jemaon, N., Abdullah, S. A., & Jamil, S. (2015). Flavonoids from *Artocarpus anisophyllus* and their bioactivities. *Natural Product Communications*, *10*(3), 393-396.

Lee, C.-C., Lin, C.-N., & Jow, G.-M. (2006). Cytotoxic and apoptotic effects of prenylflavonoid artonin B in human acute lymphoblastic leukemia cells. *Acta Pharmacologica Sinica*, *27*(9), 1165-1174.

Lee, C.-W., Ko, H.-H., Lin, C.-C., Chai, C.-Y., Chen, W.-T., & Yen, F.-L. (2013). Artocarpin attenuates ultraviolet B-induced skin damage in hairless mice by antioxidant and anti-inflammatory effect. *Food and Chemical Toxicology*, *60*, 123-129.

Lee, J.-O., Kim, E., Kim, J. H., Hong, Y. H., Kim, H. G., Jeong, D., . . . Cho, J. Y. (2018). Antimelanogenesis and skin-protective activities of *Panax ginseng* calyx ethanol extract. *Journal of Ginseng Research*, *42*(3), 389-399.

Lee, T. H., Park, S., Yoo, G., Jang, C., Kim, M.-h., Kim, S. H., . . . Kim, S. Y. (2016). Demethyleugenol β-glucopyranoside isolated from *Agastache rugosa* decreases melanin synthesis via down-regulation of MITF and SOX9. *Journal of Agricultural and Food Chemistry*, *64*(41), 7733-7742.

Levy, C., Khaled, M., & Fisher, D. E. (2006). MITF: master regulator of melanocyte development and melanoma oncogene. *Trends in Molecular Medicine*, *12*(9), 406-414.

Li, J., Lin, Z., Tang, X., Liu, G., Chen, Y., Zhai, X., . . . Cao, Y. (2020). Oxyresveratrol extracted from *Artocarpus heterophyllus* Lam. inhibits tyrosinase and age pigments *in vitro* and *in vivo*. *Food & Function*, *11*(7), 6595-6607.

Li, J., Wang, X., Zhang, T., Wang, C., Huang, Z., Luo, X., . . . Deng, Y. (2015). A review on phospholipids and their main applications in drug delivery systems. *Asian Journal of Pharmaceutical Sciences*, *10*(2), 81-98.

Li, Y.-Z., Mao, Q., Feng, F., & Ye, C.-H. (2010). Genetic diversity within a jackfruit (*Artocarpus heterophyllus* Lam.) germplasm collection in China using AFLP markers. *Agricultural Sciences in China*, *9*(9), 1263-1270.

Lin, J.-A., Fang, S.-C., Wu, C.-H., Huang, S.-M., & Yen, G.-C. (2011). Anti-inflammatory effect of the 5,7,4′-trihydroxy-6-geranylflavanone isolated from the fruit of *Artocarpus communis* in S100B-induced human monocytes. *Journal of Agricultural and Food Chemistry*, *59*(1), 105-111.

Lin, K.-W., Liu, C.-H., Tu, H.-Y., Ko, H.-H., & Wei, B.-L. (2009). Antioxidant prenylflavonoids from *Artocarpus communis* and *Artocarpus elasticus*. *Food Chemistry*, *115*(2), 558-562.

Liu, N., & Park, H.-J. (2009). Chitosan-coated nanoliposome as vitamin E carrier. *Journal of Microencapsulation*, *26*(3), 235-242.

Liu, W. J., Ye, L., Huang, W. F., Guo, L. J., Xu, Z. G., Wu, H. L., . . . Liu, H. F. (2016). p62 links the autophagy pathway and the ubiqutin–proteasome system upon ubiquitinated protein degradation. *Cellular & Molecular Biology Letters*, *21*, Article#29.

Liyanaarachchi, G. D., Samarasekera, J. K. R. R., Mahanama, K. R. R., & Hemalal, K. D. P. (2018). Tyrosinase, elastase, hyaluronidase, inhibitory and antioxidant activity of Sri Lankan medicinal plants for novel cosmeceuticals. *Industrial Crops and Products*, *111*, 597-605.

Ma, J., Guo, W., & Li, C. (2017). Ubiquitination in melanoma pathogenesis and treatment. *Cancer Medicine*, *6*(6), 1362-1377.

MacNeil, S. (2008). Biomaterials for tissue engineering of skin. *Materials Today*, *11*(5), 26-35.

Maddodi, N., Jayanthy, A., & Setaluri, V. (2012). Shining light on skin pigmentation: the darker and the brighter side of effects of UV radiation. *Photochemistry and Photobiology*, *88*(5), 1075-1082.

Madison, K. C. (2003). Barrier function of the skin: "la raison d'être" of the epidermis. *Journal of Investigative Dermatology*, *121*(2), 231-241.

Maghraby, G. M. M. E., Williams, A. C., & Barry, B. W. (2006). Can drug-bearing liposomes penetrate intact skin? *Journal of Pharmacy and Pharmacology*, *58*(4), 415-429.

Makbal, R., Villareal, M. O., Gadhi, C., Hafidi, A., & Isoda, H. (2020). *Argania spinosa* fruit shell extract-induced melanogenesis via cAMP signaling pathway activation. *International Journal of Molecular Sciences*, *21*(7), Article#2539.

Malakooti, S., Nasrollahi, S. A., Kashani, M. N., Naeimifar, A., Amiri, F., Rastegar, H., . . . Firooz, A. (2020). Formulation of triple cream for treatment of melasma. *Jundishapur Journal of Natural Pharmaceutical Products*, *15*(2), Article#e62252.

Mansky, K. C., Sankar, U., Han, J., & Ostrowski, M. C. (2002). Microphthalmia transcription factor is a target of the p38 MAPK pathway in response to receptor activator of NF-κB ligand signaling. *Journal of Biological Chemistry*, *277*(13), 11077-11083.

Marchev, A. S., & Georgiev, M. I. (2020). Plant *in vitro* systems as a sustainable source of active ingredients for cosmeceutical application. *Molecules*, *25*(9), Article#2006.

Martins, I. M., Barreiro, M. F., Coelho, M., & Rodrigues, A. E. (2014). Microencapsulation of essential oils with biodegradable polymeric carriers for cosmetic applications. *Chemical Engineering Journal*, *245*, 191-200.

Matsui, M. S., Petris, M. J., Niki, Y., Karaman-Jurukovska, N., Muizzuddin, N., Ichihashi, M., . . . Yarosh, D. B. (2015). Omeprazole, a gastric proton pump inhibitor, inhibits melanogenesis by blocking ATP7A trafficking. *Journal of Investigative Dermatology*, *135*(3), 834-841.

Matthias, F., Marie-Alexandrine, B., Hatem, F., & Stephanie, B. (2009). Topical delivery of cosmetics and drugs. Molecular aspects of percutaneous absorption and delivery. *European Journal of Dermatology*, *19*(4), 309-323.

Meybeck, A., & Dumas, M. (1992). *Composition containing a mulberry extract incorporated into hydrated lipidic lamellar phases of liposomes* (United States Patent No. 5,164,182).

Miki, H., Setou, M., Kaneshiro, K., & Hirokawa, N. (2001). All kinesin superfamily protein, KIF, genes in mouse and human. *Proceedings of the National Academy of Sciences*, *98*(13), 7004-7011.

Moan, J., Nielsen, K. P., & Juzeniene, A. (2012). Immediate pigment darkening: its evolutionary roles may include protection against folate photosensitization. *The FASEB Journal*, *26*(3), 971-975.

Morrison, I. J., Zhang, J., Lin, J., Murray, J. E., Porter, R., Langat, M. K., . . . Delgoda, R. (2021). Potential chemopreventive, anticancer and anti-inflammatory properties of a refined artocarpin-rich wood extract of *Artocarpus heterophyllus* Lam. *Scientific Reports*, *11*(1), Article#6854.

Moyal, D., Pinnell, S., & Hansenne, I. (2007). Topical application of ferulic acid, vitamins C and E protects human skin from ultraviolet A radiation‐induced erythema. *Journal of the American Academy of Dermatology*, *56*, AB163.

Murakami, H., & Arnheiter, H. (2005). Sumoylation modulates transcriptional activity of MITF in a promoter-specific manner. *Pigment Cell Research*, *18*(4), 265-277.

Musthapa, I., Latip, J., Takayama, H., Juliawaty, L. D., Hakim, E. H., & Syah, Y. M. (2009). Prenylated flavones from *Artocarpus lanceifolius* and their cytotoxic properties against P-388 cells. *Natural Product Communications*, *4*(7), 927-930.

Nagala, S., Yekula, M., & Tamanam, R. R. (2013). Antioxidant and gas chromatographic analysis of five varieties of jackfruit (*Artocarpus*) seed oils. *Drug Invention Today*, *5*(4), 315-320.

Nakamura, M., Morita, A., Seité, S., Haarmann-Stemmann, T., Grether-Beck, S., & Krutmann, J. (2015). Environment-induced lentigines: formation of solar lentigines beyond ultraviolet radiation. *Experimental Dermatology*, *24*(6), 407-411.

Namdaung, U., Aroonrerk, N., Suksamrarn, S., Danwisetkanjana, K., Saenboonrueng, J., Arjchomphu, W., . . . Suksamrarn, A. (2006). Bioactive constituents of the root bark of *Artocarpus rigidus* subsp. *rigidus*. *Chemical and Pharmaceutical Bulletin*, *54*(10), 1433-1436.

Navanesan, S., Wahab, N., Manickam, S., & Sim, K. S. (2015). Evaluation of selected biological capacities of *Baeckea frutescens*. *BMC Complementary and Alternative Medicine*, *15*(1), Article#186.

Newburger, A. E. (2009). Cosmeceuticals: myths and misconceptions. *Clinics in Dermatology*, *27*(5), 446-452.

Nguyen, J. K., Masub, N., & Jagdeo, J. (2020). Bioactive ingredients in Korean cosmeceuticals: trends and research evidence. *Journal of Cosmetic Dermatology*, *19*(7), 1555-1569.

Nguyen, M. T. T., Le, T. H., Nguyen, H. X., Dang, P. H., Do, T. N. V., Abe, M., . . . Nguyen, N. T. (2017). Artocarmins G–M, prenylated 4-chromenones from the stems of *Artocarpus rigida* and their tyrosinase inhibitory activities. *Journal of Natural Products*, *80*(12), 3172-3178.

Nguyen, N. T., Nguyen, M. H. K., Nguyen, H. X., Bui, N. K. N., & Nguyen, M. T. T. (2012). Tyrosinase inhibitors from the wood of *Artocarpus heterophyllus*. *Journal of Natural Products*, *75*(11), 1951-1955.

Nishioka, K. (1978). Particulate tyrosinase of human malignant melanoma: solubilization, purification following trypsin treatment, and characterization. *European Journal of Biochemistry*, *85*(1), 137-146.

Ochiai, Y., Kaburagi, S., Okano, Y., Masaki, H., Ichihashi, M., Funasaka, Y., . . . Sakurai, H. (2008). A Zn(II)–glycine complex suppresses UVB-induced melanin production by stimulating metallothionein expression. *International Journal of Cosmetic Science*, *30*(2), 105-112.

Ortonne, J.-P., Pandya, A. G., Lui, H., & Hexsel, D. (2006). Treatment of solar lentigines. *Journal of the American Academy of Dermatology*, *54*(5), S262-S271.

Oskoueian, E., Karimi, E., Noura, R., Ebrahimi, M., Shafaei, N., & Karimi, E. (2020). Nanoliposomes encapsulation of enriched phenolic fraction from pistachio hulls and its antioxidant, anti-inflammatory, and anti-melanogenic activities. *Journal of Microencapsulation*, *37*(1), 1-13.

Pandya, A. G., & Guevara, I. L. (2000). Disorders of hyperpigmentation. *Dermatologic Clinics*, *18*(1), 91-98.

Parvez, S., Kang, M., Chung, H. S., & Bae, H. (2007). Naturally occurring tyrosinase inhibitors: mechanism and applications in skin health, cosmetics and agriculture industries. *Phytotherapy Research*, *21*(9), 805-816.

Parvez, S., Kang, M., Chung, H. S., Cho, C., Hong, M. C., Shin, M. K., . . . Bae, H. (2006). Survey and mechanism of skin depigmenting and lightening agents. *Phytotherapy Research*, *20*(11), 921-934.

Passeron, T., & Picardo, M. (2018). Melasma, a photoaging disorder. *Pigment Cell & Melanoma Research*, *31*(4), 461-465.

Pathak, M. A. (2004). In memory of Thomas Bernhard Fitzpatrick. *Journal of Investigative Dermatology*, *122*(2), xx-xxi.

Patkar, K. (2008). Herbal cosmetics in ancient India. *Indian Journal of Plastic Surgery*, *41*, S134-S137.

Pattni, B. S., Chupin, V. V., & Torchilin, V. P. (2015). New developments in liposomal drug delivery. *Chemical Reviews*, *115*(19), 10938-10966.

Pearson, D. (1976). *Chemical analysis of food. Churchill Livingstone*.

Picardo, M., Ottaviani, M., Camera, E., & Mastrofrancesco, A. (2009). Sebaceous gland lipids. *Dermato-Endocrinology*, *1*(2), 68-71.

Pieroni, A., Quave, C. L., Villanelli, M. L., Mangino, P., Sabbatini, G., Santini, L., . . . Tomasi, M. (2004). Ethnopharmacognostic survey on the natural ingredients used in folk cosmetics, cosmeceuticals and remedies for healing skin diseases in the inland Marches, Central-Eastern Italy. *Journal of Ethnopharmacology*, *91*(2), 331-344.

Pillaiyar, T., Manickam, M., & Jung, S.-H. (2017a). Downregulation of melanogenesis: drug discovery and therapeutic options. *Drug Discovery Today*, *22*(2), 282-298.

Pillaiyar, T., Manickam, M., & Namasivayam, V. (2017b). Skin whitening agents: medicinal chemistry perspective of tyrosinase inhibitors. *Journal of Enzyme Inhibition and Medicinal Chemistry*, *32*(1), 403-425.

Plensdorf, S., & Martinez, J. (2009). Common pigmentation disorders. *American Family Physician*, *79*(2), 109-116.

Praditsangthong, R., Slakkham, B., & Bhattarakosol, P. (2021). A fear detection method based on palpebral fissure. *Journal of King Saud University - Computer and Information Sciences*, *33*, 1030-1039.

Praetorius, C., Sturm, R. A., & Steingrimsson, E. (2014). Sun-induced freckling: ephelides and solar lentigines. *Pigment Cell & Melanoma Research*, *27*(3), 339-350.

Prausnitz, M. R., Mitragotri, S., & Langer, R. (2004). Current status and future potential of transdermal drug delivery. *Nature Reviews Drug Discovery*, *3*(2), 115-124.

Price, E. R., Horstmann, M. A., Wells, A. G., Weilbaecher, K. N., Takemoto, C. M., Landis, M. W., . . . Fisher, D. E. (1998). α-melanocyte-stimulating hormone signaling regulates expression of microphthalmia, a gene deficient in Waardenburg syndrome. *Journal of Biological Chemistry*, *273*(49), 33042-33047.

Rajanala, S., Maymone, M. B., & Vashi, N. A. (2019). Melasma pathogenesis: a review of the latest research, pathological findings, and investigational therapies. *Dermatology Online Journal*, *25*(10), 1-6.

Rendon, M., Berneburg, M., Arellano, I., & Picardo, M. (2006). Treatment of melasma. *Journal of the American Academy of Dermatology*, *54*(5), S272-S281.

Roh, E., Jeong, I.-Y., Shin, H., Song, S., Kim, N. D., Jung, S.-H., . . . Kim, Y. (2014). Downregulation of melanocyte-specific facultative melanogenesis by 4-hydroxy-3-methoxycinnamaldehyde acting as a cAMP antagonist. *Journal of Investigative Dermatology*, *134*(2), 551-553.

Roméro-Graillet, C., Aberdam, E., Clément, M., Ortonne, J.-P., & Ballotti, R. (1997). Nitric oxide produced by ultraviolet-irradiated keratinocytes stimulates melanogenesis. *The Journal of Clinical Investigation*, *99*(4), 635-642.

Ryu, Y. B., Ha, T. J., Curtis-Long, M. J., Ryu, H. W., Gal, S. W., & Park, K. H. (2008). Inhibitory effects on mushroom tyrosinase by flavones from the stem barks of *Morus lhou* (S.) Koidz. *Journal of Enzyme Inhibition and Medicinal Chemistry*, *23*(6), 922-930.

Saad, H. M., Sim, K. S., & Tan, Y. S. (2018). Antimelanogenesis and anti-inflammatory activity of selected culinary-medicinal mushrooms. *International Journal of Medicinal Mushrooms*, *20*(2), 141-153.

Saito, H., Yasumoto, K.-i., Takeda, K., Takahashi, K., Fukuzaki, A., Orikasa, S., . . . Shibahara, S. (2002). Melanocyte-specific microphthalmia-associated transcription factor isoform activates its own gene promoter through physical interaction with lymphoid-enhancing factor 1. *Journal of Biological Chemistry*, *277*(32), 28787-28794.

Sangkaew, O., & Yompakdee, C. (2020). Fermented unpolished black rice (*Oryza sativa* L.) inhibits melanogenesis via ERK, p38, and AKT phosphorylation in B16F10 melanoma cells. *Journal of Microbiology and Biotechnology*, *30*(8), 1184-1194.

Sarkar, R., Ailawadi, P., & Garg, S. (2018). Melasma in men: a review of clinical, etiological, and management issues. *The Journal of Clinical and Aesthetic Dermatology*, *11*(2), 53-59.

Sayre, R. M., Agin, P. P., LeVee, G. J., & Marlowe, E. (1979). A comparison of *in vivo* and *in vitro* testing of sunscreening formulas. *Photochemistry and Photobiology*, *29*(3), 559-566.

Scherer, R., & Godoy, H. T. (2009). Antioxidant activity index (AAI) by the 2,2-diphenyl-1-picrylhydrazyl method. *Food Chemistry*, *112*(3), 654-658.

Searle, T., Ali, F. R., & Al-Niaimi, F. (2022). The versatility of azelaic acid in dermatology. *Journal of Dermatological Treatment*, *33*(2), 722-732.

Seo, E. Y., Jin, S.-P., Sohn, K.-C., Park, C.-H., Lee, D. H., & Chung, J. H. (2017). UCHL1 regulates melanogenesis through controlling MITF stability in human melanocytes. *Journal of Investigative Dermatology*, *137*(8), 1757-1765.

Seo, G.-Y., Ha, Y., Park, A.-H., Kwon, O. W., & Kim, Y.-J. (2019). *Leathesia difformis* extract inhibits α-MSH-induced melanogenesis in B16F10 cells via down-regulation of CREB signaling pathway. *International Journal of Molecular Sciences*, *20*(3), Article#536.

Shah, M. K. K., Sirat, H. M., Jamil, S., & Jalil, J. (2016). Flavonoids from the bark of *Artocarpus integer* var. silvestris and their anti-inflammatory properties. *Natural Product Communications*, *11*(9), 1275-1278.

Shamaun, S. S., Rahmani, M., Hashim, N. M., Ismail, H. B. M., Sukari, M. A., Lian, G. E. C., . . . Go, R. (2010). Prenylated flavones from *Artocarpus altilis*. *Journal of Natural Medicines*, *64*(4), 478-481.

Sharad, J. (2013). Glycolic acid peel therapy - a current review. *Clinical, Cosmetic and Investigational Dermatology*, *6*, 281-288.

Shi, V. Y., Leo, M., Hassoun, L., Chahal, D. S., Maibach, H. I., & Sivamani, R. K. (2015). Role of sebaceous glands in inflammatory dermatoses. *Journal of the American Academy of Dermatology*, *73*(5), 856-863.

Shigeta, Y., Imanaka, H., Ando, H., Ryu, A., Oku, N., Baba, N., . . . Makino, T. (2004). Skin whitening effect of linoleic acid is enhanced by liposomal formulations. *Biological and Pharmaceutical Bulletin*, *27*(4), 591-594.

Shimizu, H. (2016). Structure and function of the skin. In *Shimizu's Textbook of Dermatology* (pp. 1-42). Nakayama Shoten Co., Ltd.

Singpanna, K., Dechsri, K., Patrojanasophon, P., Limpachayaporn, P., Opanasopit, P., & Nuntharatanapong, N. (2021). Transdermal delivery, cytotoxicity and anti-melanogenic activity of p-chlorophenyl benzyl ether loaded-liposomes. *Journal of Drug Delivery Science and Technology*, *65*, Article#102746.

Sinico, C., Manconi, M., Peppi, M., Lai, F., Valenti, D., & Fadda, A. M. (2005). Liposomes as carriers for dermal delivery of tretinoin: *in vitro* evaluation of drug permeation and vesicle–skin interaction. *Journal of Controlled Release*, *103*(1), 123-136.

Slominski, A., Tobin, D. J., Shibahara, S., & Wortsman, J. (2004). Melanin pigmentation in mammalian skin and its hormonal regulation. *Physiological Reviews*, *84*(4), 1155-1228.

Sotelo, C. G., Blanco, M., Ramos, P., Vázquez, J. A., & Perez-Martin, R. I. (2021). Sustainable sources from aquatic organisms for cosmeceuticals ingredients. *Cosmetics*, *8*(2), Article#48.

Sturm, R. A. (2009). Molecular genetics of human pigmentation diversity. *Human Molecular Genetics*, *18*(R1), R9-R17.

Sulaiman, N. S. (2011). *Phytochemicals and bioactivities of Artocarpus lanceifolius roxb and Artocarpus maingayi King* [Master thesis, Universiti Teknologi Malaysia].

Sun, L., Guo, C., Yan, L., Li, H., Sun, J., Huo, X., . . . Hu, J. (2020). Syntenin regulates melanogenesis via the p38 MAPK pathway. *Molecular Medicine Reports*, *22*(2), 733-738.

Sunder, S. (2019). Relevant topical skin care products for prevention and treatment of aging skin. *Facial Plastic Surgery Clinics of North America*, *27*(3), 413-418.

Svobodova, A., Walterova, D., & Vostalova, J. (2006). Ultraviolet light induced alteration to the skin. *Biomedical Papers-Palacky University in Olomouc*, *150*(1), 25-38.

Szöllősi, A. G., Oláh, A., Bíró, T., & Tóth, B. I. (2017). Recent advances in the endocrinology of the sebaceous gland. *Dermato-Endocrinology*, *9*(1), Article#e1361576.

Taira, N., Katsuyama, Y., Yoshioka, M., Okano, Y., & Masaki, H. (2018). 3-O-Glyceryl-2-O-hexyl ascorbate suppresses melanogenesis by interfering with intracellular melanosome transport and suppressing tyrosinase protein synthesis. *Journal of Cosmetic Dermatology*, *17*(6), 1209-1215.

Taylor, S., Grimes, P., Lim, J., Im, S., & Lui, H. (2009). Postinflammatory hyperpigmentation. *Journal of Cutaneous Medicine and Surgery*, *13*(4), 183-191.

Teeranachaideekul, V., Souto, E. B., Junyaprasert, V. B., & Müller, R. H. (2007). Cetyl palmitate-based NLC for topical delivery of Coenzyme Q10 – development, physicochemical characterization and *in vitro* release studies. *European Journal of Pharmaceutics and Biopharmaceutics*, *67*(1), 141-148.

Tengamnuay, P., Pengrungruangwong, K., Pheansri, I., & Likhitwitayawuid, K. (2006). *Artocarpus lakoocha* heartwood extract as a novel cosmetic ingredient: evaluation of the *in vitro* anti‑tyrosinase and *in vivo* skin whitening activities. *International Journal of Cosmetic Science*, *28*(4), 269-276.

Tetali, B., Fahs, F. M., & Mehregan, D. (2020). Popular over-the-counter cosmeceutical ingredients and their clinical efficacy. *International Journal of Dermatology*, *59*(4), 393-405.

Tewtrakul, S., Itharat, A., Thammaratwasik, P., & Ooraikul, B. (2008). Anti-allergic and anti-microbial activities of some Thai crops. *Songklanakarin Journal of Science and Technology*, *30*(4), 467-473.

The UniProt, C. (2019). UniProt: a worldwide hub of protein knowledge. *Nucleic Acids Research*, *47*(D1), D506-D515.

Thody, A. J., Higgins, E. M., Wakamatsu, K., Ito, S., Burchill, S. A., & Marks, J. M. (1991). Pheomelanin as well as eumelanin is present in human epidermis. *Journal of Investigative Dermatology*, *97*(2), 340-344.

Tiraravesit, N., Yakaew, S., Rukchay, R., Luangbudnark, W., Viennet, C., Humbert, P., . . . Viyoch, J. (2015). *Artocarpus altilis* heartwood extract protects skin against UVB *in vitro* and *in vivo*. *Journal of Ethnopharmacology*, *175*, 153-162.

Tsatmali, M., Ancans, J., & Thody, A. J. (2002). Melanocyte function and its control by melanocortin peptides. *Journal of Histochemistry & Cytochemistry*, *50*(2), 125-133.

Van Tran, V., Moon, J.-Y., & Lee, Y.-C. (2019). Liposomes for delivery of antioxidants in cosmeceuticals: challenges and development strategies. *Journal of Controlled Release*, *300*, 114-140.

Vargas, F. S., Almeida, P. D. O., Boleti, A. P. A., Pereira, M. M., Souza, T. P., Vasconcellos, M. C., . . . Lima, E. S. (2016). Antioxidant activity and peroxidase inhibition of Amazonian plants extracts traditionally used as anti-inflammatory. *BMC Complementary and Alternative Medicine*, *16*(1), Article#83.

Victor, F. C., Gelber, J., & Rao, B. (2004). Melasma: a review. *Journal of Cutaneous Medicine and Surgery: Incorporating Medical and Surgical Dermatology*, *8*(2), 97-102.

Villareal, M. O., Han, J., Ikuta, K., & Isoda, H. (2012). Mechanism of *Mitf* inhibition and morphological differentiation effects of hirsein A on B16 melanoma cells revealed by DNA microarray. *Journal of Dermatological Science*, *67*(1), 26-36.

Walters, C., Keeney, A., Wigal, C. T., Johnston, C. R., & Cornelius, R. D. (1997). The spectrophotometric analysis and modeling of sunscreens. *Journal of Chemical Education*, *74*(1), 99-101.

Wei, B.-L., Weng, J.-R., Chiu, P.-H., Hung, C.-F., Wang, J.-P., & Lin, C.-N. (2005). Antiinflammatory flavonoids from *Artocarpus heterophyllus* and *Artocarpus communis*. *Journal of Agricultural and Food Chemistry*, *53*(10), 3867-3871.

Wen, A.-H., Choi, M.-K., & Kim, D.-D. (2006). Formulation of liposome for topical delivery of arbutin. *Archives of Pharmacal Research*, *29*(12), 1187-1192.

Wen, L., Zhao, Y., Jiang, Y., Yu, L., Zeng, X., Yang, J., . . . Yang, B. (2017). Identification of a flavonoid C-glycoside as potent antioxidant. *Free Radical Biology and Medicine*, *110*, 92-101.

Wickett, R. R., & Visscher, M. O. (2006). Structure and function of the epidermal barrier. *American Journal of Infection Control*, *34*(10), S98-S110.

Wlaschek, M., Tantcheva-Poór, I., Naderi, L., Ma, W., Schneider, L. A., Razi-Wolf, Z., . . . Scharffetter-Kochanek, K. (2001). Solar UV irradiation and dermal photoaging. *Journal of Photochemistry and Photobiology B: Biology*, *63*(1), 41-51.

Wu, M., Hemesath, T. J., Takemoto, C. M., Horstmann, M. A., Wells, A. G., Price, E. R., . . . Fisher, D. E. (2000). C-Kit triggers dual phosphorylations, which couple activation and degradation of the essential melanocyte factor Mi. *Genes & Development*, *14*(3), 301-312.

Wu, Q.-Y., Wong, Z. C.-F., Wang, C., Fung, A. H.-Y., Wong, E. O.-Y., Chan, G. K.-L., . . . Tsim, K. W.-K. (2019). Isoorientin derived from *Gentiana veitchiorum* Hemsl. flowers inhibits melanogenesis by down-regulating MITF-induced tyrosinase expression. *Phytomedicine*, *57*, 129-136.

Yamaguchi, Y., Brenner, M., & Hearing, V. J. (2007). The regulation of skin pigmentation. *Journal of Biological Chemistry*, *282*(38), 27557-27561.

Yao, X., Wu, D., Dong, N., Ouyang, P., Pu, J., Hu, Q., . . . Huang, J. (2016). Moracin C, a phenolic compound isolated from *Artocarpus heterophyllus*, suppresses lipopolysaccharide-activated inflammatory responses in murine raw264.7 macrophages. *International Journal of Molecular Sciences*, *17*(8), 1-15, Article#1199.

Yeh, C.-J., Chen, C.-C., Leu, Y.-L., Lin, M.-W., Chiu, M.-M., & Wang, S.-H. (2017). The effects of artocarpin on wound healing: *in vitro* and *in vivo* studies. *Scientific Reports*, *7*(1), Article#15599.

Yoo, J., Shanmugam, S., Song, C.-K., Kim, D.-D., Choi, H.-G., Yong, C.-S., . . . Yoo, B. K. (2008). Skin penetration and retention of L-Ascorbic acid 2-phosphate using multilamellar vesicles. *Archives of Pharmacal Research*, *31*(12), 1652-1658.

Yousef, H., Alhajj, M., & Sharma, S. (2020). Anatomy, skin (integument), epidermis. In *StatPearls [Internet]*. Treasure Island (FL): StatPearls Publishing. https://www.ncbi.nlm.nih.gov/books/NBK470464/

Zheng, Z. P., Cheng, K. W., To, J. T. K., Li, H., & Wang, M. (2008). Isolation of tyrosinase inhibitors from *Artocarpus heterophyllus* and use of its extract as antibrowning agent. *Molecular Nutrition & Food Research*, *52*(12), 1530-1538.